



**Politecnico
di Torino**

Politecnico di Torino

LINKS Foundation Internship

Master Degree Thesis

Master Science program in Electronic Engineering

**Radio frequency wave propagation
and scattering in plasmas generated
by hypersonic crafts**

Supervisor:

Prof. Giuseppe Vecchi

Co-Supervisor and Tutor:

Dr. Andrea Scarabosio

Candidate:

Giovanni Mascarino

269725

Academic year 2022/23

A mia zia Elvira

To my aunt Elvira

Acknowledgements

In English

I would like to acknowledge my supervisor, prof. Giuseppe Vecchi, and my co-supervisor Andrea Scarabosio, who offered to me this opportunity and for all the support provided during the thesis. I would like to acknowledge LACE team from LINKS Foundation, researchers and PhD students, for the cooperation and assistance.

In Italian

Vorrei ringraziare la mia famiglia, che mi è stata di supporto: a partire dai miei genitori, mio fratello, i miei zii e i miei cugini. Vorrei ringraziare altrettanto i miei amici per essermi stati accanto.

Abstract

Radio Frequency wave propagation and scattering have a huge role in aerospace, being the basis for telecommunication and radar technology. Hypersonic crafts in atmosphere generate plasma by shock wave heating of the surrounding air. The plasma free electric charges (electrons and ions) have a strong influence on the RF waves up to a point of completely blocking the wave propagation (cut-off condition). Drude model is the theoretical reference, because it is suitable for unmagnetized plasma as in this case: it defines the distribution in space of the complex permittivity due to plasma and neutrals density and temperature.

Re-entry vehicles from space, missiles, aerospace crafts, hyperloop trains are some instances of hypersonic vehicles and research has lately grown interest in them; moreover they remark the importance of their tracking due to either safety and defence purposes. A fast and accurate modelling tool for RF scattering by hypersonic plasmas would make it possible to design performing radar systems and communication links for specified purpose.

RF scattering evaluation is done on CST microwave studio, a commercial software that performs well in full-wave FDTD (finite difference time domain) method and fulfils dispersion model such as Drude reference that complies with hypersonic condition. Usefulness of that software is the spread among companies, that make it more reachable with the respect of other approximated methods implemented in research, such as asymptotic one. Unlike standard user, we operate the code via scripting to allow the implementation of complex inputs and dielectric geometries. Codes are written in VBA, but Matlab may pass directly those scripts.

RCS results (Radar Cross Section scattering) are compared with semi-analytic solution, such as Mie Series, whenever it is possible. Hypersonic RF testing is subordinated to CFD (computational fluid dynamics) extractions because physical quantities, such as permittivities and plasma frequencies, are distributed along the

hypersonic vehicle in relation with own trajectory and speed. Most critical points are on impact region, where shock wave heating is much effective, potentially leading to high density plasma with strongly real negative permittivity region. This work attempts to define the applicability of CST on this hard and computationally challenging conditions.

Contents

List of Figures	V
List of Tables	IX
Nomenclature	X
1 Introduction	1
1.1 Introduction description and desired achievements	1
2 EM wave propagation, RCS and plasmas	3
2.1 Propagation Theory	4
2.1.1 Maxwell's Equations	4
2.1.2 Permittivity and Permeability	5
2.1.3 Wave Equation	6
2.1.4 Plane Wave	7
2.1.5 Radar Cross Section	9
2.1.5.1 CST simulation	10
2.1.6 Mie Series	11
2.2 Plasma Physics	14
2.2.1 Drude Model	14
2.2.2 Computational Fluid Dynamics simulation provided quantities	16

Contents

3	CST code and its application to plasmas	20
3.1	Solver	20
3.1.1	Differencing formulas	21
3.1.2	Time Domain Finite Difference method	22
3.1.2.1	Linear discretization	22
3.1.2.2	Three-Dimensional Discretization	23
3.2	Geometry model implementation in CST	24
3.2.1	Geometry Definition	25
3.2.1.1	VBA	26
3.2.2	Material Definition	26
3.2.2.1	Space Map	28
3.2.3	CST simulation of dielectric shells in radial distribution	29
3.2.3.1	Inhomogeneous shells around PEC sphere	30
3.2.4	RCS Result - Spherical Coordinates	31
3.3	Simulation experience	33
4	RCS of plasma with spherical geometry	35
4.1	Inhomogeneous dielectric with discontinuities - negative permittivities shells around PEC sphere	36
4.1.1	Frequency of 100 MHz	36
4.1.2	Conclusion on CST simulations for discontinuous shells	40
4.2	Inhomogeneous dielectric with continuities permittivity distribution around PEC sphere	41
4.2.1	Positive permittivities in inhomogeneous continuous plasmas	43
4.2.1.1	CST spherical shells with permittivity variable at 0.1, $f = 100$ [MHz]	43
4.2.1.2	Space map with permittivity variable at 0.5, $f = 250$ [MHz]	44

4.2.1.3	Space map with permittivity variable at 0.1, f = 100 [MHz]	47
4.2.1.4	Space map with permittivity variable at 0.1, f = 250 [MHz]	47
4.2.2	Negative permittivities in inhomogeneous continuous plasmas	50
4.2.2.1	Space map with permittivity variable at -0.1, f = 100 [MHz]	50
4.2.2.2	Space map with permittivity variable at -0.1, f = 250 [MHz]	51
4.3	Conclusions on analytic plasmas profile	51
5	RCS in presence of realistic hypersonic plasma flows	53
5.1	PTFE sphere with Mach 10 flow	53
5.1.1	RCS in vacuum background	54
5.1.2	Plasma distribution	55
5.1.2.1	Extraction of spherical symmetric plasma distri- bution from 3D CFD	56
5.1.2.2	CFD plasma reproduced by [1] implemented in CST	58
5.1.3	PTFE with plasma reproduced by [1] and source angle by 10 degrees	59
5.2	RCS of simple hypersonic vehicle	61
5.2.1	RCS for hypersonic vehicle in plasma flow	62
5.2.2	Negative dielectric permittivity shell around vehicle	65
5.3	Conclusions	65
6	Summary and Conclusions	69
	References	71

Contents

Appendix A Homogeneous dielectric - spheres in vacuum - fixed ka around	
31.4	73
A.1 PEC sphere CAD model	74
A.2 PTFE sphere CAD model	74
A.2.1 PTFE Filled sphere CAD model	74
A.2.2 PTFE Hollowed sphere CAD model	75
A.3 PTFE filled sphere space map material	81
A.4 Conclusions on homogeneous dielectric sphere EM evaluation in vacuum	82
Appendix B Mie Solution for continuous permittivity distribution and imaginary component of relative permittivity contribution	85
B.1 Mie Solution evaluation	85
B.1.1 Imaginary component contribution	86
B.1.1.1 Step for input dielectric	88
B.2 Implementation of a relevant imaginary component	90
B.2.1 Permittivity distribution with negative and zero values substituted with very tiny positive values	90
B.2.2 Conclusions	93
Appendix C MATLAB code for shells with permittivity profile and CST geometry implementation	95

List of Figures

2.1	Plane Wave - linear polarization - 3D plot	8
2.2	Monostatic radar simple scheme	10
2.3	Bistatic radar simple scheme	10
2.4	Mie Series implementation in Spherical Coordinates	11
2.5	Scattering regime regions with the respect of a/λ_0 physical parameter from figure 2.9 in [2] page 34	13
2.6	CFD reproduce by [1] - temperature around 150 mm diameter PTFE sphere as primarily proposed in [3] paper - inspired by figure 2 in [3]	17
2.7	CFD reproduce by [1] - ions around 150 mm diameter PTFE sphere as primarily proposed in [3] paper - inspired by figure 2 in [3]	17
2.8	CFD reproduce by [1] - Plasma Frequency in GHz around 150 mm diameter PTFE sphere as primarily proposed in [3] paper - inspired by figure 2 in [3]	18
2.9	CFD reproduce by [1] - ϵ_r around 150 mm diameter sphere primarily proposed in [3] - inspired by figure 2 in [3]	19
3.1	Curve and its derivative	22
3.2	Linear discretization in one dimension	23
3.3	Grid and Yee's cell	24
3.4	CST window for sphere model generation	25
3.5	CST window New Material definition	27

List of Figures

3.6	Drude model verification for $\epsilon_r = -6 - j1 \cdot 10^{-4}$ at 150 MHz on CST	31
3.7	3D half cut model on CST for plasma distribution described in figure 4.1	31
3.8	Spherical coordinates system and polarization planes referment . . .	32
3.9	Plots of table A.1 trends for ASCII file size and width for space map material of 2 meter radius sphere	34
4.1	Sphere shelling with negative permittivities	37
4.2	CST view of space mapped material at 100 MHz for negative shells	37
4.3	RCS for $f = 100 \text{ MHz}$ and $\epsilon_r' = -3$ for plasma distribution described in figure 4.1 - Geometry	38
4.4	RCS for $f = 100 \text{ MHz}$ and $\epsilon_r' = -3$ for plasma distribution described in figure 4.1 - Space Map	39
4.5	RCS for $f = 150 \text{ MHz}$ and $\epsilon_r' = -3$ for plasma distribution described in figure 4.1	40
4.6	Radial permittivity distribution related to equation 4.1	42
4.7	Distribution of relative permittivity as equation (4.1) and $\epsilon_c = 0.1$	43
4.8	Portion of halved concentric 55 shells generated for CST	44
4.9	RCS with ϵ_r profile provided by (4.1) with $\epsilon_c = 0.1$, $\epsilon_r'' = 1 \cdot 10^{-4}$, frequency = 100 MHz and 55 shells around PEC sphere	45
4.10	Space map cut for analytic plasma from distribution defined in (4.1) with $\epsilon_c = 0.5$	46
4.11	RCS of space mapped analytic plasma from distribution defined in (4.1) with $\epsilon_c = 0.5$, $f = 250 \text{ MHz}$	47
4.12	RCS of space mapped analytic plasma from distribution defined in (4.1) with $\epsilon_c = +0.1$, $f = 100 \text{ [MHz]}$ and $\epsilon_r'' = 1 \cdot 10^{-4}$	48
4.13	Space map cut for analytic plasma from distribution defined in (4.1) with $\epsilon_c = 0.1$	48
4.14	RCS of space mapped analytic plasma from distribution defined in (4.1) with $\epsilon_c = 0.1$, $f = 250 \text{ [MHz]}$ and $\epsilon_r'' = 0$	49

List of Figures

4.15 RCS of space mapped analytic plasma from distribution defined in (4.1) with $\epsilon_c = -0.1$, $f = 100$ [MHz], $\epsilon_r'' = 1 \cdot 10^{-4}$	50
4.16 RCS of space mapped analytic plasma from distribution defined in (4.1) with $\epsilon_c = -0.1$, $f = 250$ [MHz] and $\epsilon_r'' = 1 \cdot 10^{-4}$	51
5.1 Comparison between f_p in [3] and with CFD provided by [1]	54
5.2 Monostatic RCS from figure 3 in paper [3] in vacuum condition with reproduced simulation on CST for this thesis and Mie Solution	55
5.3 From CFD reproduced by [1] with model proposed in [3] - high- lighted region from ϵ_r cut map inspired by figure 2 of [3]	56
5.4 Space Maps radial dependence for f_p extraction from CFD provided by [1]	57
5.5 Space Maps radial dependence for ϵ_r' extraction with $f = 3$ [GHz] from CFD provided by [1]	58
5.6 RCS for radial extraction of CFD provided by [1] and at $f = 3$ [GHz]	59
5.7 RCS for PTFE sphere of Mach 10 as proposed in [3] with CFD provided by [1] and at $f = 3$ [GHz]	60
5.8 Comparisons between figure 5.6 and figure 5.7	61
5.9 Proposed Model and its plasma for Mach 10	63
5.10 RCS for model in figure 5.9a with multiple plasma frequencies mapped from figure 5.9b with multiplying factor	64
5.11 Vehicle surrounded by constant complex permittivity shell - half cut	65
5.12 Model and corresponding RCS for $f = 600$ [MHz] from [4] figure 7	66
5.13 RCS for model in figure 5.9a with negative shell with $\epsilon_r = -3 + j1 \cdot$ 10^{-4} around	68
A.1 Sphere in vacuum CAD Models in CST	74
A.2 Time Domain Solver for PEC sphere with $k_0 \cdot a \approx 31.4$	76
A.3 Integral Equation Solver for PEC sphere with $k_0 \cdot a \approx 31.4$	77
A.4 Time Domain Solver for PTFE filled sphere with $k_0 \cdot a \approx 31.4$	78

List of Figures

A.5	Integral Equation Solver for PTFE filled sphere with $k_0 \cdot a \approx 31.4$. . .	79
A.6	RCS of PTFE hollowed sphere in vacuum	80
A.7	Instance of space map for a filled PTFE sphere by 2 meter radius . . .	81
A.8	RCS of filled PTFE sphere space mapped with width on run1 in table A.1 and a CST simulation with CAD model	83
A.9	RCS of filled PTFE sphere space mapped with all widths reported in table A.1	84
B.1	Convergence for imaginary part implementation for $\epsilon_c = 0.1$ in distribution equation (4.1)	86
B.2	RCS of ϵ_r from equation (4.1) Mie Solution with $\epsilon_c = -0.1$ and additive imaginary component	87
B.3	RCS convergence of ϵ_r by equation (4.1) with $\epsilon_c = 0.5$	88
B.4	RCS convergence for ϵ_r by equation (4.1) with $\epsilon_c = 0.1$	89
B.5	RCS of ϵ_r from equation (4.1) Mie Solution for $\epsilon_c = -0.1$	91
B.6	Profile of permittivity distribution	92
B.7	RCS for permittivity distribution in equation (4.1) with $\epsilon_c = -0.1$ and $\epsilon_r'' = 0.05$ with and without substitution $\forall \epsilon_r' < 0 \Rightarrow \epsilon_r' = 1 \cdot 10^{-3}$	92
B.8	Accuracy for Mie Solution of ϵ_r from equation (4.1) with $\epsilon_c = -0.1$ and $\epsilon_r'' = 0.05$	93
B.9	RCS with $\epsilon_c = -0.1$ from profile defined in (4.1) - $\epsilon_r \in \mathbb{C}$	94

List of Tables

2.1	Fundamental EM physical quantities	5
2.2	Plane Wave formulas	7
2.3	Physical quantities for plasma Frequency	15
2.4	Format of CFD file for PTFE sphere described in section 2.2	16
3.1	FourColumns Format for CST Space Map Material	28
3.2	VBA variables definition for Drude Model	29
4.1	Parameters description for permittivity analytic profile	41
5.1	Monostatic RCS value for $\theta = 0^\circ$ at $f = 3$ [GHz]	58
5.2	Monostatic RCS for $\theta = 10$ comparison between extraction from figure 3 in [3] and our simulations	61
A.1	Trends for different runs of space mapped permittivity for a PTFE filled sphere of 2 meter radius in width and ASCII generated file size	81

Nomenclature

Roman Symbols

CST CST microwave studio software by Dassault Systèmes

Ma Mach Number

Other Symbols

ϵ_r'' Imaginary part of relative permittivity

ϵ_r' Real part of relative permittivity

ν_c Collision Frequency [Hz]

ω_p Plasma Angular Frequency [rad/s]

f_p Plasma Frequency [Hz]

Acronyms / Abbreviations

CFD Computational Fluid Dynamics

EM Electromagnetic

FDTD Finite Difference Time Domain method

PDE Partial Differential Equations

PEC Perfectly Electric Conducting material

PTFE Polytetrafluoroethylene material

RCS Radar Cross Section

Nomenclature

RF Radio Frequency

RX Receiver / Reception

TX Transmitter / Transmission

VB(A) Visual Basic (for Applications)

Chapter 1

Introduction

1.1 Introduction description and desired achievements

Last century has signed the development of aerospace and now plenty of flying vehicles may overcome the sound barrier. Hypersonic vehicles are those that reach a flight speed higher than Mach 5 ¹.

$$1 [Ma] \approx 330 [m/s] \quad (\text{speed of sound in air})$$

Nowadays hypersonic crafts are implemented in many circumstances such as: re-entry vehicles from the space, missiles and military aircrafts. Those instances are subjects of interest for RF research, because radio communication has a huge role in aerospace, mainly for either communication and radar detection, and the atmosphere impacts hardly on EM wave propagation whenever certain flight rates are reached.

In the following chapters it will be explained how the impact with atmosphere generates a plasma around the hypersonic vehicle and how this behaviour may be implemented in RF simulation setup.

Thesis work aims to study RCS response to hypersonic vehicles enveloped by a dispersive and dissipative media called plasma. The shock-wave in front of the

¹The Mach number makes a relation between flight speed and sound speed, where 1 Ma corresponds to sound speed as shown in equation (speed of sound in air).

Introduction

hypersonic vehicle heats up, dissociates and ionises the surrounding atmosphere creating a mixture of partially ionised gases (plasma). For unmagnetised plasmas, the Drude model links plasma parameters such as the electron number density to the dielectric properties of the media ϵ_r . The plasma parameters may be spatially inhomogeneous and thus is the electrical permittivity.

For sufficiently high plasma density the cut-off phenomenon occurs where the local refractive index (and ϵ_r) goes to zero and the EM wave cannot further propagate. The cut-off regions are of particular interest to this study because they strongly influence the RCS. In realistic conditions with complex vehicles geometry, the RCS is computed using numerical code also in vacuum. Many commercial codes (and different algorithm) are available for this task but only very few implements the Drude model necessary for simulation with plasma media.

One of them is CST Microwave Studio by Dassault System. CST features a Finite Difference Time Domain solver with the possibility to consider dispersive media as for the Drude model. A major aim of this thesis is to explore the applicability of CST to the RCS problem of hypersonic object surrounded by a plasma. We initially use simple analytic plasma model with spherical symmetry where semi-analytic RCS solutions exist and compare with CST results.

In real-life conditions, complex Computational Fluid Dynamic (CFD) models are typically used to simulate the hypersonic plasma creation and dynamics. The CFD results are not computed in this thesis but instead are taken as input to build the EM wave propagation media. A few example of RCS with complex hypersonic plasma are given at the end of this thesis and, where possible, compared to already published results.

All results are part of an intership at **LINKS Foundation** company, that provided support as workstation access, together with LACE team collaborations, in continuous contact together with the professor supervisor.

Chapter 2

EM wave propagation, RCS and plasmas

Theory references for wave propagation might be applied properly to physics. This chapter briefly reviews essential elements of electromagnetic wave propagation, the Drude model applied to plasma-like media e semi-analytic solution to the Maxwell's equations extensively used in this thesis such as the Mie series.

Realistic plasma distributions are obtained through CFD software, that derives physical distribution of ions and chemical compounds. Through these parameters is possible to extract physical quantities of interest, that will be implemented in Drude model: plasma frequency and collision frequency. Through selected model those quantities generate equivalent complex permittivity distributed in space and varying with the respect of frequency. In some critical area permittivity may be hardly negative: later on it will be shown how negative permittivities may lead to convergence issues in semi-analytic Mie Solution and moreover in FDTD based simulations.

Once extracted plasma frequency and collision frequency is possible to import them on CST microwave studio through a space mapped implementation. The way in which this map has to be defined has strict conditions for homogeneous grid, but plasma distribution is defined in an irregular grid distribution.

2.1 Propagation Theory

RF wave propagation is related to Maxwell's Equations. Whenever a reduction may help it has to be applied and in this case is not much important how hypersonic vehicles reacts to different kind of sources, but rather how plasma may generate cut-off phenomena along frequency domain.

There are two way to represent time-varying vectors: the time-varying one is represented as a cursive character \mathcal{A} , while the instantaneous one related to working frequency $f = 2\pi\omega$ is represented as a bold letter \mathbf{A} for complex amplitude. Following equation explains their relationship from equation (1.10) of [5] page 8:

$$\mathcal{A}(r,t) = \Re[\mathbf{A}(r) \cdot e^{j\omega t}] \quad (2.1)$$

Vectors are represented as underlined letter \underline{A} .

In this section definitions, procedures and equations are implemented from [5] chapter 1 and [6] chapter 7 for subsections: 2.1.1, 2.1.2, 2.1.3, 2.1.4 and 2.1.5, while citation from [7] are implemented in 2.1.6.

2.1.1 Maxwell's Equations

Maxwell's Equations are fundamentals for EM propagation and they describe behaviour of electric field and magnetic field both in static and dynamic conditions. Below they are reported as differential definition:

$$\begin{cases} \nabla \cdot \mathcal{D}(r,t) = \rho_v \\ \nabla \cdot \mathcal{B}(r,t) = 0 \\ \nabla \times \mathcal{E}(r,t) = -\frac{\partial \mathcal{B}(r,t)}{\partial t} \\ \nabla \times \mathcal{H}(r,t) = \frac{\partial \mathcal{D}(r,t)}{\partial t} + \mathcal{J} \end{cases} \quad (2.2)$$

2.1 Propagation Theory

and in complex amplitude form, assumed as time harmonic dependence $e^{j\omega t}$, becomes:

$$\begin{cases} \nabla \cdot \mathbf{D}(r) = \rho_v \\ \nabla \cdot \mathbf{B}(r) = 0 \\ \nabla \times \mathbf{E}(r) = -j\omega \mathbf{B}(r) \\ \nabla \times \mathbf{H}(r) = j\omega \mathbf{D}(r) + \mathbf{J} \end{cases} \quad (2.3)$$

where r is space dependence. Fields are supposed to be time harmonic dependent, therefore physical quantities of interest are reported:

Table 2.1 EM basic physics inspired by [5] page 6-7

\mathbf{E}	electric field intensity $[V/m]$
\mathbf{H}	magnetic field intensity $[A/m]$
$\mathbf{D} = \varepsilon \cdot \mathbf{E}$	electric flux density $[C/m^2]$
$\mathbf{B} = \mu \cdot \mathbf{H}$	magnetic flux density $[Wb/m^2 = T]$
$\mathbf{J} = \sigma \mathbf{E}$	electric current density $[A/m^2]$
ρ	electric charge density $[C/m^3]$
σ	electric conductivity $[S/m]$
ε	electric permittivity $[F/m]$
μ	magnetic permeability $[H/m]$

these are the base physical quantities for electromagnetism. ε and μ are defined in coming subsection 2.1.2.

2.1.2 Permittivity and Permeability

For EM simulations in different mediums other key parameters are the following:

$$\begin{aligned} \varepsilon &= \varepsilon_0 \cdot \varepsilon_r \\ \mu &= \mu_0 \cdot \mu_r \end{aligned} \quad (2.4)$$

EM wave propagation, RCS and plasmas

ϵ_0 ¹ is a constant related to vacuum permittivity and μ_0 ² is the corresponding vacuum constant for permeability, while ϵ_r and μ_r are relative coefficients that change together with material. In particular for the thesis being plasma unmagnetized the permittivity will be a variable in space and in frequency, while permeability is set as a constant vacuum condition, so $\mu_r = 1$.

Those quantities may be defined in a complex way, due to phasor domain and losses, so being unmagnetized case analysis let's focus on complex permittivity:

$$\epsilon = \epsilon' - j\epsilon'' = \epsilon_0 \cdot (\epsilon'_r - j\epsilon''_r) \quad (2.5)$$

in this case definition is assumed as:

$$\epsilon' = \epsilon_0 \cdot \epsilon'_r \quad (2.6)$$

$$\epsilon'' = \frac{\sigma}{\omega} = \epsilon_0 \cdot \epsilon''_r \quad (2.7)$$

if imaginary part is negligible or avoided because medium is lossless then permittivity belongs to $\epsilon_r = \epsilon'_r$ in equation (2.4).

2.1.3 Wave Equation

EM propagation is a wave behaviour, so it may be defined through Helmholtz equation, a wave equation derived from Maxwell's equations (2.3) implemented for solutions of complex amplitude time harmonic dependent propagations:

$$\begin{cases} \nabla^2 \mathbf{E} + k^2 \mathbf{E} = 0 \\ \nabla^2 \mathbf{H} + k^2 \mathbf{H} = 0 \end{cases} \quad (2.8)$$

with propagation constant in lossless medium reduced to wave number k :

$$k = \omega \sqrt{\mu \epsilon} \quad [1/m] \quad (2.9)$$

¹ $\epsilon_0 \simeq 8.854 \cdot 10^{-12} [F/m]$

² $\mu_0 = 4\pi \cdot 10^{-7} \simeq 1.257 \cdot 10^{-6} [H/m]$

2.1 Propagation Theory

parameter	symbol	expression
wave number	k	$\omega\sqrt{\epsilon\mu}$
wavelength	λ	$\frac{c}{f} \cdot \frac{1}{\sqrt{\mu_r \cdot \epsilon_r}}$
electric field component	$E_{0_z}(z)$	$E_{0_z}^+ e^{-jk \cdot x} + E_{0_z}^- e^{jk \cdot x}$
magnetic field component	$H_{0_y}(z)$	$-j \frac{k}{\omega \cdot \mu} [E_{0_z}(x)]$
incident wave	$A_0^+(z)$	boundary condition terms
reflected wave	$A_0^-(z)$	

Table 2.2 Plane Wave formulas for linear polarization with propagation constant along \hat{x} , E along \hat{z} and H along \hat{y} as similarly proposed in [5] chapter 1 section 4

The wave propagates along a direction \hat{n} and field components are perpendicular to this direction, as shown in figure 2.1. For sake of simplicity medium may be considered lossless in this chapter.

2.1.4 Plane Wave

Plane Wave in lossless medium, as simplest case analysis, is the solution of wave equation (2.8). Moreover for sake of simplicity, as proposed by [5] chapter 1 section 4, propagation direction is put along only one axis, in this case \hat{x} , so field component would be on another perpendicular axis, for instance \hat{z} , and for magnetic component will remain \hat{y} axis. This is a linear polarized propagation of EM wave.

Below in Figure 2.1 the case explained as instance is plotted. Each plane represent front of the propagated wave with same phase. Table 2.2 shows main quantities and equations for simplified case reported.

In general a field may have components along all three-dimensional axis:

$$\mathbf{E}_0 = E_{0_x} \cdot \hat{x} + E_{0_y} \cdot \hat{y} + E_{0_z} \cdot \hat{z} \quad (2.10)$$

where \underline{E}_0 is the field in the origin axis, and space variation belongs to \underline{r} as follows:

$$\underline{r} = x \cdot \hat{x} + y \cdot \hat{y} + z \cdot \hat{z} \quad (2.11)$$

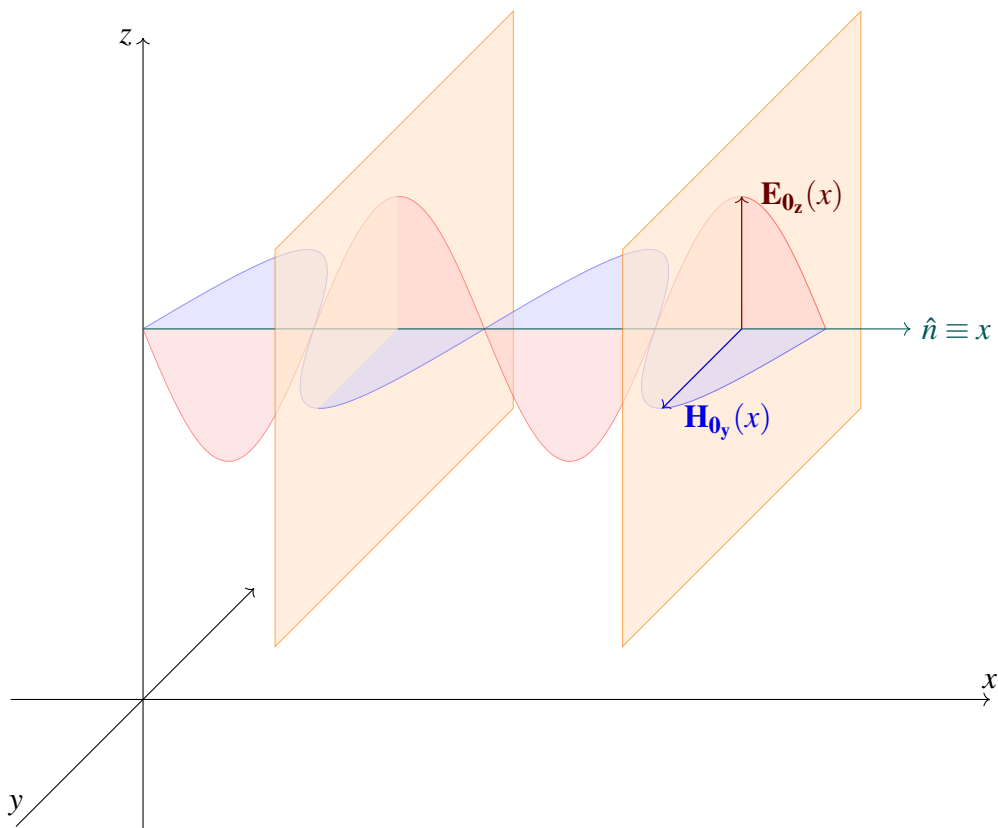


Fig. 2.1 Plane Wave with linear polarization propagating in space, inspired by figure 7-5 [6] page 319

2.1 Propagation Theory

So the general equation for a plane wave with only progressive propagation will be seen as:

$$\mathbf{E} = \mathbf{E}_0 e^{-j\mathbf{k}\cdot\mathbf{r}} \quad (2.12)$$

and wave number, along propagation direction \hat{n} is defined in three components:

$$\underline{k} = k_x \cdot \hat{x} + k_y \cdot \hat{y} + k_z \cdot \hat{z} = k_0 \cdot \hat{n} \quad (2.13)$$

A plane wave is a useful condition that study propagation effects, and may be considered also an approximation of real propagations such as antenna, radar, spherical waves but at long distances from the source.

In our simulations plane wave will have linear polarization and along a single axis.

2.1.5 Radar Cross Section

In this subsection equations and definitions are extracted from [7] page 8-9 and [6], chapter 10 section 6.

Any field is affected by reflection, refraction and diffraction phenomena whenever different permittivities are encountered. Altogether the EM field is "scattered" in space giving rise to the concept of radar cross-section (RCS) that is related to the scattered field as defined in equation (2.1-5) page 9 of [7]:

$$\sigma = 4\pi \lim_{r \rightarrow +\infty} r^2 \frac{(\mathbf{E}_{\text{scattered}} \cdot \mathbf{E}_{\text{scattered}}^*)}{(\mathbf{E}_{\text{incident}} \cdot \mathbf{E}_{\text{incident}}^*)} \quad [m^2] \quad (2.14)$$

Where $\mathbf{E}_{\text{scattered}}$ "is the scattered electric field and" $\mathbf{E}_{\text{incident}}$ "is the incident field" as defined in [7] page 8. Moreover in page 9 of [7], together with equation (2.1-4), "scattered field is defined as the difference between total field (with target present) and incident field (the total field that would exist if there is no target present)":

$$\mathbf{E}_{\text{scattered}} = \mathbf{E}_{\text{total}} - \mathbf{E}_{\text{incident}} \quad (2.15)$$

In our simulations transmitted signal is simplified as a plane wave, then scattering field is measured on a receiver. If TX and RX are in the same space point as shown in figure 2.2, angle variation in RCS plot is called *monostatic*, therefore if the transmitter

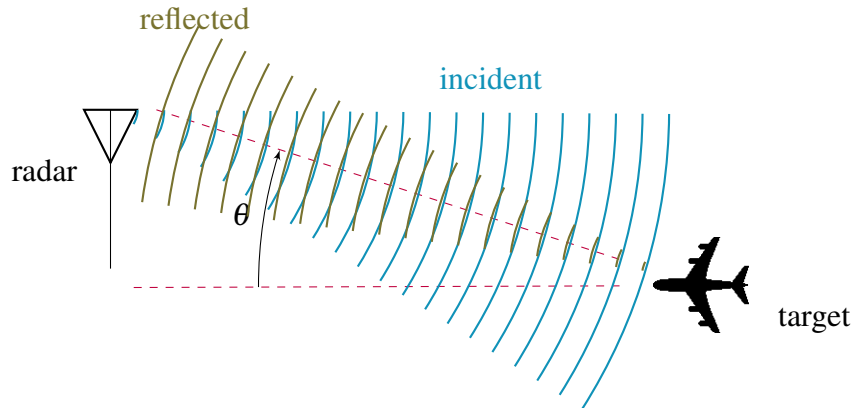


Fig. 2.2 Simple scheme of a monostatic radar, inspired by figure 10-14 [6] page 468

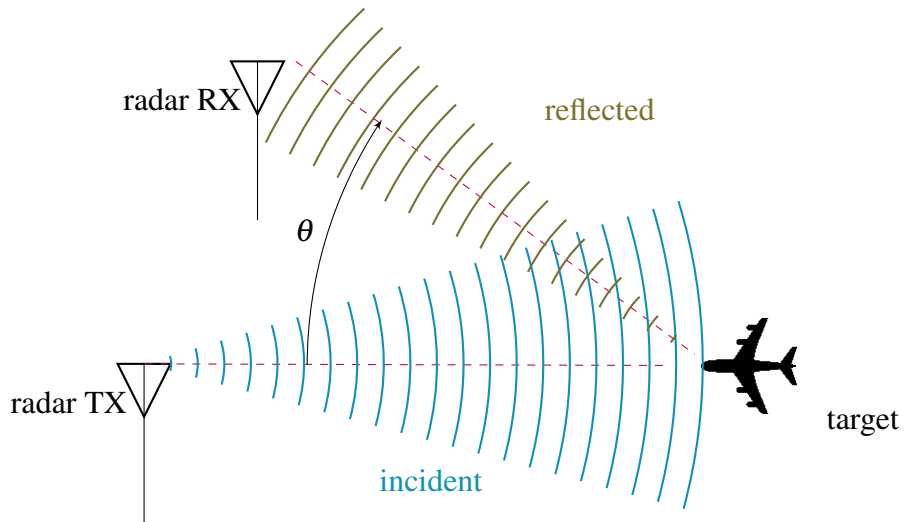


Fig. 2.3 Simple scheme of a bistatic radar, inspired by figure 10-14 [6] page 468

is fixed in space and receiver angle vary as shown in figure 2.3, RCS plot angle is called *bistatic*.

2.1.5.1 CST simulation

In our simulations evaluated plot are RCS with bistatic angle and they are expressed as dBm^2 , decibel square meter³: σ is evaluated by the solver as declared in CST microwave studio guide in this way⁴:

$$^3 1 [dBsm] = 10 \cdot \log_{10} \left(\frac{RCS_{in} [m^2]}{1 [m^2]} \right)$$

⁴from [8] Home | 3D Simulation | Post-Processing | Post-Processing Results | Farfield Calculation Overview

$$RCS(\theta, \phi) = 4\pi \cdot \frac{\text{power radiated per unit solid angle}}{\text{irradiance due to incoming plane wave}} \quad [dBm^2]$$

that belongs similarly as in equation (2.14).

2.1.6 Mie Series

Simplest geometry of analysis for dispersive model analyzed in following section 2.2.1 is sphere, due to its symmetry. Following definitions are extracted from [7], chapter 3.

The solution for scattering from a sphere is attributed to Mie Series, or more in general without a defined maximum number of mode to Mie Solution. These semi-analytic solutions evaluate scattering through geometrical simplification, such as given by spherical and cylindric coordinate systems. A convention has to be established as mentioned in [7] chapter 3.1 in following way:

- Source is an incident plane wave (propagation constant is along $-\hat{z}$)
- Evaluation on phasors (harmonic time dependence)
- Linear polarization of incident field (along \hat{x} direction)
- Observation point put outside of the defined permittivity varying sphere, and this point is defined as $P(\theta, \phi)$

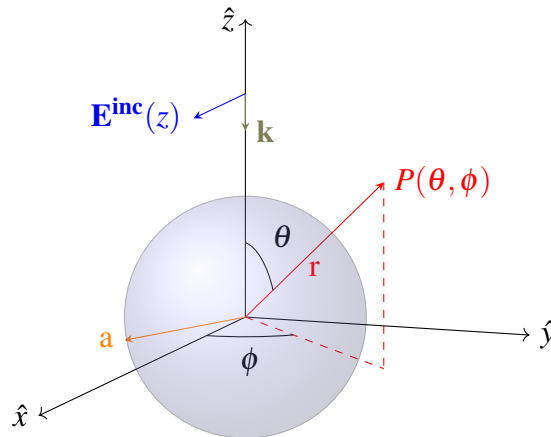


Fig. 2.4 Mie Series implementation in Spherical Coordinates, from figure 3.1 of [7] page 141

So from table 2.2 but with corresponding direction of this subsection:

$$\begin{aligned}\mathbf{E}^{inc}(z) &= E_0 \hat{x} e^{-jk \cdot z} \\ \mathbf{H}^{inc}(z) &= -\sqrt{\frac{\epsilon_0}{\mu_0}} E_0 \hat{y} e^{-jk \cdot z}\end{aligned}\quad (2.16)$$

in this case is considered only incident field. General solution for Mie Series is provided as:

$$\begin{aligned}\mathbf{E}(P, \omega) &= \sum_{n=1}^{\infty} (A_n \cdot \mathbf{M}_{\mathbf{o1n}}(P) + B_n \cdot \mathbf{N}_{\mathbf{e1n}}(P)) \\ \mathbf{H}(P, \omega) &= -j \sqrt{\frac{\epsilon_0}{\mu_0}} E_0 \sum_{n=1}^{\infty} (B_n \cdot \mathbf{M}_{\mathbf{e1n}}(P) + A_n \cdot \mathbf{N}_{\mathbf{o1n}}(P))\end{aligned}\quad (2.17)$$

where $\mathbf{N}_{\mathbf{e-o1n}}$ and $\mathbf{M}_{\mathbf{e-o1n}}$ are functions of spherical wave for each P position, while A_n and B_n are constant and they are related to property of the sphere, in this case permittivity distribution along radius.

In [7] are provided equations for the evaluations of each coefficient and component, through spherical Bessel and Hankel functions, and they are provided in the script implemented in MATLAB from [9] for RCS semi-analytic evaluation.

In coding a key parameter is maximum mode number related to Bessel and Hankel functions, that should be as higher as possible. A trade off between frequency and maximum mode number has to be done: for higher frequencies lower mode number has to be reached. This limit is due to computation constraints.

The ratio between geometry dimension and vacuum wavelength a/λ_0 defines the scattering regime as reported in figure 2.5

For a spherically symmetric geometry the physical parameter that follows scattering regime is defined in equation:

$$k_0 \cdot a = \frac{2\pi}{\lambda_0} \cdot a = \frac{2\pi f}{c} \cdot a \quad (2.18)$$

where a is the sphere radius as shown in figure 2.4 and k_0 is the propagation constant in vacuum as defined in equation (1.29b) of [6] page 25, related to vacuum wavelength λ_0 .

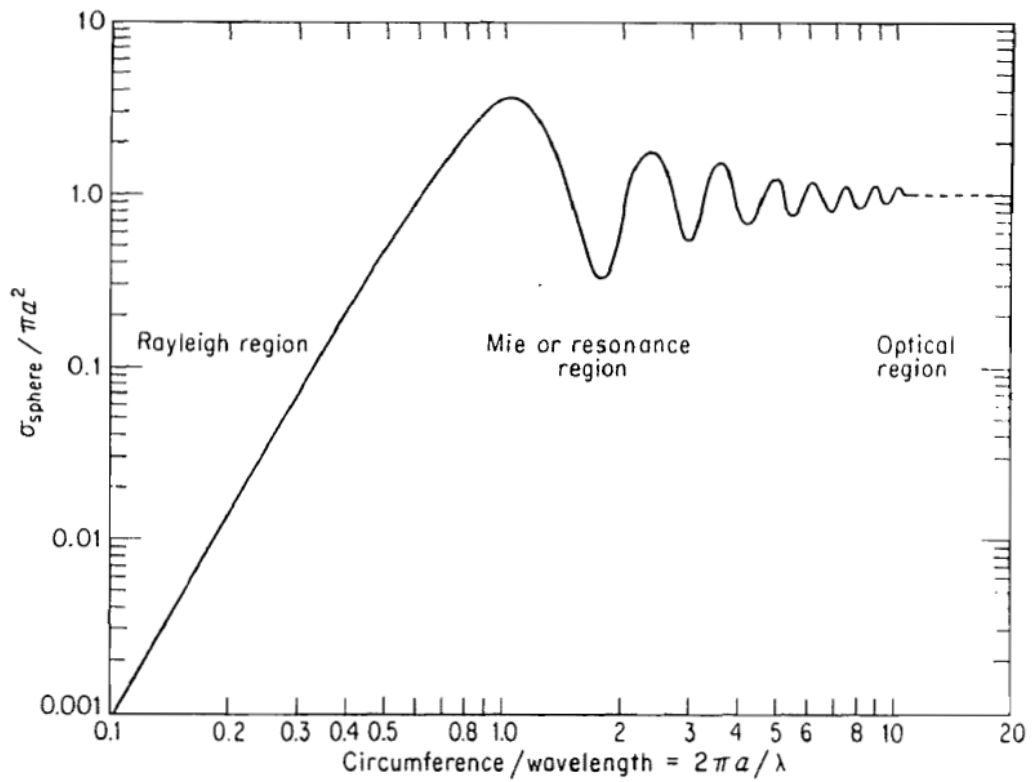


Fig. 2.5 Scattering regime regions with the respect of a/λ_0 physical parameter from figure 2.9 in [2] page 34

2.2 Plasma Physics

Hypersonic vehicles generate plasma due to collision with surrounding air. Heating produces ions and neutrals distributed in space in relation with thermofluid-dynamics theory. In this case EM propagation medium should be considered a dispersive model due to electric charges, so complex permittivity ϵ is defined in space, while plasma is considered unmagnetized with $\mu_r = 1$ as already told. Each physical quantity in space is provided from a CFD software simulation.

2.2.1 Drude Model

Drude model may be implemented for unmagnetized cold plasmas, leading to evaluation of complex permittivity in space. From [10] page 44, and in [3] equation (6) where dispersion Drude model has been implemented:

$$\epsilon_r(\omega) = \epsilon_\infty - \frac{\omega_p^2}{\omega(\omega - j\nu_c)} \quad (2.19)$$

where ϵ_∞ is the default value of medium, in this case considered as vacuum with $\epsilon_\infty = 1$, ω_p [rad/s] as plasma radial frequency and ν_c [1/s] as collision frequency. Those quantities are extracted from CFD or given by simple analytic formulas implemented in CST microwave studio for EM propagation simulation. Moreover plasma radial frequency is extracted and might be converted in hertz for plots as follows:

$$\omega_p = \sqrt{\frac{n_e \cdot e^2}{\epsilon_0 \cdot m_e}} \quad [\text{rad/s}] \quad (2.20)$$

Equation (2.20) from [11] equation (10) pag 685 and from equation (2) in [3].

$$f_p = 2\pi\omega_p \quad [\text{Hz}] \quad (2.21)$$

quantities are described in table 2.3, where n_e is provided from CFD as a mapped parameter and ϵ_0 is the constant vacuum permittivity as already mentioned in subsection 2.1.2.

parameter	symbol	value	unit
electron density	n_e	mapped	$[1/m^3]$
constant electron charge	e	$\simeq 1.6 \cdot 10^{-19}$	$[C]$
constant electron mass	m_e	$\simeq 9.11 \cdot 10^{-31}$	$[kg]$

Table 2.3 Physical quantities for Plasma Frequency as explained in [3] section III.A

A first approximation mostly adopted is a negligible v_c , as reported in equation (9) page 685 of [11], reducing equation (2.19) in:

$$\varepsilon_r(\omega) = \varepsilon_\infty - \left(\frac{\omega_p}{\omega}\right)^2 \quad (2.22)$$

Material corresponding quantities for plasma frequency and collision frequency at a fixed working frequency and given permittivity may be extracted from equation (2.19) with two equation systems defined through real and imaginary part component system equations:

$$\begin{cases} \varepsilon'_r = \Re\text{al}[\varepsilon_r(\omega)] = \varepsilon_\infty - \frac{\omega_p^2}{\omega^2 + v_c^2} \\ \varepsilon''_r = -\Im\text{ag}[\varepsilon_r(\omega)] = \frac{\omega_p^2 \cdot v_c}{\omega \cdot (\omega^2 + v_c^2)} \end{cases} \quad (2.23)$$

possible solution is obtained making negligible v_c for real component ε'_r equation, then obtained plasma frequency ω_p generates corresponding collision frequency from imaginary component equation.

Equation (2.23) for only real relative permittivity is shown below:

$$\varepsilon'_r = \varepsilon_\infty - \frac{\omega_p^2}{\omega^2 + v_c^2} \quad (2.24)$$

In plasmas with sufficiently high electron density the plasma frequency may equate or overcome the wave EM frequency and lead to zero or negative real permittivity. In the limit where $v_c = 0$, the frequency $\omega = \omega_p$ is called cut-off frequency. Furthermore, as ω_p increases with fixed ω and v_c , ε'_r will decrease towards negative values:

$$\lim_{\omega_p \rightarrow +\infty} \varepsilon'_r = -\infty \quad (2.25)$$

The cut-off frequency as a consequence may reflect propagating wave toward the source, leading to an higher back-scattering value. This may lead to a convergence issue because back-scattering is the point for monostatic scattering in which propagating and reflected waves are concentrating, making the computation by the solver more difficult to be managed.

2.2.2 Computational Fluid Dynamics simulation provided quantities

For each model analysed the quantities of interest are provided from a CFD evaluation. The simplest model for plasma generated by shocking wave is a sphere, in particular this section refers to the sphere from [3]: a PTFE ($\epsilon_r = 2.1$) sphere of 150 mm diameter with a shell of 5 mm and Mach 10 in atmosphere. Being the model a sphere the plot has symmetries, and plots are cut at the center of the sphere. CFD simulation are reproduced by a PhD student as cited in [1] and reported results are coming from a provided *csv* file as follows:

Label	NO+ nd	E nd	Temperature	X	Y	Z
Descript.	nitrosonium density	electron density	heat	coordinates		
Unit	[1/m ³]		kelvin	meter		

Table 2.4 Format of CFD file for sphere described

From this file data are extracted and evaluated: following figures are reported as inspired by figure 2 in [3], starting from figure 2.6 that shows temperature plot distribution:

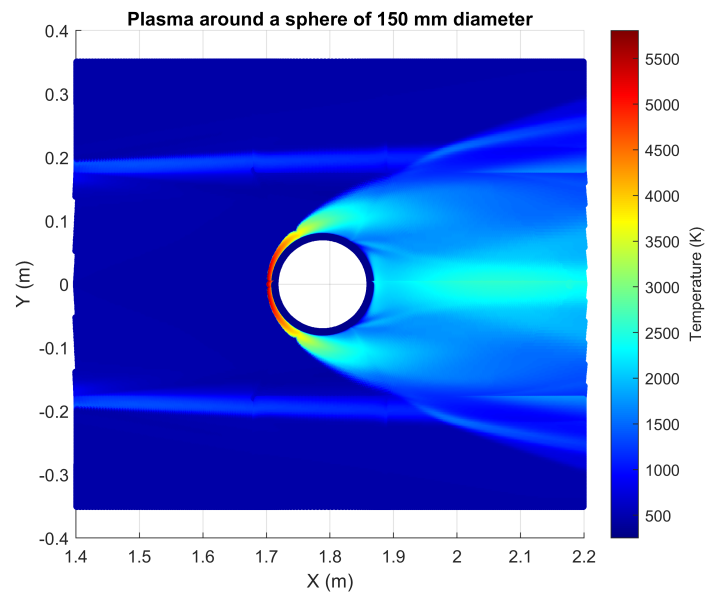


Fig. 2.6 CFD reproduce by [1] - temperature around 150 mm diameter PTFE sphere as primarily proposed in [3] paper - inspired by figure 2 in [3]

highest temperatures are reached on impact region, that is on the left side. Electron density distribution is given as well and is shown in figure 2.7:

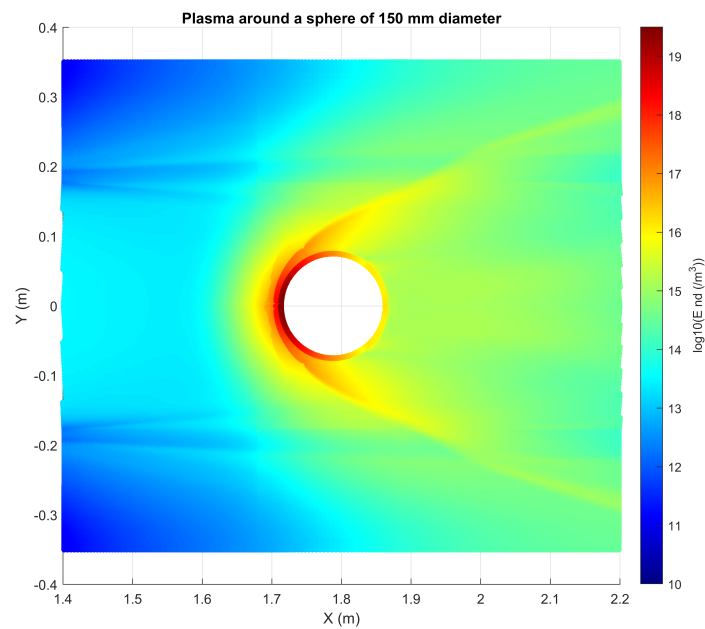


Fig. 2.7 CFD reproduce by [1] - ions around 150 mm diameter PTFE sphere as primarily proposed in [3] paper - inspired by figure 2 in [3]

EM wave propagation, RCS and plasmas

highest densities are concentrated similarly to highest temperatures. From these quantities is possible to extract Plasma Frequency from equation (2.20) and to express it in GHz through relation equation (2.21).

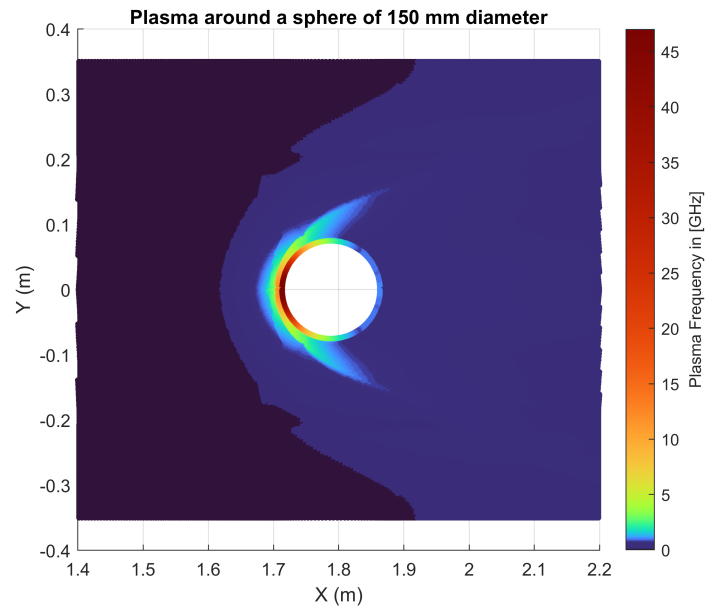


Fig. 2.8 CFD reproduce by [1] - Plasma Frequency in GHz around 150 mm diameter PTFE sphere as primarily proposed in [3] paper - inspired by figure 2 in [3]

From plasma frequency is possible to extract corresponding permittivity for each working frequency from equation (2.22), as a first approximation without collision frequency ν_c . As instance $f = 3GHz$, but $\omega = \frac{f}{2\pi}$ is implemented.

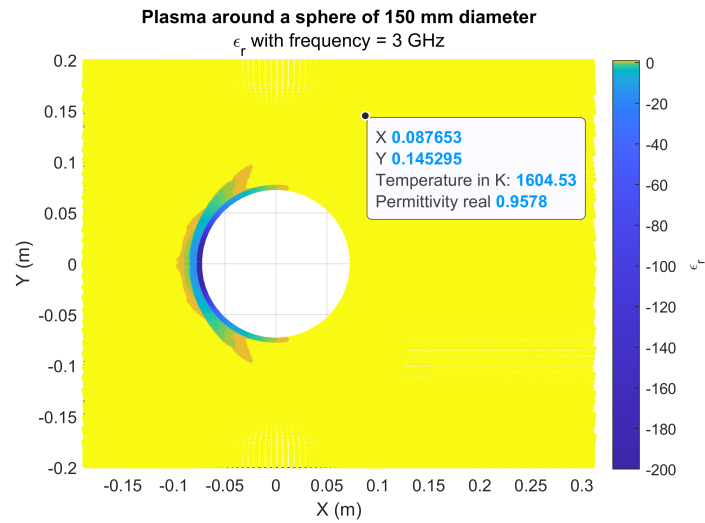


Fig. 2.9 CFD reproduce by [1] - ϵ_r around 150 mm diameter sphere primarily proposed in [3] - inspired by figure 2 in [3]

on impact region it shows that permittivity may become negative at certain frequencies, generating a cut-off condition, with very high absolute values with the respect of permittivities from vacuum and positive sign. We will see later on this thesis that this might generate convergence issues in RCS evaluation in both semi-analytic Mie Solution and FDTD based solver.

Chapter 3

CST code and its application to plasmas

This chapter describe the basic feature of the CST solver algorithms used in this thesis and the non-conventional way we operated the code via Visual Basic and Matlab scripting. CST microwave studio by Dassault Systèmes, a widely spread software for research and commercial purposes in EM propagation evaluations.

The solver mostly adopted in CST will be the time domain one, because it is the only one that implements the Drude model. It is possible to define directly the desired geometries or to import them from files. This software aims to be as much as possible user friendly, but for plasma frequency mapped implementation is required a scripting through VBA. Visual Basic is a language implemented in many commercial software on Windows Operating Systems, in order to create and compute directly from scripts any possible implementation.

3.1 Solver

In CST microwave studio there are different solvers, in particular there are reported from guide [8] the solvers that are implemented in High Frequency Simulation for thesis purposes:

- Time Domain Solver

- Integral Equation Solver

Time Domain Solver is the main solver implemented in our simulations. As told in [8] it works with Finite Domains, so space is mapped in grids, defined in mesh section. Time domain solver mainly adopts Finite Integration Technique, a discretization method that implements integral form of Maxwell Equations instead of differential one as defined in subsection 2.1.1, leading to a much performing solver for curved structures.¹ FDTD approach as a simpler model of this solver can be studied in cartesian coordinates system.

In this section focus is on FDTD solver; then equations, procedures and definitions are extracted from [10] chapter 8.

3.1.1 Differencing formulas

Maxwell's Equations (2.2) are partial differential equations and they require boundary conditions. The Finite Method aims to make these PDEs available at computational level, transforming them into an algebraic form. This approach requires discretization, so it is necessary to subdivide volume in microregions.

The first simplification is made on derivative operator that is defined in approximation form as a little increasing, called *forward differencing*:

$$f'(x) \approx \frac{f(x + \Delta x) - f(x)}{\Delta x} \quad (3.1)$$

or as a little decreasing, called *backward differencing*:

$$f'(x) \approx \frac{f(x) - f(x - \Delta x)}{\Delta x} \quad (3.2)$$

a third way of definition is an average between equation (3.1) and (3.2):

$$f'(x) \approx \frac{f(x + \Delta x) - f(x - \Delta x)}{2\Delta x} \quad (3.3)$$

In figure 3.1 there is an instance of the derivative approximated on a curve, and the figure shows how close are the points with the respect of the derivative straight line.

¹from [8] - 3D simulation - Solvers - High Frequency - Time Domain Solver - Time Domain solver overview.

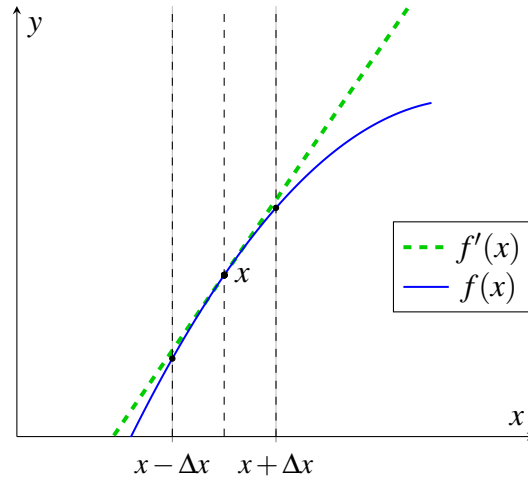


Fig. 3.1 Curve and its derivative, from figure 8.1 of [10] page 386

Being an approximation, accuracy is a parameter that increases as resolution increases, therefore as Δx spacing decreases. Taylor's expansion may be implemented, but up to now the focus is on a simple discretized differential operator based on *central differencing formula* (3.3).

3.1.2 Time Domain Finite Difference method

3.1.2.1 Linear discretization

As a simpler case is considered the solution for Wave Equation (2.8) with real propagation constant and time dependent form, so rewritten as [10] page 389 with time-varying equations:

$$\nabla \times \nabla \times \mathcal{E} + \mu \varepsilon \frac{\partial^2 \mathcal{E}}{\partial t^2} + \mu \frac{\partial \mathcal{J}_i}{\partial t} = 0 \quad (3.4)$$

Considering field hold on axis \hat{z} and varying only along direction axis \hat{x} then it comes:

$$\frac{\partial^2 \mathcal{E}_z}{\partial x^2} - \mu \varepsilon \frac{\partial^2 \mathcal{E}_z}{\partial t^2} = \mu \frac{\mathcal{J}_z^i}{\partial t} \quad (3.5)$$

This solution is solved in one dimension discretization, subdividing x axis domain in N interval of spacing Δx , as shown in figure 3.2, so $x = i\Delta x$ with $i = 0, 1, \dots, N$. Discretization is done also on time variable that becomes $t = 0, 1, \dots, M$ with spacing

Δt between time instants, so $t = m\Delta t$. Adopted notation is from [10] page 388:

$$\mathcal{E}_z(x, t) = \mathcal{E}_z(i\Delta x, m\Delta t) = \mathcal{E}_z^m(i) \quad (3.6)$$

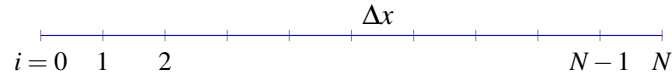


Fig. 3.2 Linear discretization in one dimension, from figure 8.2 of [10] page 388

This wave equation is also named *hyperbolic partial differential equation* and it is solved through Finit Element Method in discretized intervals, adopting central differencing formula (3.3), then equation becomes as expressed in [10] page 389 (8.2.12):

$$\frac{\mathcal{E}_z^m(i+1) - 2\mathcal{E}_z^m(i) + \mathcal{E}_z^m(i-1)}{(\Delta x)^2} - \mu\epsilon \frac{\mathcal{E}_z^{m+1}(i) - 2\mathcal{E}_z^m(i) + \mathcal{E}_z^{m-1}(i)}{(\Delta t)^2} = \mu \frac{\mathcal{J}_z^{m+1}(i) - \mathcal{J}_z^{m-1}(i)}{2\Delta t} \quad (3.7)$$

this formula could be computed with initial boundary conditions: sources value, and initial field value. Also the initial values for time variation is required, for instant $m = 0$ and also $m = 1$, because there is the second derivative in time. \mathcal{J}_i is an additional source from (3.8).

3.1.2.2 Three-Dimensional Discretization

One dimension discretization is the simplest case for analysis, but for EM wave propagation three-dimensional discretization is required. Yee's FDTD algorithm is based on finite differencing as described above in this subsection, but discontinuities between different layers and material occur. To overcome this problem Yee's algorithm adopts a discretization in three-dimensions, similarly as done previously on one dimension: figure 3.3a shows how a volume region, the one marked in blue, could be subdivided in many cells.

Solver adopted the last two Maxwell's Equation with time dependance (2.2) shown in equation (3.8) and extracts them into six scalar equations (three equations

varying independently on cartesian axis for each Maxwell's equation). Anyone who is interested in those equations may find them in subsection 8.4.2 of [10].

$$\begin{cases} \nabla \times \mathcal{E} = -\mu \frac{\partial \mathcal{H}}{\partial t} \\ \nabla \times \mathcal{H} = \epsilon \frac{\partial \mathcal{E}}{\partial t} + \sigma \mathcal{E} + \mathcal{J}_i \end{cases} \quad (3.8)$$

with \mathcal{J}_i as additional source with the respect of the equation seen in subsection 2.1.1.

As shown in figure 3.3b each cell has components of electric field at center of each edge and magnetic field at center of each face.

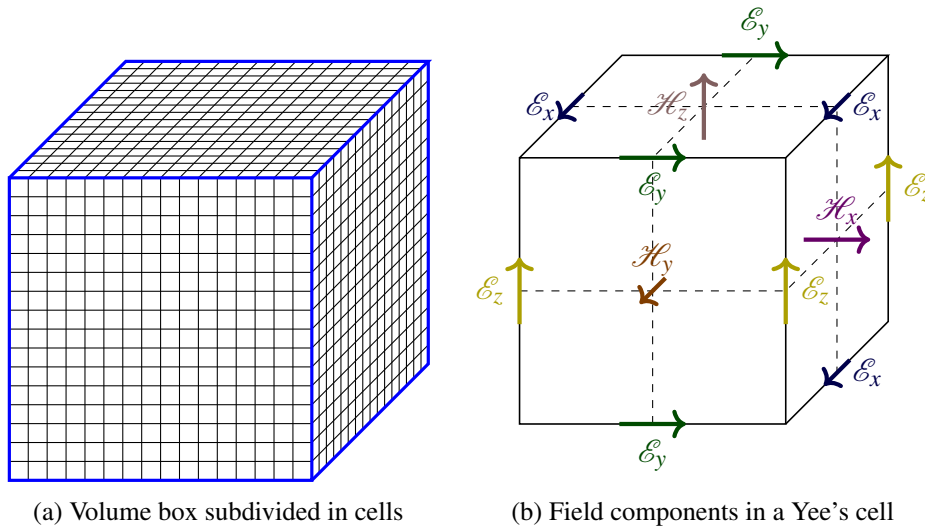


Fig. 3.3 Grid and Yee's cell from from figure 8.6 of [10] page 400

3.2 Geometry model implementation in CST

CST microwave studio is a commercial software with license. In previous section there is a general description of basis algorithm for EM scattering evaluation, but licensed software do not lay possibility to view and analyse all the entire process of computation. In this section there is a brief description of the interfaces implemented on thesis for simulations.

3.2.1 Geometry Definition

In CST the main way in which geometry is defined is through user friendly windows, and possible geometries might be: spheres, cylinders, parallelepipeds, so on and so forth. This software allows to generate any kind of geometry through instructions from [8] for basic geometries definition and their transformations. Any transformation in scale, rotation, translation may be done. Even shelling and extrusions might be applied. CST microwave studio works as well with CAD models imported and exported. In figure 3.4 is reported as instance the window dialogue for PEC (perfectly electric conductor) sphere by 1 as radius (in corresponding unit project) and centered in cartesian coordinates system.

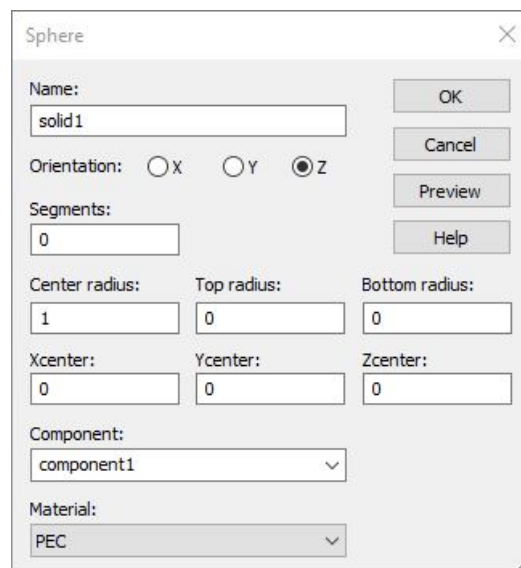


Fig. 3.4 CST window for sphere model generation

Flexibility through Visual Basic coding is provided for complex geometries and space mapping for material. A built-in application allows direct coding in CST environment, but even external interactions might be applied, for instance through MATLAB.²

²from [8] - Automation and Scripting - VBA Overview

3.2.1.1 VBA

Visual Basic for Applications is an object-oriented scripting language³, so external applications may communicate to CST through Visual Basic procedure defined in CST guide. An external function for MATLAB might be implemented: the ones in this thesis may be executed through source code cited in [12] that translates scripts from MATLAB to VBA and communicates directly with CST microwave studio software.

This automation allows scripting for complex geometries and it is required to import space mapped material. VB scripts manage software project in each step: unit definition, import/export, boundary conditions, parameters management, geometry and material definition, transformations, excitation and monitor definition, but even solver execution and file management. Below is reported as instance the corresponding code for sphere generation as done in window in figure 3.4. Plenty of commands may be done in whichever way it is desired.

```
With Sphere
    .Reset
    .Name "sphere_name"
    .Component "default"
    .Material "PEC"
    .Axis "z"
    .CenterRadius "1"
    .BottomRadius "0"
    .Center "0", "0", "0"
    .Segments "0"
    .Create
End With
```

`With` command is used in VB macros for multiple methods calling in same object and it leads to compact and readable scripts.

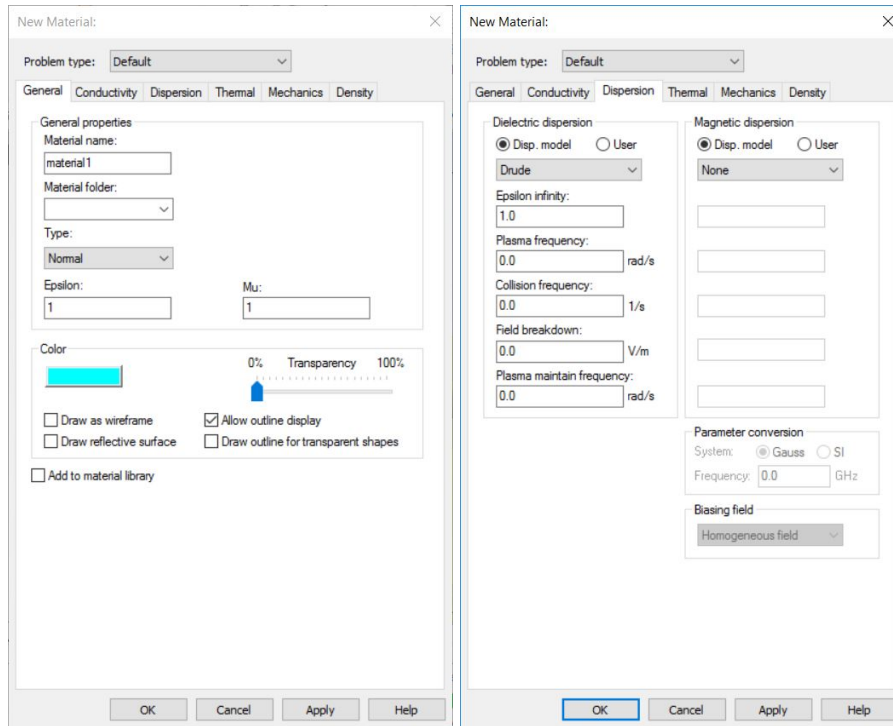
3.2.2 Material Definition

CST microwave studio defines a material for each solid. In material there are defined all possible physical components for material interaction in EM propagation. In previous chapter for unmagnetized plasma key elements were permittivity (subsection 2.1.2) and Drude model (subsection 2.2.1).

³description from CST guide - Automation and Scripting - VBA overview

3.2 Geometry model implementation in CST

Permittivity is the primary parameter implemented in CST and for plenty of materials there is a library with provided quantities. Dispersion material may be implemented such as Drude Model: CST allows as inputs plasma radiant frequency and collision frequency that in EM simulation are implemented in same way as defined in subsection 2.2.1.⁴



(a) General section

(b) Dispersion section

Fig. 3.5 CST window New Material definition

In figure 3.5a the window for material creation shows that general parameters are named *Epsilon* for relative permittivity ϵ_r and *Mu* for relative permeability μ_r . In dispersion section is possible to define Drude model parameters as shown in figure 3.5b. As previously explained with solid, those settings may be done through Visual Basic.

Relative imaginary permittivity component $\epsilon_r'' = \epsilon'' / \epsilon_0$ may be implemented in CST for permittivity material through σ conductivity component (described in table

⁴from [8] - 3D simulation - Creating and Visualizing Models - Material Overview (HF) - Dispersive Materials - Cold Plasma Materials

CST code and its application to plasmas

2.1) extracted from equation (2.7):

$$\sigma = \varepsilon'' \cdot \omega \quad [S/m] \quad (3.9)$$

being considered imaginary component from a relative permittivity, for CST implementation $\varepsilon'' = \varepsilon_r'' \cdot \varepsilon_0$.

$$\sigma = \varepsilon_r'' \cdot \varepsilon_0 \cdot \omega \quad [S/m] \quad (3.10)$$

3.2.2.1 Space Map

Material properties may change in space and CST accepts a cartesian property grid through Visual Basic scripting. For each desired quantity an input ASCII file has to be imported within possibilities given by CST guide. From [8] chosen file format is called *FourColumns*, shown in 3.1, where header is optional and for each coordinate x , y and z is possible to define their own unit. Last column is for mapped parameter.⁵

x [mm]	y [mm]	z [mm]	key parameter
x(1)	y(1)	z(1)	parameter(1)
x(2)	y(2)	z(2)	parameter(2)
...
x(i)	y(i)	z(i)	parameter(i)
...
x(N)	y(N)	z(N)	parameter(N)

Table 3.1 FourColumns Format for CST Space Map Material described in [8]

The key parameter, as explained in CST guide, may be "eps" for relative permittivity, "mu" for relative permeability and for chosen dispersion model as expressed in table 3.2, where *eps* at the end means that dispersion model is adopted for permittivity distribution:

⁵All procedure and tables and images of this paragraph explained from [8] - Automation and Scripting - Visual Basic (VBA) - 3D Simulation VBA - VBA Objects - Material - Space Map Based Materials

3.2 Geometry model implementation in CST

CST VB variable	corresponding physical quantity	unit
dispcoeff1eps	plasma radial frequency	[rad/s]
dispcoeff2eps	collision frequency	[1/s]

Table 3.2 VBA variables definition for Drude Model

Once generated the file with format reported in table 3.1, the script reported below has to be implemented, where for each dispersion parameter described in table 3.2 an ASCII file as input has to be created and then corresponding binary files have to be generated by CST itself.

In green there are comments for specific methods explained in CST guide and default values for imported coefficients are required. Once defined space mapped material is possible to define it in a brick solid.

```

With Material
    .Reset ' reset all methods in Material Object

    ''' DEFINE THE MODEL - in this case Drude dispersion model is required
    .DispModelEps "Drude" ' select the model
    .EpsInfinity "1" ' background value
    .DispCoeff1Eps "2e10" ' default value for plasma frequency
    .DispCoeff2Eps "2e7" ' default value for collision frequency

    ' this method converts input ASCII file into a binary file with extension .m3d
    ' once done the conversion this line could be commented and avoided for other scripts
    .ConvertMaterialField "file_path\file_plasma_frequency.txt", "w_p.m3d"

    ' this method defines which parameter is defined and that is 3D varying mapped
    .SpaceMapBasedOperator "dispcoeff1eps", "3DimportHex"

    ' this method executes from binary file the import in CST project
    .AddSpaceMapBasedMaterialStringParameter "dispcoeff1eps", "map_filename", "w_p.m3d"

    ' same procedure for collision frequency
    .ConvertMaterialField "file_path\file_collision_frequency.txt", "nu_c.m3d"
    .SpaceMapBasedOperator "dispcoeff2eps", "3DimportHex"
    .AddSpaceMapBasedMaterialStringParameter "dispcoeff2eps", "map_filename", "n_uc.m3d"

    .Name "Plasma_space_mapped" ' name of material
    .Colour "0.55", "0.45", "0.65" ' color
    .Transparency "50" ' transparency in percentage
    .Create ' this method creates the material with all above parameters
End With

```

3.2.3 CST simulation of dielectric shells in radial distribution

Sphere is a simple model of a target and RCS evaluation may be done also through Mie Solution as explained in subsection 2.1.6.

3.2.3.1 Inhomogeneous shells around PEC sphere

Plasmas might be generated with an inhomogeneous analytic profile defined on spherical geometries generated around a sphere target. Plasma shells might be defined in two possible ways for material definition:

- **Permittivity non dispersive model:** CST does not allow negative and zero permittivity. Each negative ϵ_r must be approximated to a very small quantity, as instance $\epsilon_r = 1 \cdot 10^{-3}$.
- **Drude dispersive model:** CST allows negative permittivities through dispersion model, in this case Drude model. ω_p may be implemented alone if there is an approximation with only real permittivity map, and v_c might be implemented as well. Their corresponding values are extracted from equation 2.23.

Geometry may be modelled in two possible ways:

- **CST solid-based geometry definition:** spheres directly defined in CST workspace and then shelled one inside the other. In figure 3.7a there is shown an example of CST CAD geometry with two shells around target PEC sphere.
- **Space Mapped Material:** material may be space mapped as described in 3.2.2.1, then a brick solid is generated and created space map based material is assigned to it. In figure 3.7b there is shown an example of space mapped brick around PEC sphere. Even in this case a shelling between defined brick for plasma and target might be done.

Each material with dispersive Drude model definition without space map may be verified on CST as shown in figure 3.6. CST geometry model implementation is done in automation through a MATLAB script as described in subsection 3.2.1.1:

1. A new project is created with assigned units and frequency range
2. All materials are created in CST with a desired profile described in MATLAB script reported as instance in Appendix C for proposed model in subsection 4.2.1.1

3.2 Geometry model implementation in CST

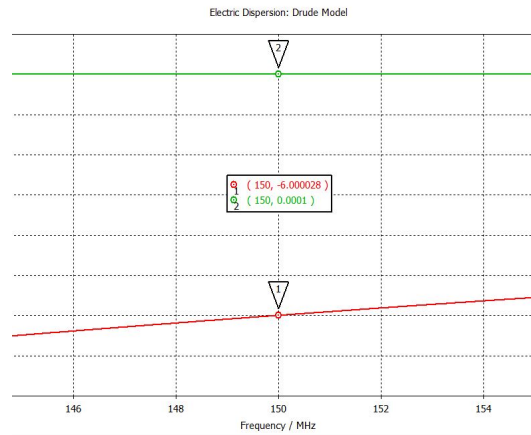


Fig. 3.6 Drude model verification for $\epsilon_r = -6 - j1 \cdot 10^{-4}$ at 150 MHz on CST

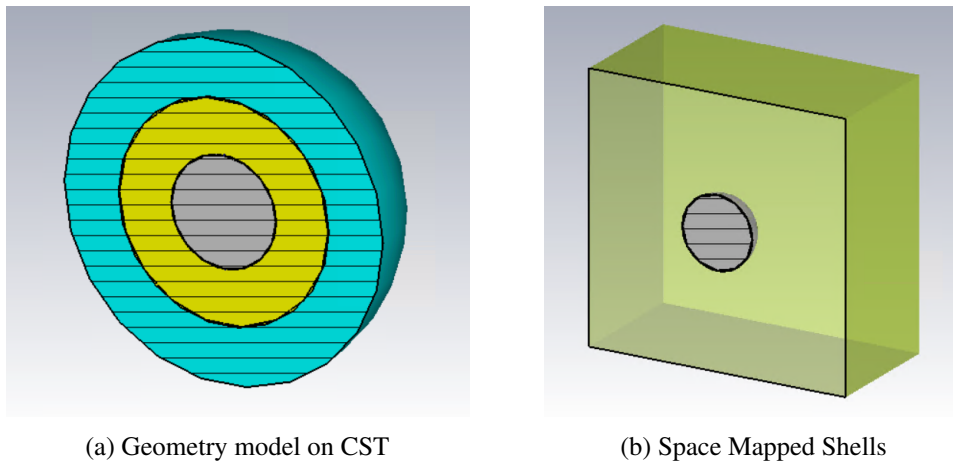


Fig. 3.7 3D half cut model on CST for plasma distribution described in figure 4.1

3. Each shell is defined at corresponding radius value with the assigned corresponding material, then a shelling operation may be done, in order to define concentric spheres non-overlapped.

A post processing might be done on generated dispersive materials with an another script, for value validation as shown for single material in figure 3.6.

3.2.4 RCS Result - Spherical Coordinates

CST adopts both cartesian coordinates system, implemented in solid generation, and spherical coordinates system for result plots. RCS result farfield cuts are based on θ

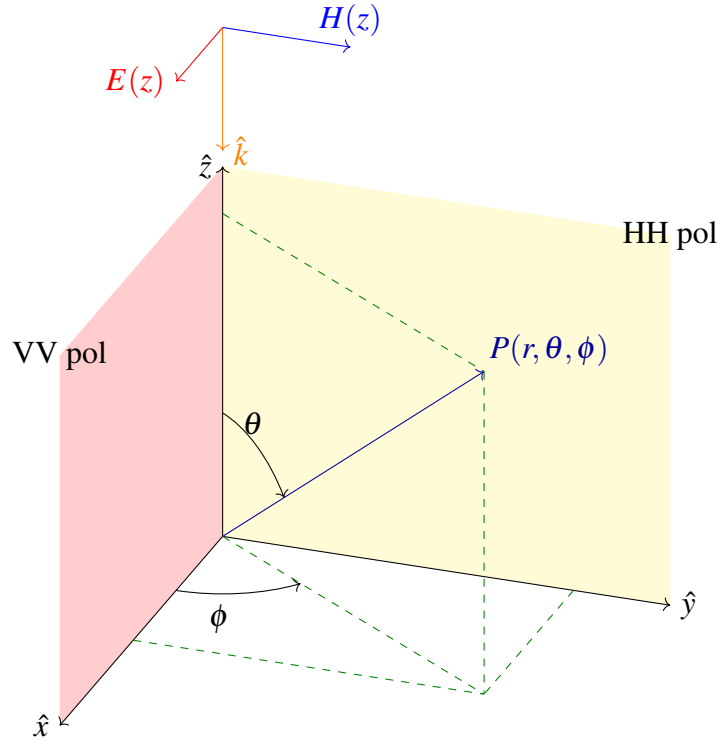


Fig. 3.8 Spherical coordinates system and polarization planes referment

and ϕ angles variation: one is fixed and the other varies. In figure 3.8 is shown the spherical coordinates system with $0 [rad] \leq \theta \leq \pi [rad]$ and $0 [rad] \leq \phi \leq 2\pi [rad]$.

In general in CST trajectory of sphere is put along \hat{z} axis, with $+z$ direction. As excitation a plane wave linearly polarized is put with direction in $-z$ and electric field along \hat{y} axis in $+x$ direction. Vertical plane is the one that contains $E(z)$ field, while horizontal plane is the one containing $H(z)$.

definition	acronym	range [rad]
<i>vertical polarization</i>	VV	$\phi = 0$ and $0 \leq \theta \leq \pi$
<i>horizontal polarization</i>	HH	$\phi = \pi/2$ and $0 \leq \theta \leq \pi$

Back-scattering, also known as monostatic radar, is the point in which EM reflection from propagation is coming back toward transmitter radar, so in this case for $\theta = 0 [rad]$, while front-scattering in in the opposite point placed at $\theta = \pi [rad]$.

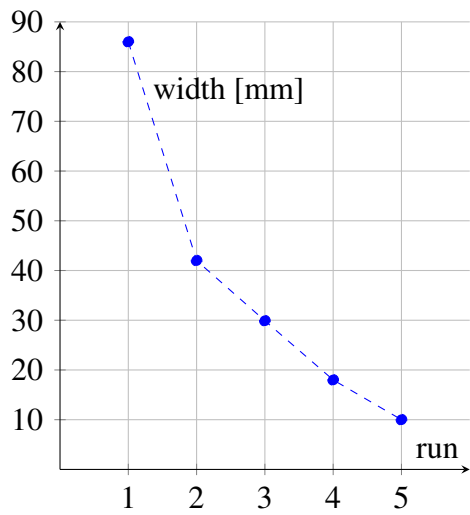
Whenever a spherical symmetry is encountered (e.g. a sphere in vacuum or surrounded by spherical layers), vertical and horizontal planes may be defined as

polarization planes with the respect of plane wave source; vice-versa if there is no spherical symmetry it is required a double simulation for each polarization plane.

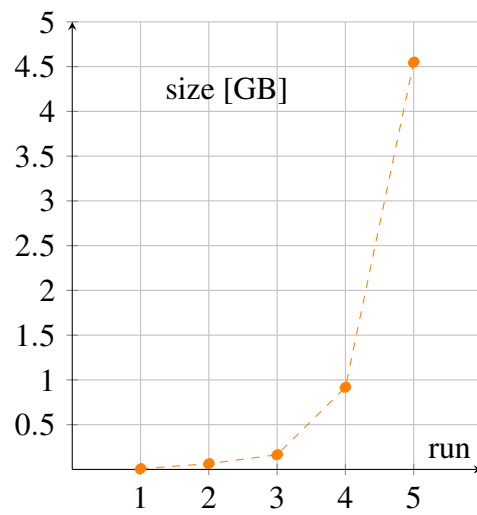
3.3 Simulation experience

CST microwave studio allows to control discretization, now on called mesh by the software, through window commands or VB scripting. The most important parameter is the maximum number of cells per wavelength $cells/\lambda$, that defines resolution: as increases this parameter, number of cells of the project increases as well. In principle higher is the number of cells, higher would be the reliability of results, but longer time computation is required. A trade-off between time and resolution has to be done, because simulation may become time consuming, in particular if CPU computing power is limited or there is no GPU available.

ASCII file required for material space map definition may be a limit, because increases quickly its size with the respect of width of generated grid (the width is the minimum distance between points in ASCII file). In figure A.7 the curve shows an high slope for the size of ASCII generated files as width decreases: ASCII file writes variables with a defined number of bit per character, while in binary files simplification or interpolation may be done.



(a) Width trend for each run



(b) ASCII size trend for each run

Fig. 3.9 Plots of table A.1 trends for ASCII file size and width for space map material of 2 meter radius sphere

Chapter 4

RCS of plasma with spherical geometry

In this chapter we provide the RCS results for inhomogeneous dielectric (e.g. plasma) distribution with a spherical symmetry. This choice has two advantages: first, for this geometry semi-analytic RCS solution via Mie Series (see chapter 2.1.6) can be easily computed for direct and quantitative comparison; second, a lot of already published numerical work and even experiments are available in this geometry and will be used for comparison with other methods.

We consider cases with and without a core solid sphere surrounded by an inhomogeneous media. The core sphere can be made of PEC or standard dielectric materials with specified permittivity. Initial test with homogeneous dielectric have also been performed with CST and Mie series and have been described in Appendix A for the interested reader.

As described in subsection 2.2.1, Drude dispersion model might be implemented and whenever cut-off frequency is overcome then negative relative permittivities occur.

Permittivity analytic distribution might be *discontinuous* at the vacuum-plasma boundary, leading to an hard disconnection between outer layer of generated plasma and vacuum permittivity. Otherwise permittivity distribution may be *continuous* if the outer shell of plasma shares same vacuum $\epsilon_r' = 1$ as background. Mie Series, as described in subsection 2.1.6, might be implemented for these geometries through a MATLAB script from [9]. Mie Solution is a reliable semi-analytic result

implemented in comparison with CST simulations allowing software performance evaluation.

Throughout this thesis we explore scattering in the Mie or resonance regime as reported in figure 2.5, characterized by a typical electrical size in the range $1 \lesssim k_0 \cdot a \lesssim 10$.

This choice of lowish frequencies are favoured on one side by the lowest computational cost required for the simulation (grid size scales with $1/\lambda$) and on the other side because other numerical techniques exist for the high frequency range also in presence inhomogeneous dielectric: higher $k_0 \cdot a$ values toward optical region may adopt other method such as Ray Tracing one, explained in [13]: Ray Tracing is an asymptotic method that explores optical geometry with approximation on optical physics.

For instance in [13] a ray-tracing method, combining geometrical optics and physical optics approximation, is applied to study scattering by hypersonic plasmas.

4.1 Inhomogeneous dielectric with discontinuities - negative permittivities shells around PEC sphere

In this section there is the implementation of inhomogeneous plasmas with negative permittivity outer shells, as described in paper [4] section III.B . The analysed sphere has two shell of negative permittivity as shown in figure 4.1, with negative ϵ'_r . Simulations are done adopting these values: permittivity parameter as $\epsilon'_r = -3$ and frequency as $f = 100$ [MHz] and $f = 150$ [MHz].

Generated plasma is inhomogeneous because there is a discontinuity between the vacuum background condition and the plasma surrounding the PEC¹ sphere.

4.1.1 Frequency of 100 MHz

Outer radius of figure 4.1 by 1 meter and the working frequency set at 100 MHz: $k_0 \cdot a \approx 2$ from equation (2.18).

¹acronym for Perfectly Electric Conducting

4.1 Inhomogeneous dielectric with discontinuities - negative permittivities shells around PEC sphere

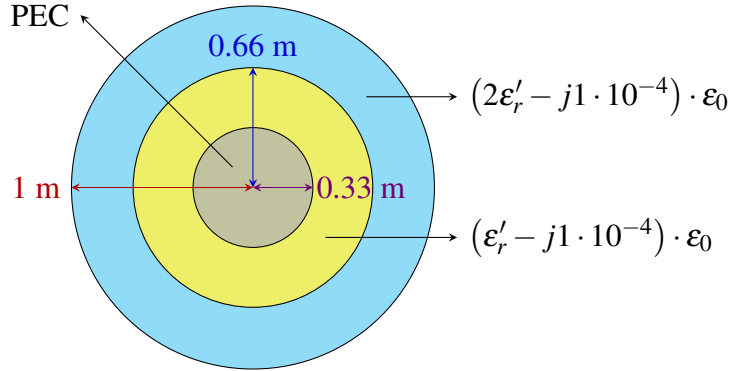


Fig. 4.1 Sphere shelling with negative permittivities from figure 6(a) in [4]

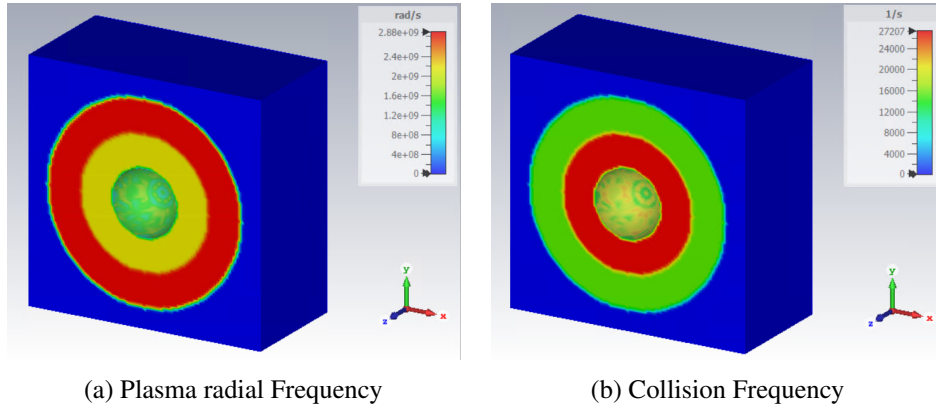


Fig. 4.2 CST view of space mapped material at 100 MHz for negative shells

Simulation are done both with geometry direct definition on CST as shown in figure 3.7a with RCS reported in figure 4.3, and space map material in CST reported in figure 4.2. We study the convergence properties of the algorithm by changing the parameter $cell/\lambda$ term, that is a key parameter for mesh resolution in CST: higher is this parameter, therefore higher will be the number of cells and the resolution of the simulation.

The results for a 50% higher frequency, with a $k_o \cdot a = \pi$ are presented in figure 4.5 for the case of space-map dielectric model.

With some surprise we don't observe a clear trend with increasing grid resolution. Although in qualitative agreement with the Mie serie, the FDTD solution is very sensitive to the particular grid. For a $cell/\lambda$ in the range of 20-30 we get however the best accuracy for both space-map and solid shells models and frequencies. The reasons for this behaviour are clear and could perhaps investigated in future work.

RCS of plasma with spherical geometry

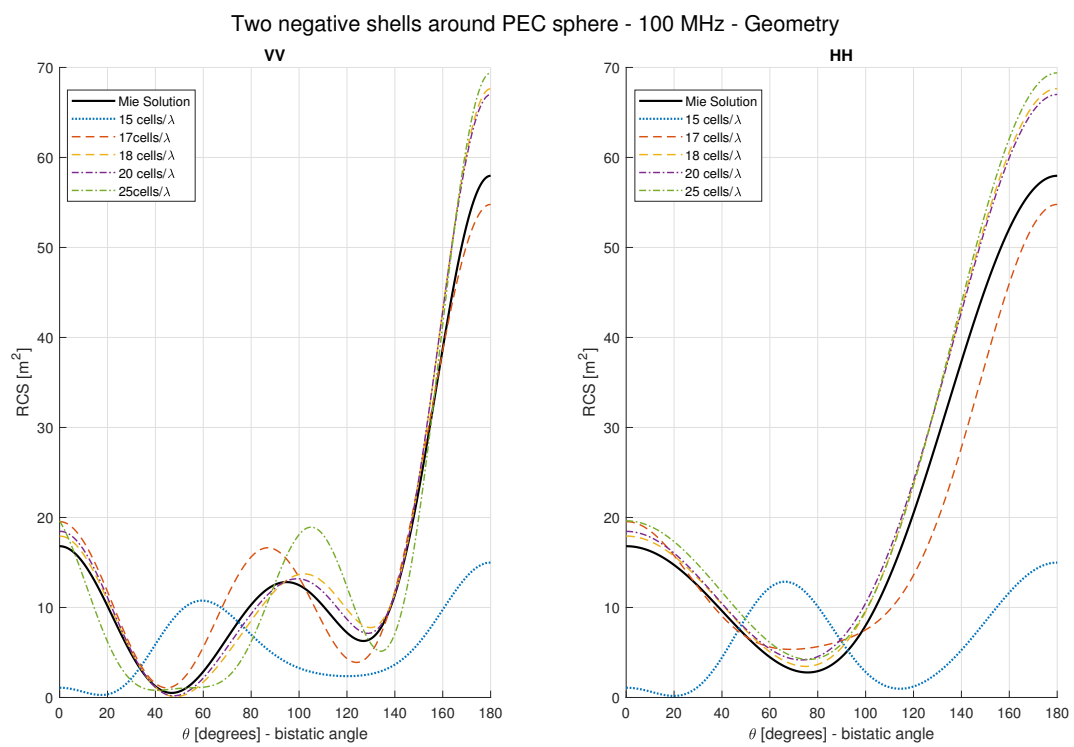


Fig. 4.3 RCS for $f = 100 \text{ MHz}$ and $\epsilon'_r = -3$ for plasma distribution described in figure 4.1 - Geometry

4.1 Inhomogeneous dielectric with discontinuities - negative permittivities shells around PEC sphere

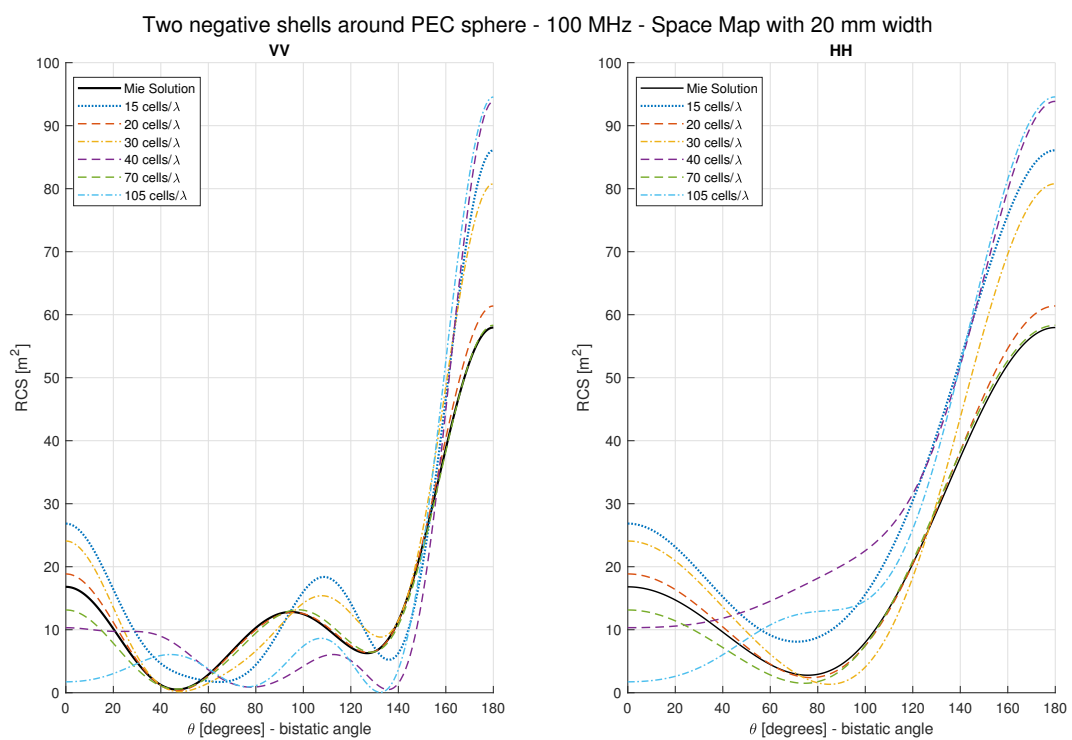


Fig. 4.4 RCS for $f = 100 \text{ MHz}$ and $\epsilon_r' = -3$ for plasma distribution described in figure 4.1 - Space Map

RCS of plasma with spherical geometry

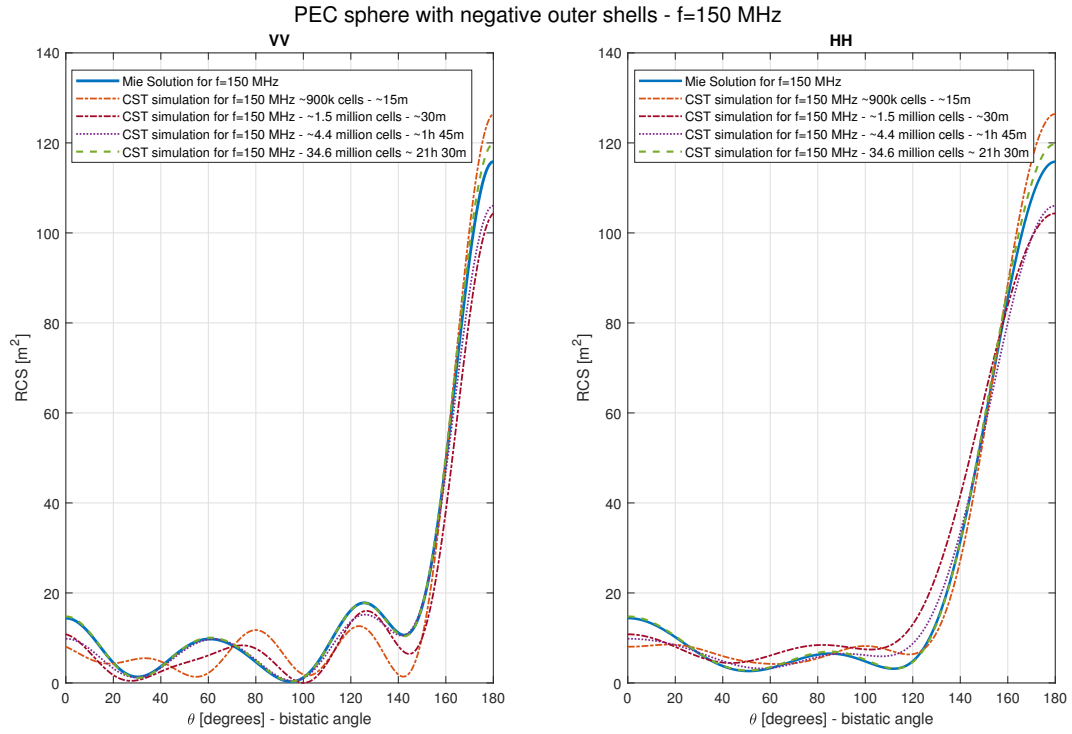


Fig. 4.5 RCS for $f = 150$ MHz and $\epsilon_r' = -3$ for plasma distribution described in figure 4.1

This result may cast doubts on the ability of the CST-FDTD method to produce numerically stable and reliable RCS.

We will see in the next section in fact, that for a continuous and smooth plasma distribution more accurate and stable results with a clear trend with grid resolution can be achieved. A plasma model with sharp discontinuities shall be regarded as numerically challenging configuration.

4.1.2 Conclusion on CST simulations for discontinuous shells

There is no accuracy for proposed shells with the respect of resolution increase: this may lead to a computational limit of CST FDTD solver for proposed shields with very high negative permittivity.

4.2 Inhomogeneous dielectric with continuities permittivity distribution around PEC sphere

parameter	symbol	value
radius outer shell	R_{out}	3 [m]
radius inner shell	R_{in}	1 [m]
permittivity at outer shell	ϵ_{ext}	1
permittivity at inner shell	ϵ_c	variable

Table 4.1 Parameters description for permittivity analytic profile of equation (4.1) extracted from [13] section A.2

4.2 Inhomogeneous dielectric with continuities permittivity distribution around PEC sphere

In this section there is a smoother profile: plasma is distributed with a cosine function. Required parameters for this implementation are reported in table 4.1: $R_{out} = 3$ [m], while $R_{in} = 1$ [m]; there is still a ratio between plasma outer shell radius and target radius by 3 with the respect of previous analysed case in figure 4.1 with $R_{out} = 1$ [m] and $R_{in} = 0.33$ [m], leading to uniform plasma extension for both distributions.

In equation (4.1) is reported the analytic permittivity profile adopted for continuous permittivity distribution, from [13] equation (16):

$$\epsilon'_r(r) = \frac{\epsilon_c + \epsilon_{ext}}{2} \cdot \left[1 + \frac{\epsilon_c - \epsilon_{ext}}{\epsilon_c + \epsilon_{ext}} \cdot \cos \left(\pi \frac{r - R_{in}}{R_{out} - R_{in}} \right) \right] \quad (4.1)$$

where r is the radial variable within the range $R_{in} \leq r \leq R_{out}$. Input $\epsilon'_r(r)$ and r have to be implemented with a finite sampling: uniform discretization may be adopted as shown in figure 3.2, moreover last interval close to target sphere might be non-uniform with the respect of the other intervals. In this case resolution is a key parameter and has to be studied, in particular for negative permittivities generation. Three permittivities distributions with ϵ_c variable are considered:

$$(I) \quad \epsilon_c = 0.5$$

$$(II) \quad \epsilon_c = 0.1$$

$$(III) \quad \epsilon_c = -0.1$$

These three cases are reported in figure 4.6, in relation with equation (4.1) with vacuum as material background, therefore $\epsilon_{ext} = 1$ as reported in table 4.1. In figure

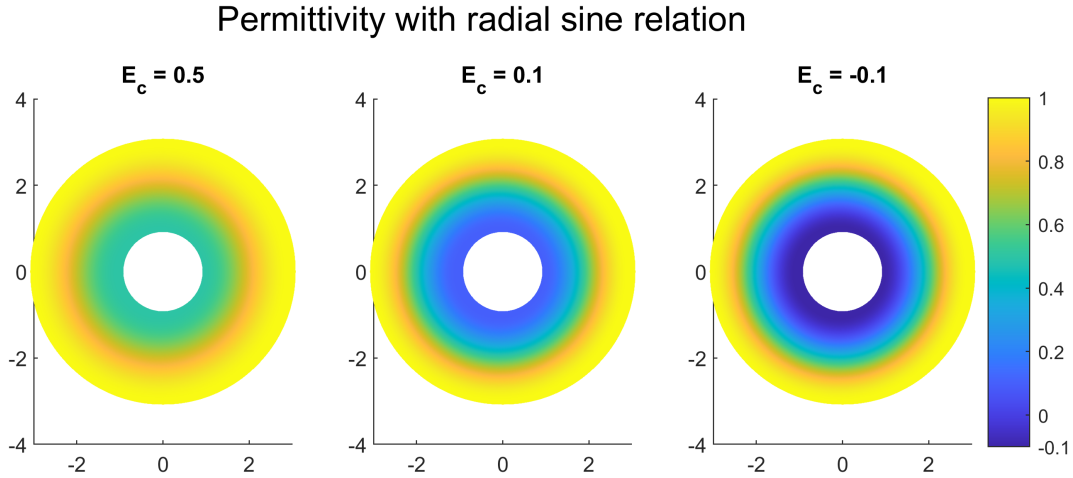


Fig. 4.6 Radial permittivity distribution from figure 12 of [13] with three ϵ_c values

4.7a is reported the profile of equation 4.1 with $\epsilon_c = 0.1$, then with this profile a space map material as described in subsection 3.2.2 is generated, then resolution has to be properly adapted to CST input file. 3D space map profile is shown as instance in figure 4.7b.

Drude model allows negative equivalent permittivities, in chosen case up to $\epsilon_r = -0.1$. For Drude Model it is required a fixed frequency for each generated plasma, in order to respect equivalent permittivity map: chosen frequencies are:

- $f = 100$ [MHz] $\Rightarrow k_0 \cdot a \approx 6.30$
- $f = 250$ [MHz] $\Rightarrow k_0 \cdot a \approx 15.7$

Whenever a negative relative permittivity is encountered, dispersion model might be applied to CST simulation, due to positive relative permittivity software limitation in material definition.

In appendix B there is explained the imaginary component implementation due to convergence issue in Mie Solution RCS, moreover there is reported the analysis for ϵ_r'' value leading to $\epsilon_r'' = 1 \cdot 10^{-4}$ whenever an imaginary component without reshaped RCS has to be implemented.

4.2 Inhomogeneous dielectric with continuities permittivity distribution around PEC sphere

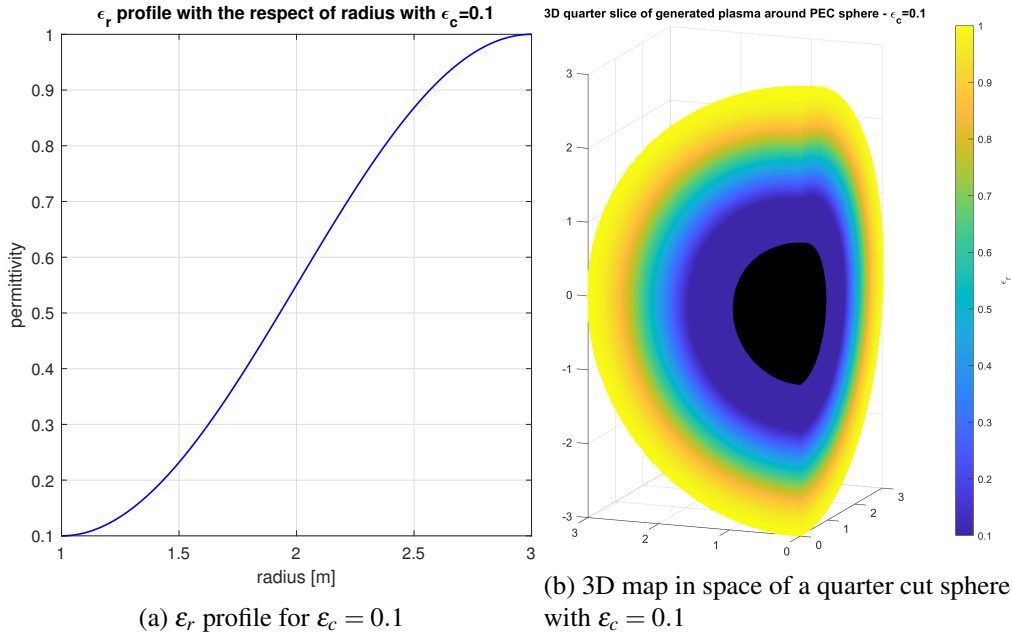


Fig. 4.7 Distribution of relative permittivity as equation (4.1) and $\epsilon_c = 0.1$

4.2.1 Positive permittivities in inhomogeneous continuous plasmas

Primary evaluations are done with only positive permittivities distribution. In this case whichever material definition between permittivity and Drude model might be implemented without approximations.

4.2.1.1 CST spherical shells with $\epsilon_c = 0.1$, $f = 100$ [MHz]

As described in subsection 3.2.3.1 primary implementation may be done with solid definition on CST with concentric shells of defined relative permittivities. Proposed frequency is set as $f = 100$ [MHz] leading to a $k_0 \cdot a \approx 6$ from equation (2.18), then for $\epsilon_r'' = 1 \cdot 10^{-4}$ corresponding conductivity is $\sigma \approx 556$ [nS/m] from equation (3.10): this quantity is implemented in material definition for each shell.

Number of shells is properly chosen such implementing the minimum number of concentric shells that leads to a solution close to the "continuous" Mie Solution, and as continuous is meant with a very high resolution as mentioned in Appendix B.2. Therefore the chosen radial step size from outer shell towards inner shell is 37 mm.

RCS of plasma with spherical geometry

Moreover in figure 4.8 is shown portion of the composed geometry, where each layer is defined with corresponding permittivity as defined in equation (4.1) with 55 shells generated as described in subsection 3.2.3.1.

The MATLAB code implemented for the generation of the spheres with corresponding material is reported in Appendix C.

The RCS are shown in figure 4.9

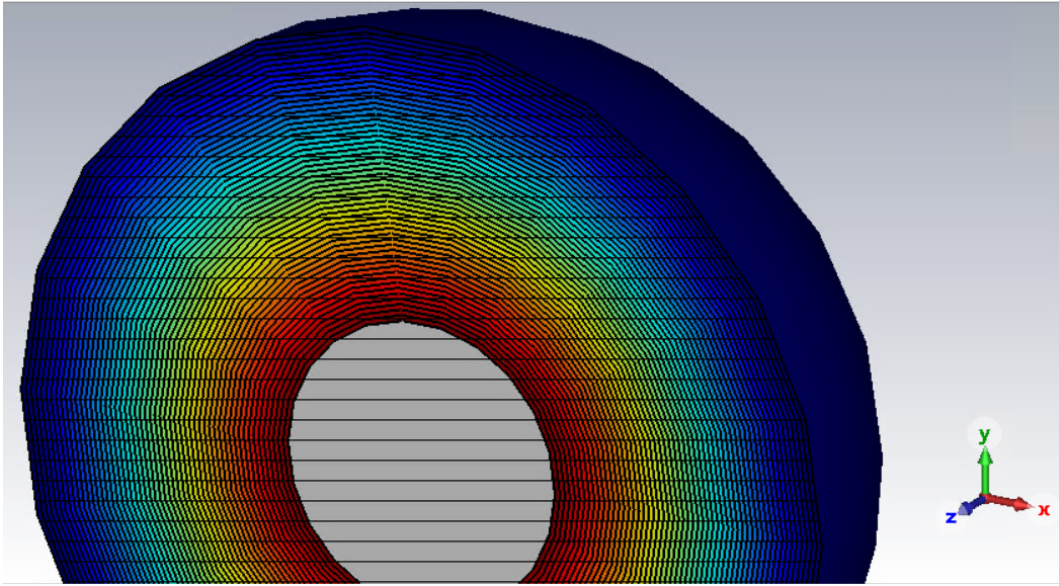


Fig. 4.8 Portion of halved concentric 55 shells generated for CST

4.2.1.2 Space map with $\epsilon_c = 0.5$, $f = 250$ [MHz]

In figure 4.10 there are reported the space maps of an analytic plasma generated through equation (4.1) with $\epsilon_c = 0.5$ and two corresponding widths for generated files: 50 mm with permittivity mapped (Fig. 4.10a) and 15 mm with permittivity (Fig. 4.10b) and plasma frequency (Fig. 4.10c) mapped. Working frequency is set to 250 [MHz], leading to a $k_0 \cdot a \approx 15.7$.

Permittivity profile is defined only through real values, thus $\epsilon_r'' = 0$.

In figure 4.11 there are the equivalent RCSs obtained through three CST simulation: all simulations respect mostly Mie Series trend, but with an undesired back-scattering defined in $\theta = 0$ [rad]. The simulation with a more refined input

4.2 Inhomogeneous dielectric with continuities permittivity distribution around PEC sphere

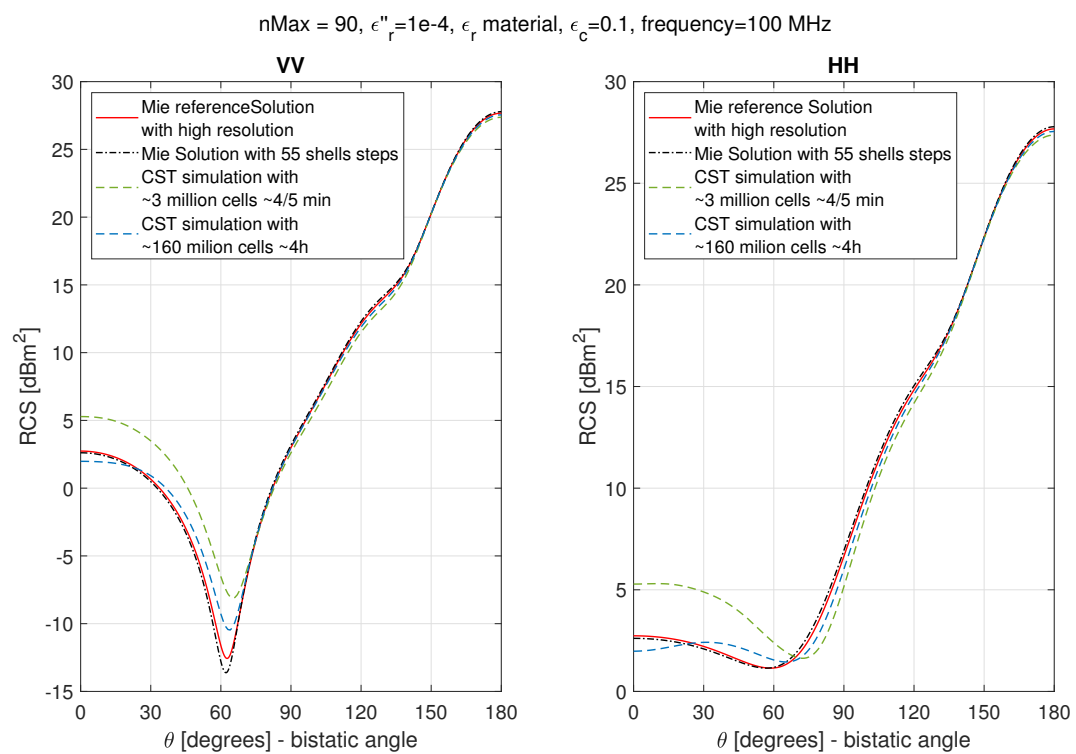


Fig. 4.9 RCS with ϵ_r profile provided by (4.1) with $\epsilon_c = 0.1$, $\epsilon_r'' = 1 \cdot 10^{-4}$, frequency = 100 MHz and 55 shells around PEC sphere

RCS of plasma with spherical geometry

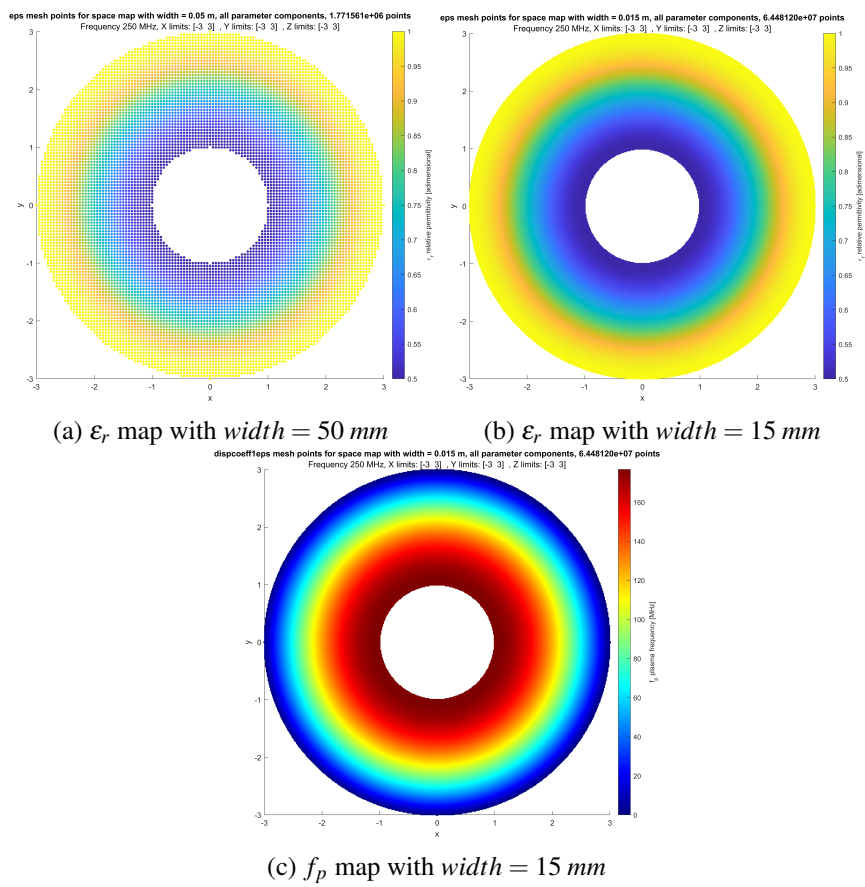


Fig. 4.10 Space map cut for analytic plasma from distribution defined in (4.1) with $\epsilon_c = 0.5$

4.2 Inhomogeneous dielectric with continuities permittivity distribution around PEC sphere

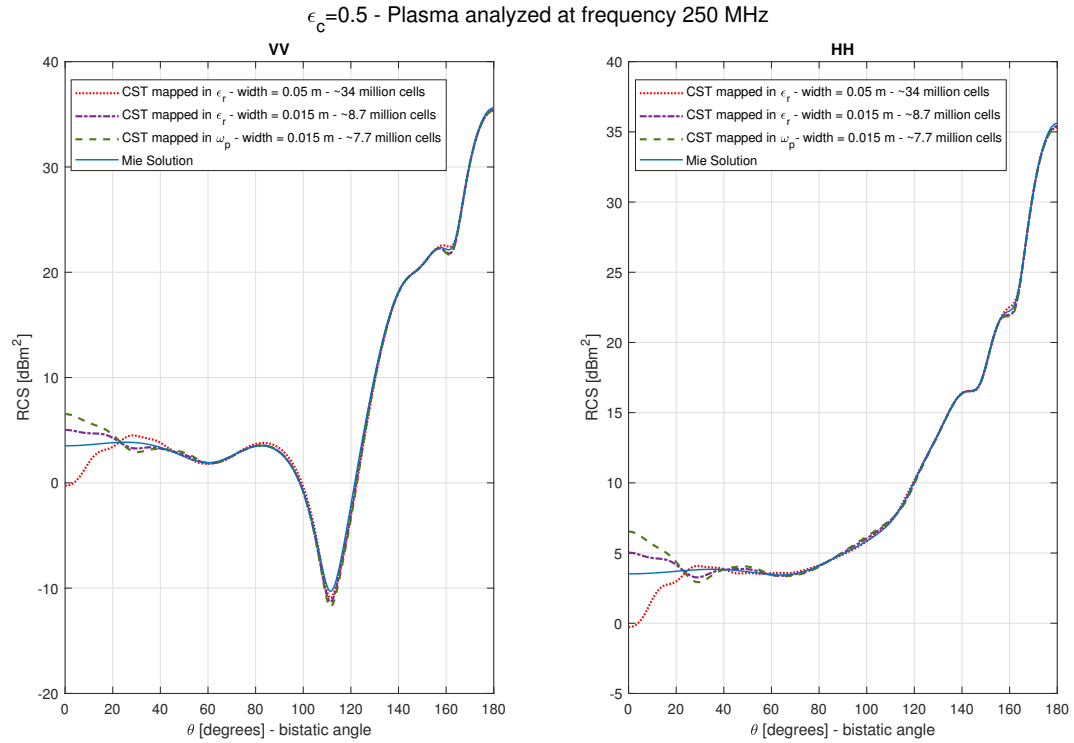


Fig. 4.11 RCS of space mapped analytic plasma from distribution defined in (4.1) with $\epsilon_c = 0.5$, $f = 250$ MHz

space map has a closer back-scattering to the semi-analytic solution. Oscillation may be encountered.

4.2.1.3 Space map with $\epsilon_c = 0.1$, $f = 100$ [MHz]

In figure 4.12 there is shown the RCS for permittivity distribution with $\epsilon_c = +0.1$ space mapped material with input file width by 20 mm. CST resolution is shown in legend: as number of cells increases, back-scattering seems to be accurate with the respect of Mie Solution one.

4.2.1.4 Space map with $\epsilon_c = 0.1$, $f = 250$ [MHz]

Same procedure is adopted for $\epsilon_c = 0.1$ and $\epsilon_r'' = 0$ with widths: 50 mm for permittivity space map (figure 4.13a) and 15 mm for plasma frequency space map (figure 4.13b). Simulation results are reported in figure 4.14: permittivity and plasma frequency implementations have different value in back-scattering.

RCS of plasma with spherical geometry

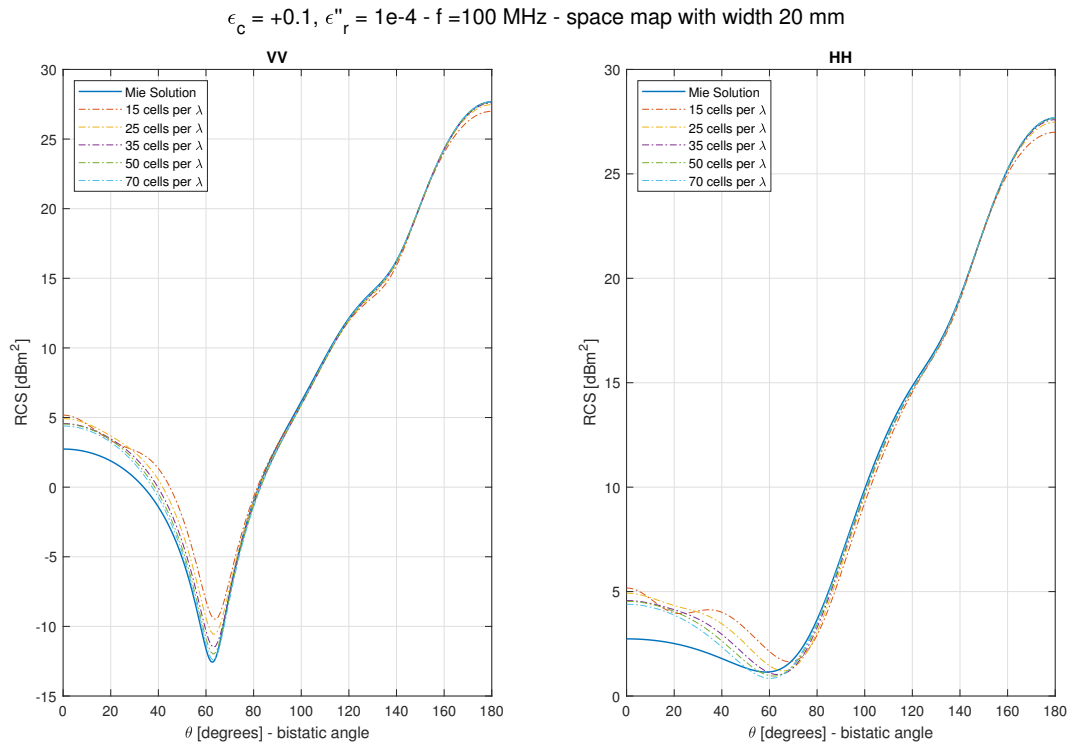


Fig. 4.12 RCS of space mapped analytic plasma from distribution defined in (4.1) with $\epsilon_c = +0.1, f = 100 \text{ [MHz]}$ and $\epsilon_r'' = 1 \cdot 10^{-4}$

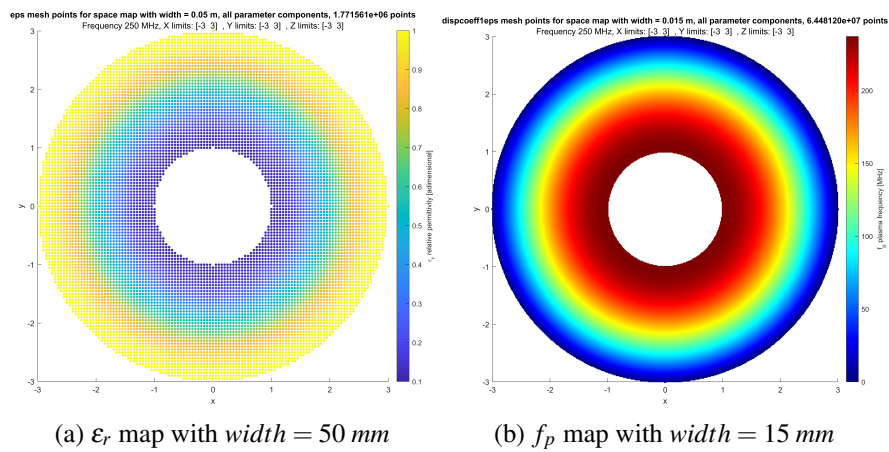


Fig. 4.13 Space map cut for analytic plasma from distribution defined in (4.1) with $\epsilon_c = 0.1$

4.2 Inhomogeneous dielectric with continuities permittivity distribution around PEC sphere

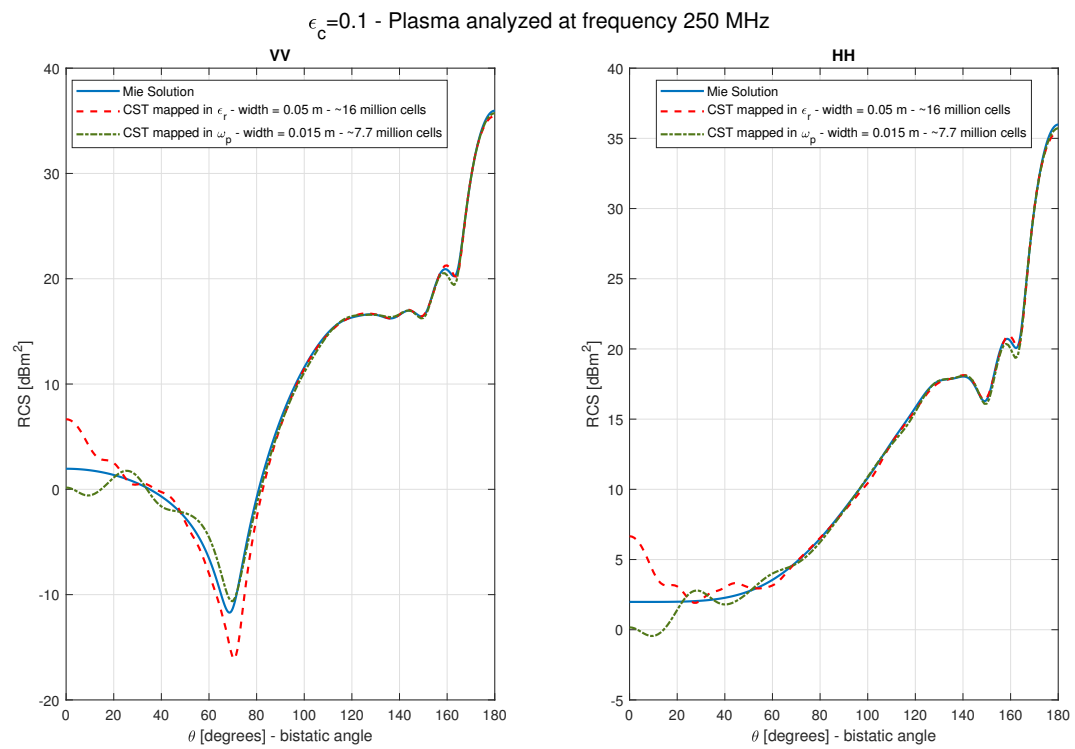


Fig. 4.14 RCS of space mapped analytic plasma from distribution defined in (4.1) with $\epsilon_c = 0.1$, $f = 250$ [MHz] and $\epsilon_r'' = 0$

RCS of plasma with spherical geometry

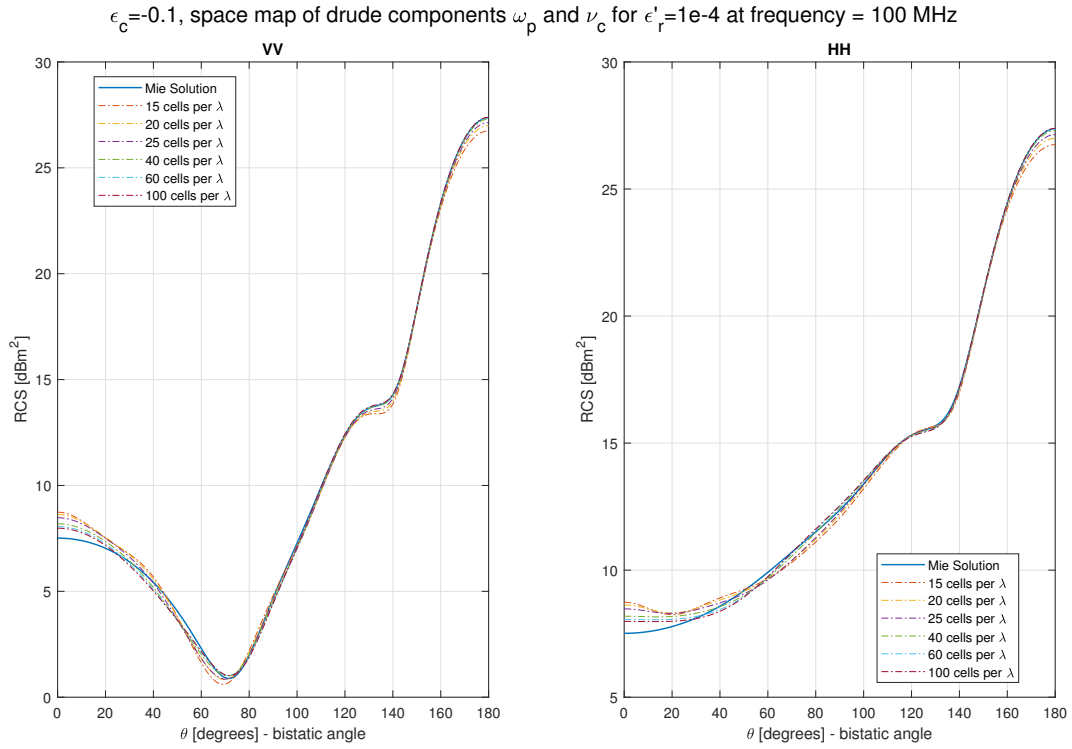


Fig. 4.15 RCS of space mapped analytic plasma from distribution defined in (4.1) with $\epsilon_c = -0.1$, $f = 100$ [MHz], $\epsilon_r'' = 1 \cdot 10^{-4}$

4.2.2 Negative permittivities in inhomogeneous continuous plasmas

Last case analysed is the implementation of negative permittivities: $\epsilon_c = -0.1$.

4.2.2.1 Space map with $\epsilon_c = -0.1$, $f = 100$ [MHz]

A space map material is generated with an high resolution such as 20 mm width and imported in CST with both ω_p and ν_c components, such having $\epsilon_r'' = 1 \cdot 10^{-4}$. In figure 4.15 there are reported RCS for corresponding simulation with the respect of mesh resolution $cells/\lambda$: as resolution increases, results become more accurate with the respect of Mie Solution.

4.3 Conclusions on analytic plasmas profile

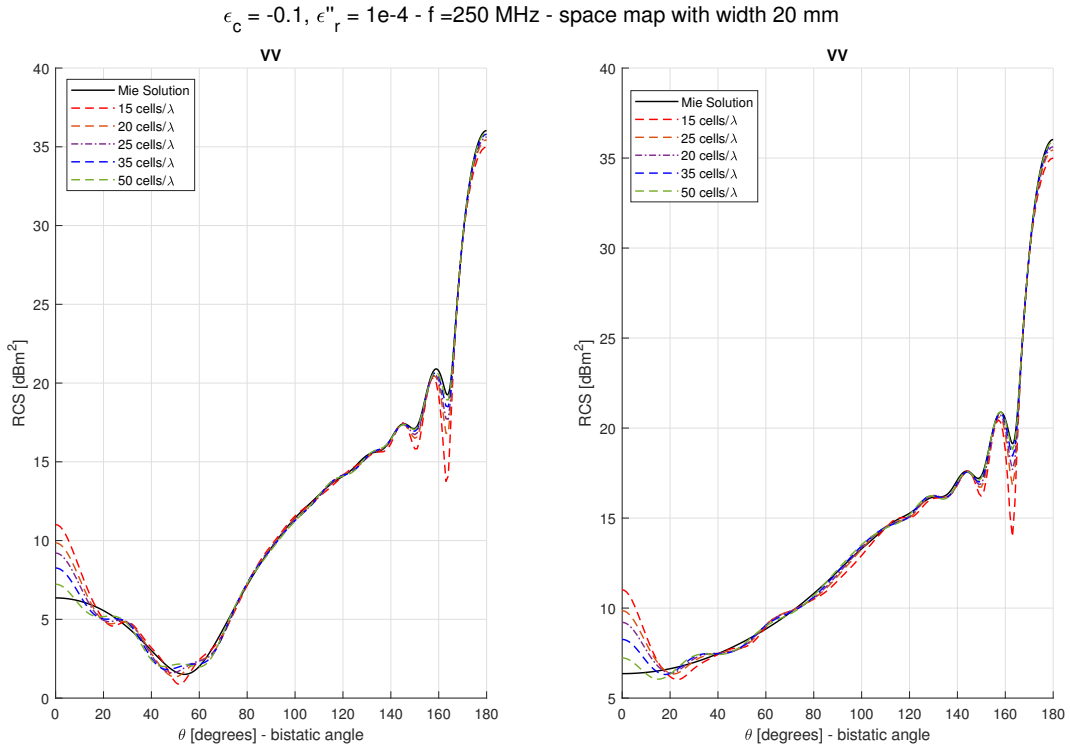


Fig. 4.16 RCS of space mapped analytic plasma from distribution defined in (4.1) with $\epsilon_c = -0.1$, $f = 250 \text{ [MHz]}$ and $\epsilon_r'' = 1 \cdot 10^{-4}$

4.2.2.2 Space map with $\epsilon_c = -0.1$ at 250 MHz

A space map material is generated for $\epsilon_c = -0.1$ profile and $\epsilon_r'' = 1 \cdot 10^{-4}$ with width 20 mm. In figure 4.16 there are reported RCS with CST resolution $cells/\lambda$: as resolution increases, the CST back-scattering seems to be more accurate with the respect of Mie Solution one.

4.3 Conclusions on analytic plasmas profile

We calculated RCS in presence of spherical symmetric plasma-like inhomogeneous media and compared the results with reference Mie solutions. The study of analytic plasmas is useful in finding limits and issues in the FDTD based method in the CST code.

For continuous smooth permittivity profiles good accuracy in the bistatic RCS can be found with reasonable computational effort. The largest differences are invariably

RCS of plasma with spherical geometry

found for small scattering angle, corresponding the back-scattering or monostatic RCS. The accuracy typically increases with grid resolution. Given the fact that number of grid cells necessary for a certain accuracy scales with $1/\lambda$ larger electric size scatterer (larger $k_0 \cdot a$) are harder to compute and require more computation power.

We have tested a space-map based and solid-shell based model implementation of the inhomogeneous background media. Both method gives similarly provided the space-map is given with sufficiently high resolution so to correctly represent the gradients in the propagating media.

RCS of plasma distribution with sharp discontinuities are more difficult to compute. No clear trend with grid resolution is found. Nevertheless, for a $cell/\lambda$ of about 20-30, quite good comparison with the Mie reference solution is observed.

Chapter 5

RCS in presence of realistic hypersonic plasma flows

In this chapter we calculate the RCS of two objects surrounded by a realistic plasma distribution generated by hypersonic flows.

The plasma is calculated with state-of-the-art CFD methods implemented in [1] and taken as input. In the first example, we consider a PTFE sphere with a Mach 10 hypersonic flow as in the laboratory experiment described in [3]. The second example consider a simple vehicle in hypersonic atmospheric flight from [1].

5.1 PTFE sphere with Mach 10 flow

This model is extracted from [3]: a PTFE sphere by 75 mm of radius and 5 mm of thickness. EM evaluations are done in vacuum and in plasma conditions. Plasma frequency is extracted from CFD results provided by [1] as described in subsection 2.2.2.

The purpose is to analyse the model proposed in [3] and to possibly compare available results, moreover being the flow reproduced by [1] starting from scratch, the results and parameters may differ from the ones in cited paper. In [3] EM simulations are evaluated through space map material based on their own CFD n_e electron density distribution.

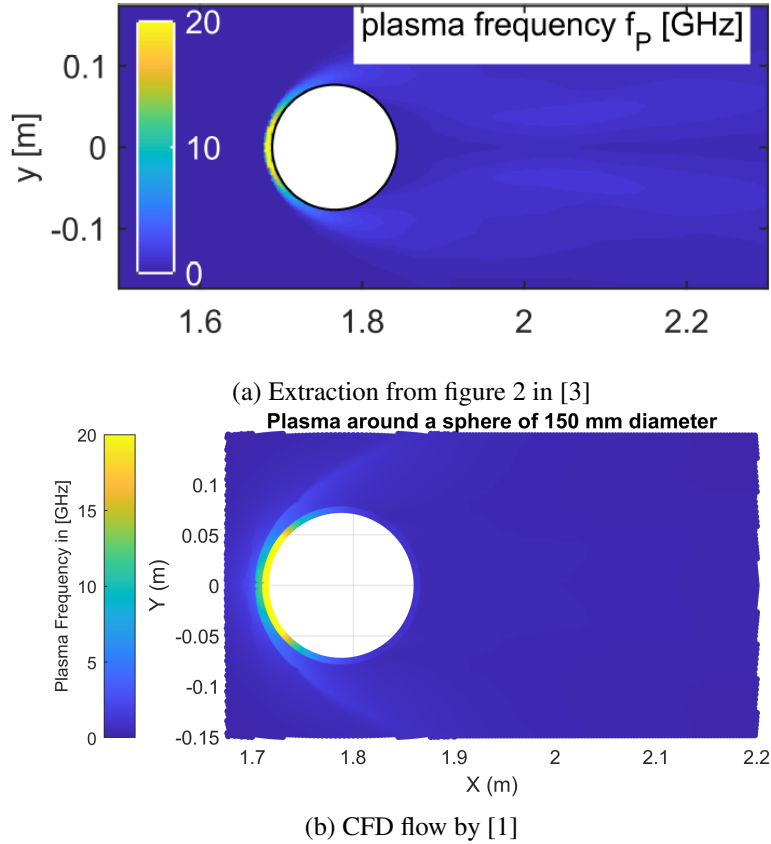


Fig. 5.1 Comparison between f_p in [3] and with CFD provided by [1]

In figure 5.1 there is a comparison between the two plasma distributions: CFD provided by [1] reported in figure 5.1b has behaviour similar with the respect of the one in figure 5.1a from [3] but not the same for the reasons explained above.

In monostatic RCS reflected EM waves are measured in same point of transmitted source as shown in figure 2.2.

5.1.1 RCS in vacuum background

Primary monostatic RCS evaluations may be done in vacuum condition. Proposed range of frequencies in figure 3 of [3] is from 3 GHz to 15 GHz, therefore $k_0 \cdot a$ coefficient is evaluated from (2.18): lowest $k_0 \cdot a \approx 4.7$ for $f = 3$ [GHz], while highest $k_0 \cdot a \approx 23.6$ for $f = 15$ [GHz].

5.1 PTFE sphere with Mach 10 flow

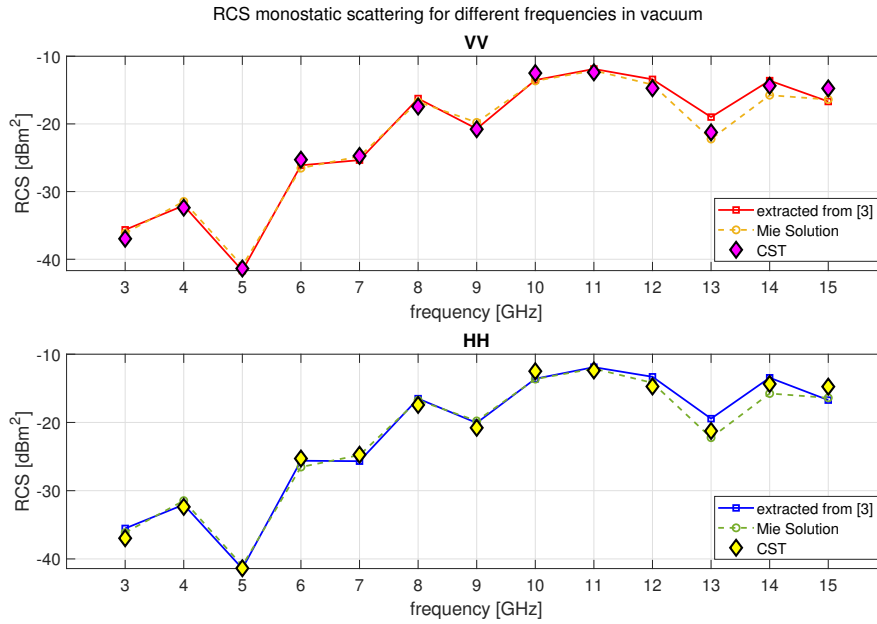


Fig. 5.2 Monostatic RCS from figure 3 in paper [3] in vacuum condition with reproduced simulation on CST for this thesis and Mie Solution

In vacuum condition with a sphere target the symmetries occur and it is possible to evaluate both vertical and horizontal polarizations with a singular simulation, while monostatic RCS results does not change for any position of the source plane wave with the respect of angle θ .

In vacuum condition for this set of $k_0 \cdot a$ values the obtained results from CST simulations for monostatic RCS are compatible with the respect of Mie Solution and results in [3] as shown in figure 5.2.

5.1.2 Plasma distribution

A step further is to implement a plasma around sphere model from a CFD simulation for an hypothetical collision in atmosphere at an hypersonic speed, as instance Mach 10 as proposed in paper [3], with reproduced CFD from [1] and provided for the EM analysis in this thesis. In section 2.2.2 there are reported the fluid physical quantities required for plasma frequency evaluation shown as instance in figure 5.1b extracted from CFD results provided by [1], while in section 3.2.2.1 there is described

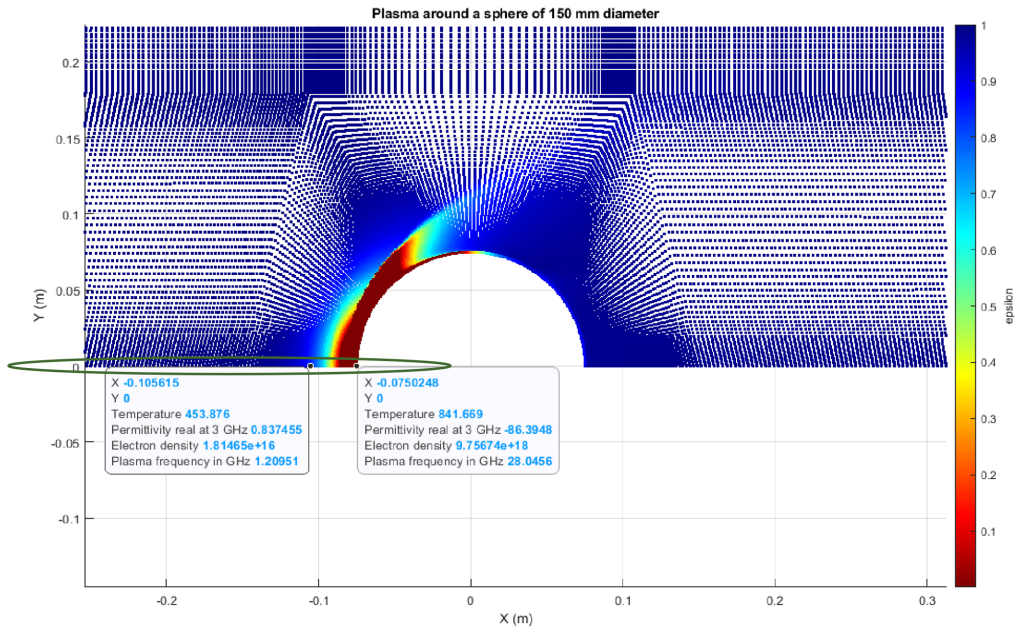


Fig. 5.3 From CFD reproduced by [1] with model proposed in [3] - highlighted region from ϵ_r cut map inspired by figure 2 of [3]

the implementation with space map material useful for scattered inhomogeneous dielectric.

In CST the source is placed with direction $\hat{n} = -\hat{z}$ while the direction of the target is in \hat{z} direction, therefore in space map material generation a rotation by 90° with the respect of \hat{y} axis has to be done.

5.1.2.1 Extraction of spherical symmetric plasma distribution from 3D CFD

Primary analysis may be done with a radial extraction, as done in previous Chapter 4 leading to Mie Solution implementation providing a reliable comparison with CST model of proposed target. In figure 5.3 it is possible to view the chosen region of interest for $\theta = 0^\circ$ on CST: therefore $Y = 0$ [m] and -0.2 [m] $\lesssim X < 0$ [m] on proposed figure.

The choice of that region is due to symmetry of the plane, moreover in region on surface target there is the highest n_e density concentration as shown in figure 2.7.

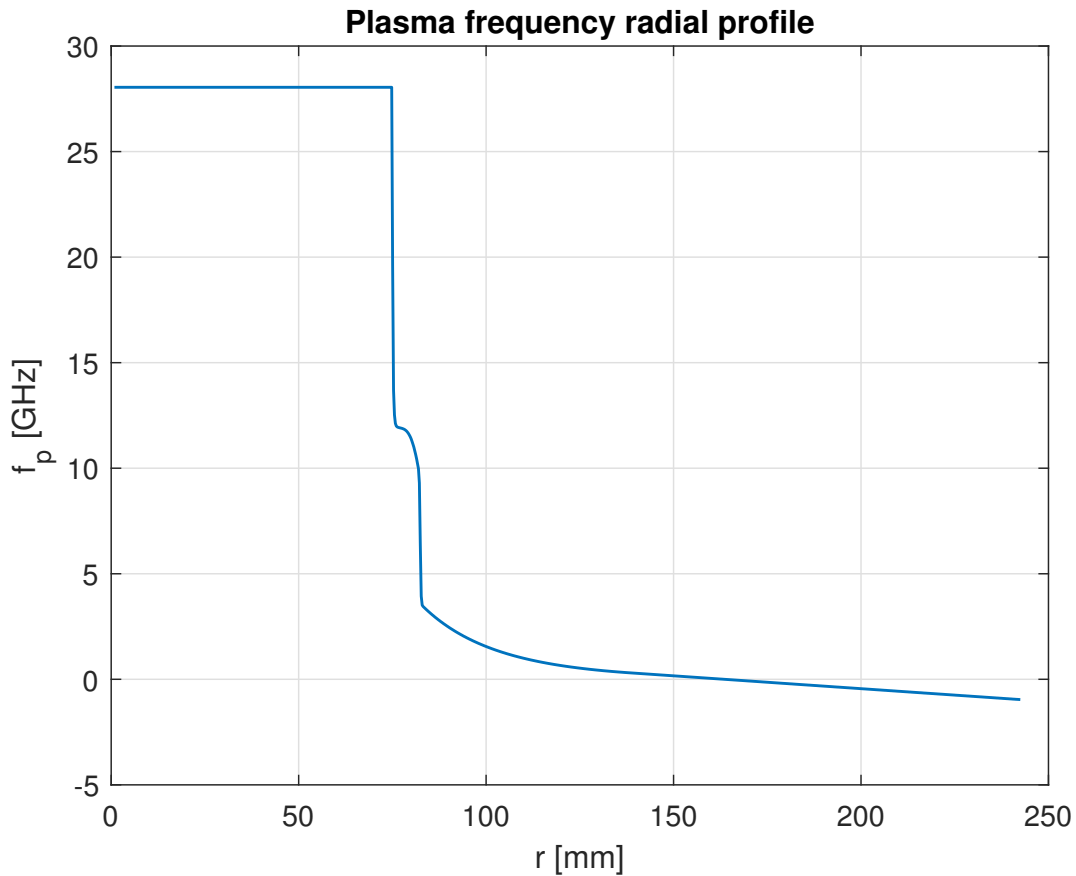


Fig. 5.4 Space Maps radial dependence for f_p extraction from CFD provided by [1]

A space map material is produced through MATLAB, with radial dependence as shown in figure 5.4 and then is imported in CST. The ω_p value is extracted directly from provided CFD, while ν_c is set such giving a low imaginary relative permittivity profile.

Working frequency is set to $f = 3$ [GHz], therefore the permittivity should be mapped as shown in figure 5.5. Evaluated RCS are reported in figure 5.6 together with Mie Solution. Simulation has general good agreement and in particular also the monostatic RCS is accurate with the respect of Mie one. A comparison with the respect of vacuum monostatic RCS from figure 5.2 is done in table 5.1: with plasma radial distribution the cut-off has increased with the respect of vacuum one, leading to the RCS of the target sphere of PEC material and reflection for propagated waves is much more effected as expected in a reflective layer.

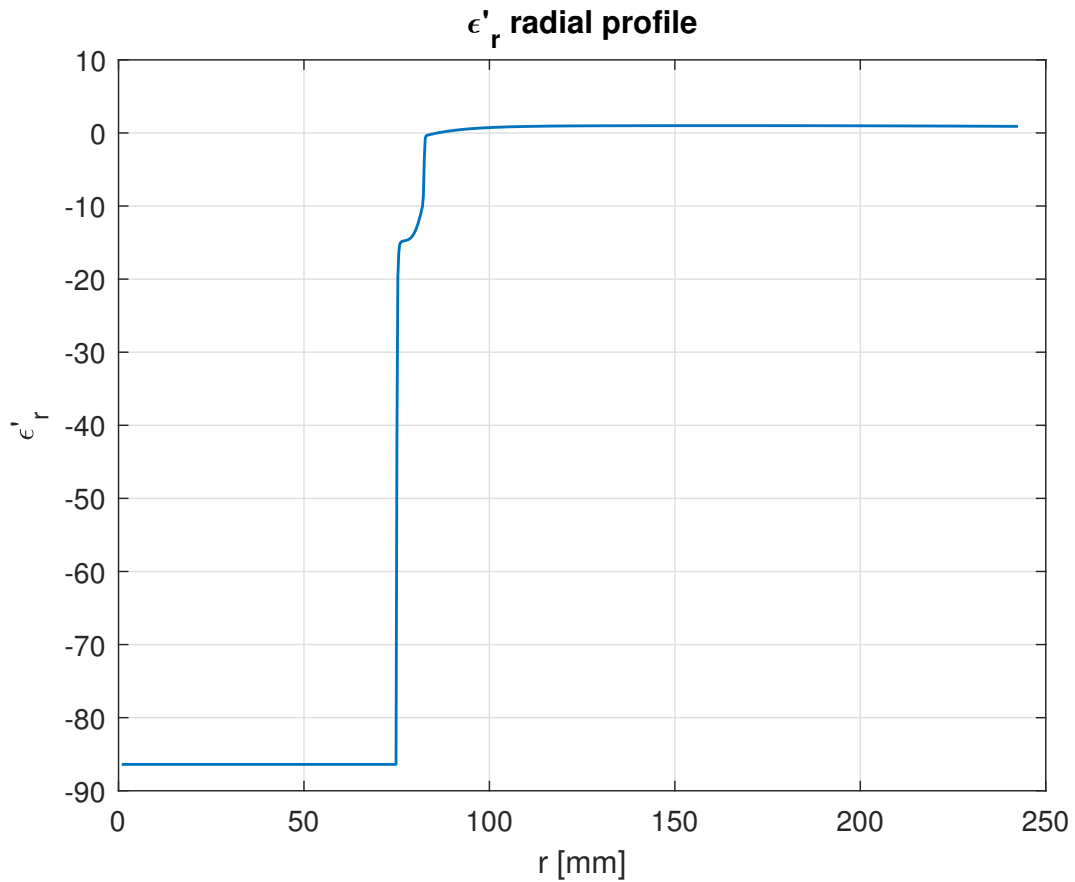


Fig. 5.5 Space Maps radial dependence for ϵ_r' extraction with $f = 3$ [GHz] from CFD provided by [1]

RCS monostatic for $\theta = 0^\circ$	-37 [dBm ²]	-16.6 [dBm ²]
	vacuum	with plasma

Table 5.1 Monostatic RCS value for $\theta = 0^\circ$ at $f = 3$ [GHz]

5.1.2.2 CFD plasma reproduced by [1] implemented in CST

We next consider the full 3D plasma distribution. As can be seen from figure 5.1 the main 3D effect is a wake of dense plasma detaching from sphere surface and expanding outward and backward. We will see that this contribution seems to increase the back-scattering as might be expected by a reflective layer.

5.1 PTFE sphere with Mach 10 flow

Radial extraction from CFD of PTFE sphere by 150 mm diameter surrounded by plasma for Mach 10 at frequency 3 GHz

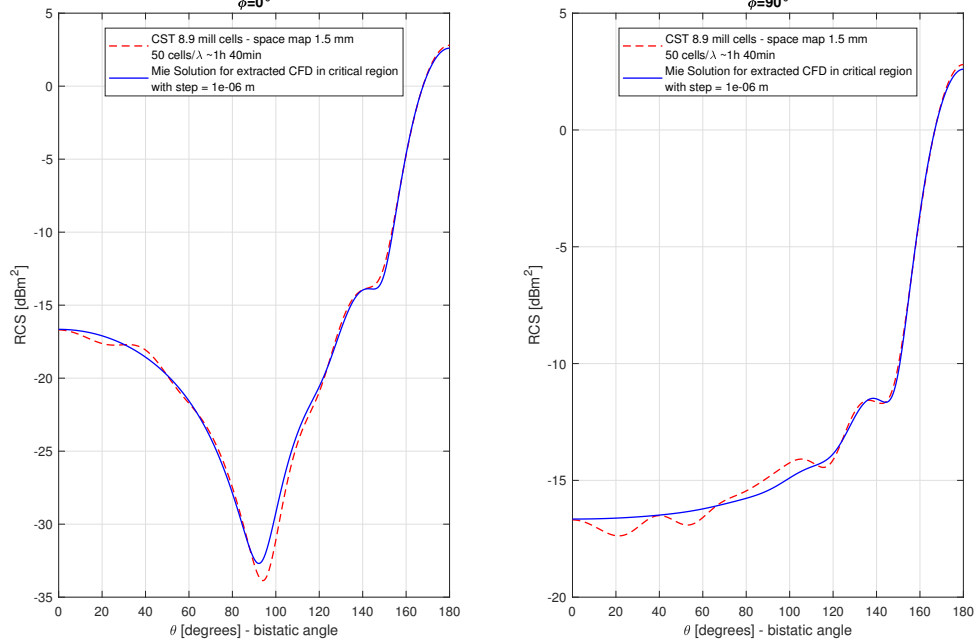


Fig. 5.6 RCS for radial extraction of CFD provided by [1] and at $f = 3$ [GHz]

Bistatic RCS are shown in figure 5.7. We include the vacuum case for comparison. We also show three level of computation grid refinement. The results are quite sensitive to the grid but a resolution of 50 cells per wavelength seems to provide a stable output in particular for the back-scattering value which seems to converge toward a value of about -10 [dBm²].

In comparison with the symmetric case (see figure 5.8) back-scattering is considerable higher and we argue that this is due to the plasma wave as previously described.

5.1.3 PTFE with plasma reproduced by [1] and source angle by 10 degrees

As previously done in vacuum condition, a monostatic RCS is computed from the plasma evaluated by [1], moreover the source plane wave is incident with a monostatic angle $\theta = 10^\circ$, while previously the monostatic angle was $\theta = 0^\circ$ in figure 5.2. Source wave is E_x polarised.

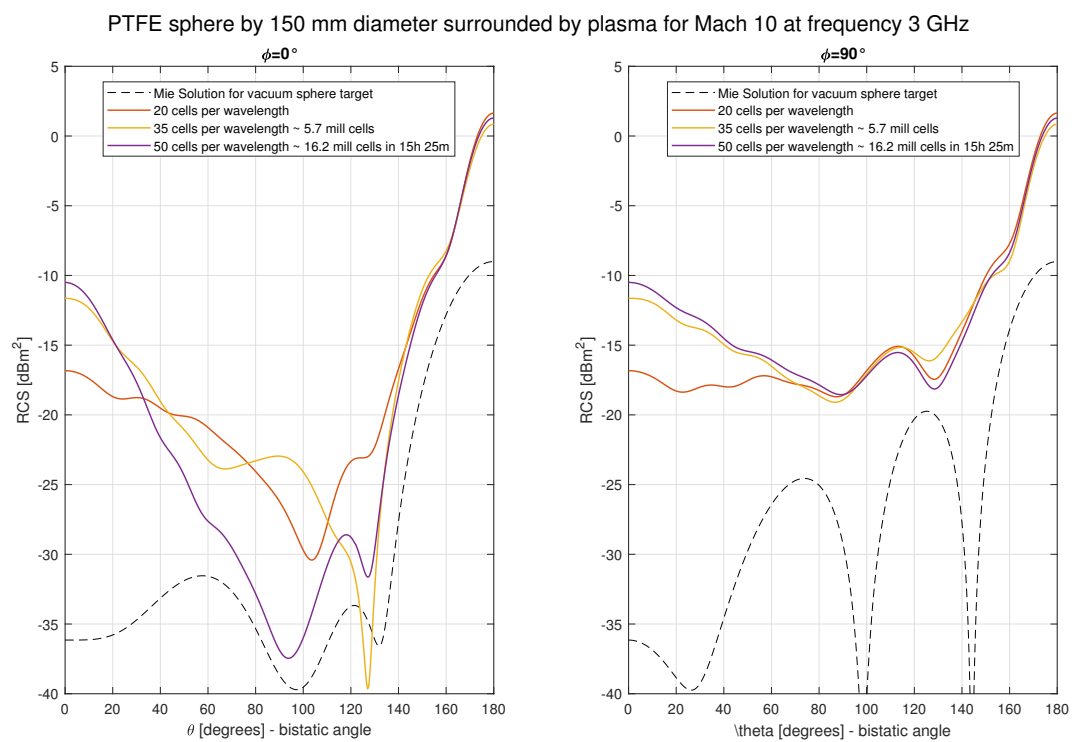


Fig. 5.7 RCS for PTFE sphere of Mach 10 as proposed in [3] with CFD provided by [1] and at $f = 3$ [GHz]

5.2 RCS of simple hypersonic vehicle

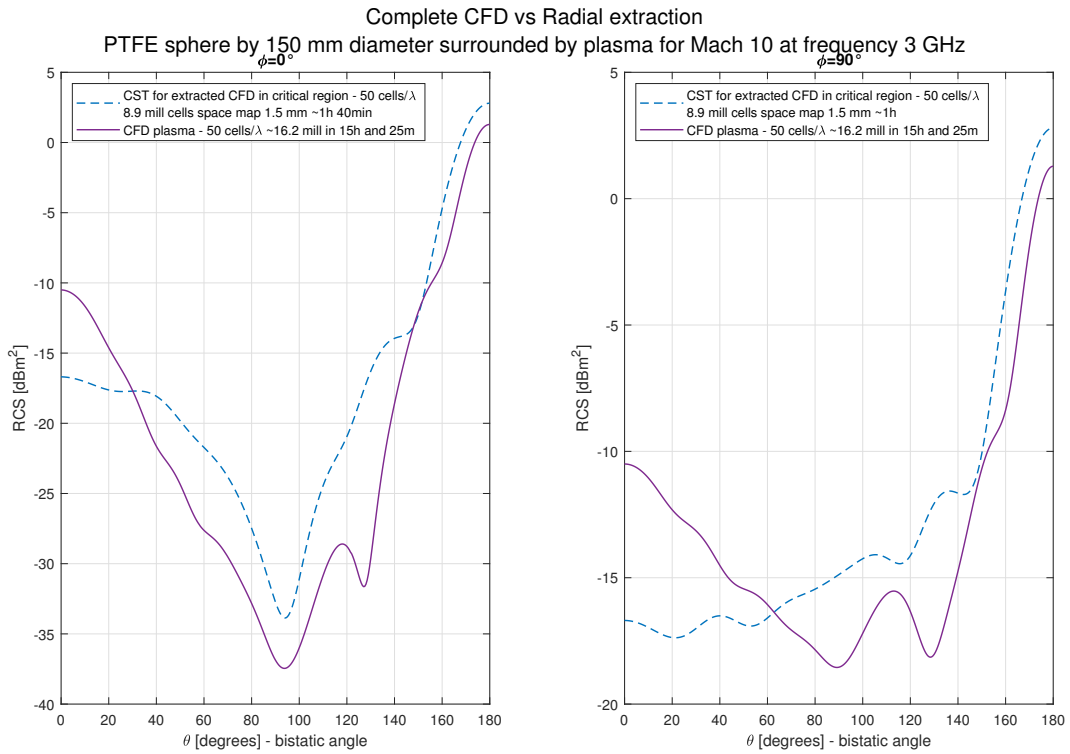


Fig. 5.8 Comparisons between figure 5.6 and figure 5.7

In figure 3 of [3] there is reported the monostatic RCS for $\theta = 10^\circ$ with plasma. Paper reported value is $RCS_{\theta=10^\circ} \approx -16.8[dBm^2]$ and as shown in table 5.2 as resolution increases, monostatic RCS becomes close to the one in [3].

extracted from [3]	thesis simulations results	cells/ λ
$-16.8 [dBm^2]$	$-13.92 [dBm^2]$	20
	$-16.75 [dBm^2]$	40

Table 5.2 Monostatic RCS for $\theta = 10^\circ$ comparison between extraction from figure 3 in [3] and our simulations

5.2 RCS of simple hypersonic vehicle

A step further is given by a model of a simple aerospace vehicle provided by LINK Foundation as shown in figure 5.9a from a CAD model file. The length of the model is 50 cm. From that model there is provided a plasma sheath defined similarly as

described in subsection 2.2.2 for Mach 10 by [1] as shown in figure 5.9b. Another proposed implementation could be a uniform shield of defined complex permittivity.

5.2.1 RCS for hypersonic vehicle in plasma flow

We set a working frequency of 1 [GHz] which is the one of interest both for radar detection and for telecommunication. With this we have an electrical length $k_0 \cdot a \approx 10.5$. This is on the upper end of what we think is doable with the present tool and computational power.

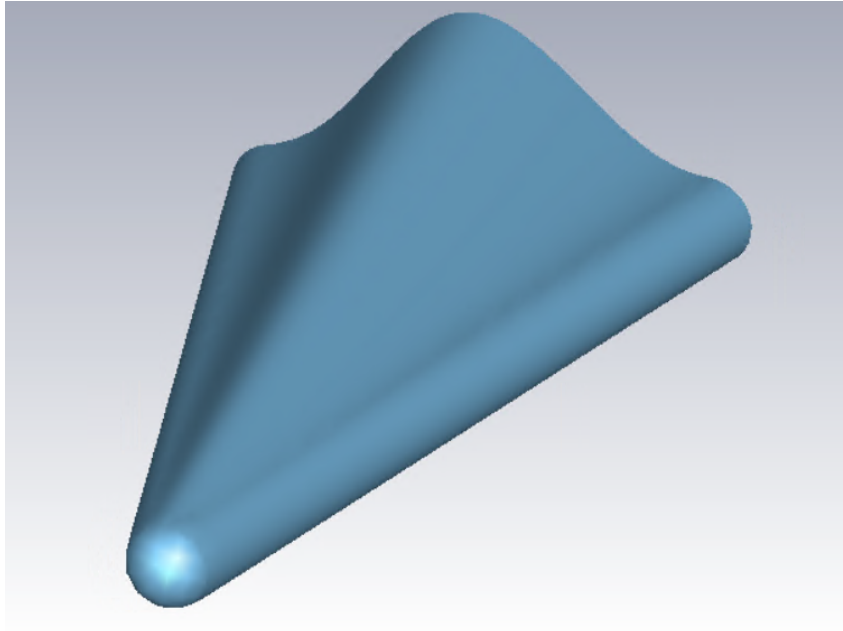
The baseline CFD plasma at Mach 10 has a maximum plasma frequency of about 180 [MHz]. This higher plasma density region is also very localised near the front of the vehicle so that small effects are expected.

Figure 5.10 shows the bistatic RCS for E_x and E_y polarised wave with and without plasmas. The effect of the baseline plasma are indeed found to be negligible. In order to enhance them we artificially multiply the plasma frequency by a fixed factor of 15 and 60 respectively. A factor of fifteen makes the peak plasma frequency of around 2.7 [GHz] that is above the cut-off value. However the cut-off reflective plasma layer is apparently too small to produce any effect as seen in figure 5.10 with the respect of RCS in vacuum.

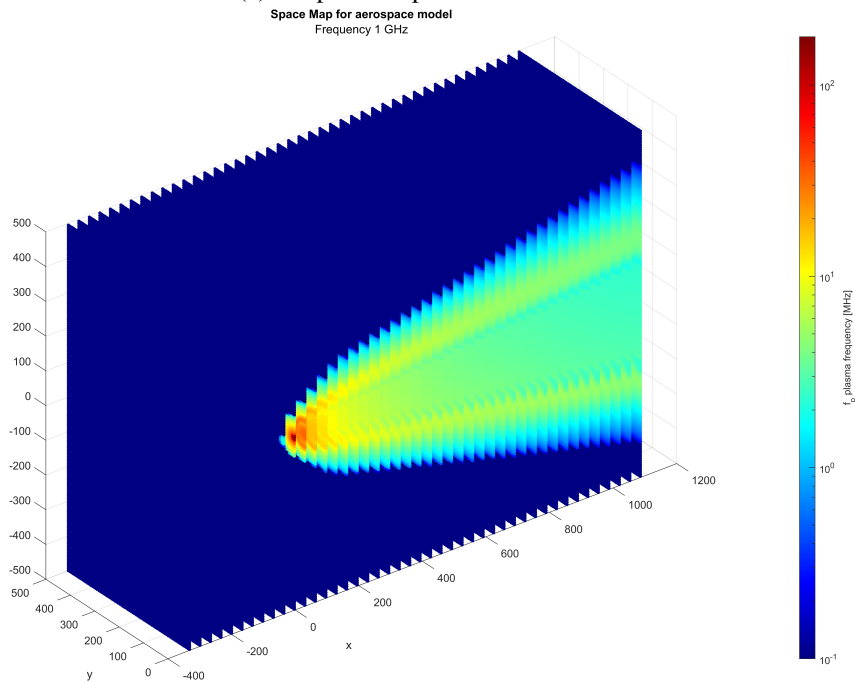
With a multiplication factor of 60 the cut-off layer extends to most of the front part of the vehicle but the rear plasma remain below cut-off. The effect on the RCS is now strong (see dashed line in fig 5.10). For most of the angular range the RCS is reduced compared to vacuum as it is for the particular case of the back-scattering $\theta = 0^\circ$ by several [dBm²]. A reduction in the RCS might be seen as non intuitive results because we are in presence of a reflective layer which should reflect the incoming EM wave similarly as a PEC surface. Here, however, the cut-off layer is thin and localised at the front of the vehicle whereas the rest of the plasma diffract and deflect the radiation in a continuous fashion altering the global scattering properties of the object.

We note also that reduced RCS have been calculated in [14] for similar vehicle geometry and plasma conditions. Nevertheless in [4] it has been shown that a dense plasma with negative real permittivity increases the RCS as expected. In the next section we thus perform a similar test.

5.2 RCS of simple hypersonic vehicle



(a) Simple aerospace vehicle model



(b) Plasma around model in figure 5.9a

Fig. 5.9 Proposed Model and its plasma for Mach 10

RCS of vehicle in PLASMA at 1 GHz -- all polarization -- 25 mill cell

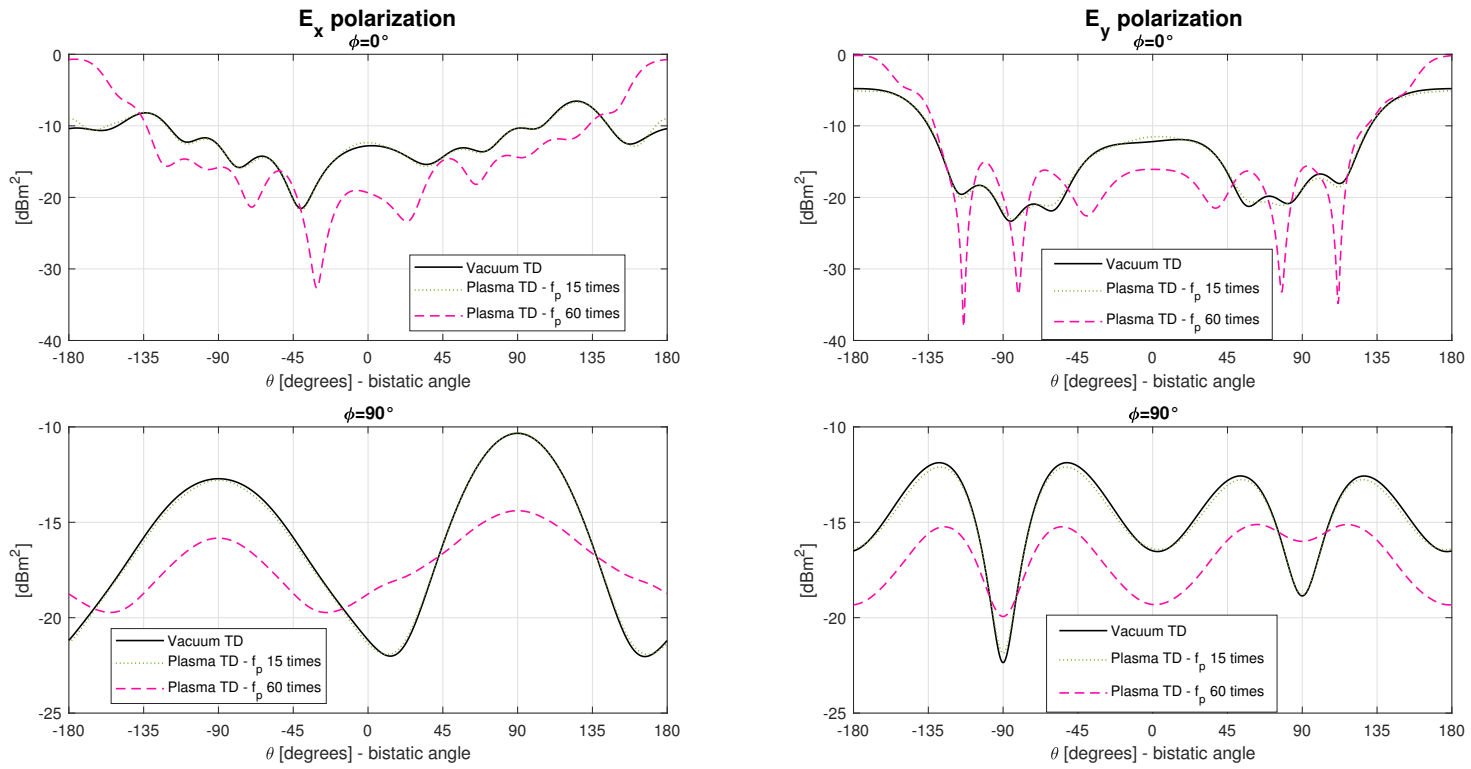


Fig. 5.10 RCS for model in figure 5.9a with multiple plasma frequencies mapped from figure 5.9b with multiplying factor

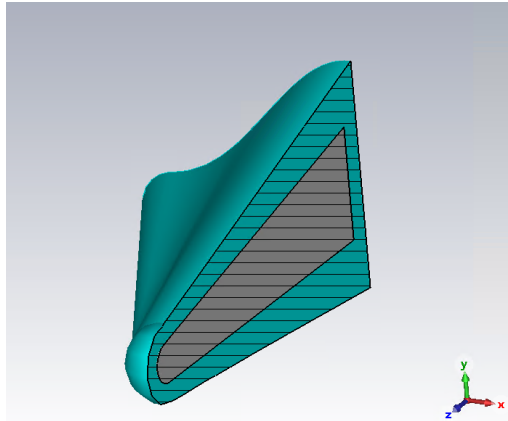


Fig. 5.11 Vehicle surrounded by constant complex permittivity shell - half cut

5.2.2 Negative dielectric permittivity shell around vehicle

A shell is generated such to obtain equivalent $\epsilon_r = -3 + j1 \cdot 10^{-4}$. The shell with constant complex with negative real part permittivity is placed uniformly around the vehicle as shown in figure 5.11.

In 5.13 there are reported the results for proposed model: back-scattering and front-scattering values have increased.

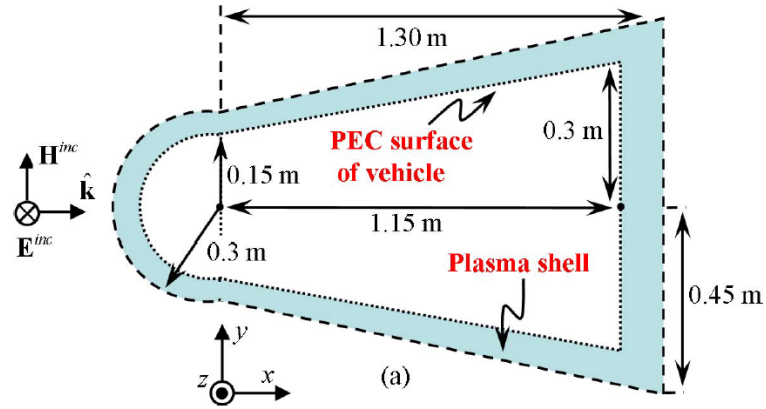
In [4] section III.C there is proposed a geometry close to the one implemented in our simulations and shown in figure 5.12a, then RCS for $f = 600$ [MHz] are reported in figure 5.12b. Length of the model proposed in figure 5.12a is 1.3 m, if there is considered $a = 1.3$ [m] for equation (2.18), therefore equivalent $k_0 \cdot a \approx 16.3$. Plasma is distributed around proposed target as shown in figure 5.12c: up to $\epsilon_r' = -8.2$.

In figure 5.12b back-scattering is for $\theta = -90^\circ$, while front-scattering is for $\theta = +90^\circ$. With a plasma shield in [4] there is clearly shown the mirroring effect that a negative ϵ_r' plasma shell should perform.

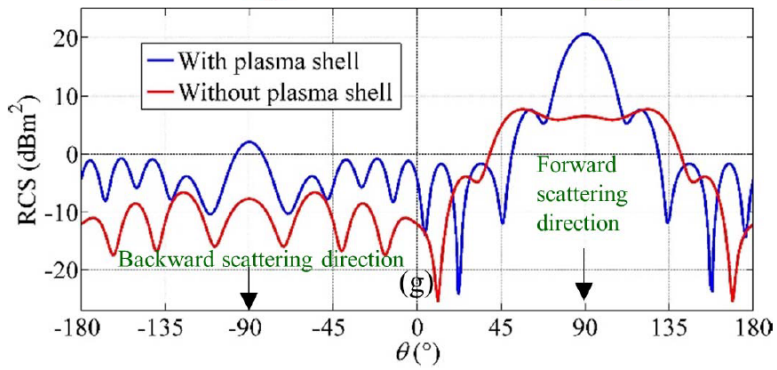
Our simulation met the same condition as proposed in [4].

5.3 Conclusions

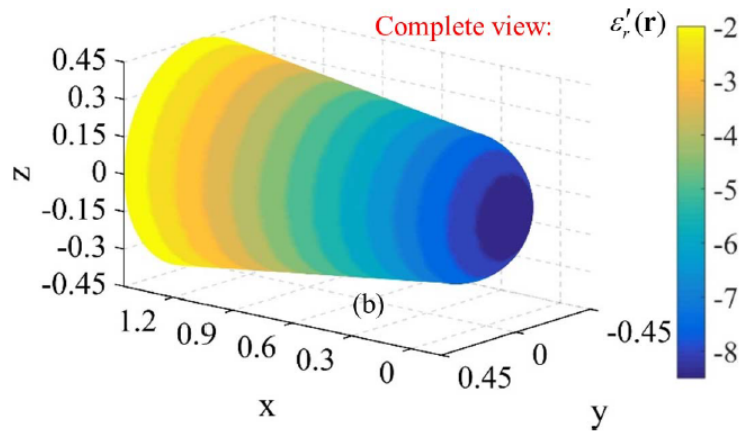
The results in this chapter are reliable for proposed models: the plasma flow modify RCS with the respect of vacuum condition. The evaluated RCS may have higher



(a) figure 7(a) of [4]



(b) figure 7(g) of [4]



(c) Shell of negative ϵ'_r from figure 7(b) of [4]

Fig. 5.12 Model and corresponding RCS for $f = 600[MHz]$ from [4] figure 7

back-scattering values if cut-off condition in shells become considerable, or they may decrease as plasma has a continuous distribution with cut-off condition concentrated in a limited region.

In literature those behaviours are encountered: in [14] for a continuous plasma profile in a model of an hypersonic vehicle there is a decrease of back-scattering as found in subsection 5.2.1 too for the aerospace model proposed in thesis, while in paper [4] the proposed case of a shell with high cut-off behaviour increases back-scattering as obtained in subsection 5.2.2 with our model.

Cut-off behaviour leads the RCS to a reflective layer such as a PEC target, whenever it is consistent.

Finally, in general CST follows a trend for higher resolutions, leading to a possible increase of the accuracy of proposed simulations.

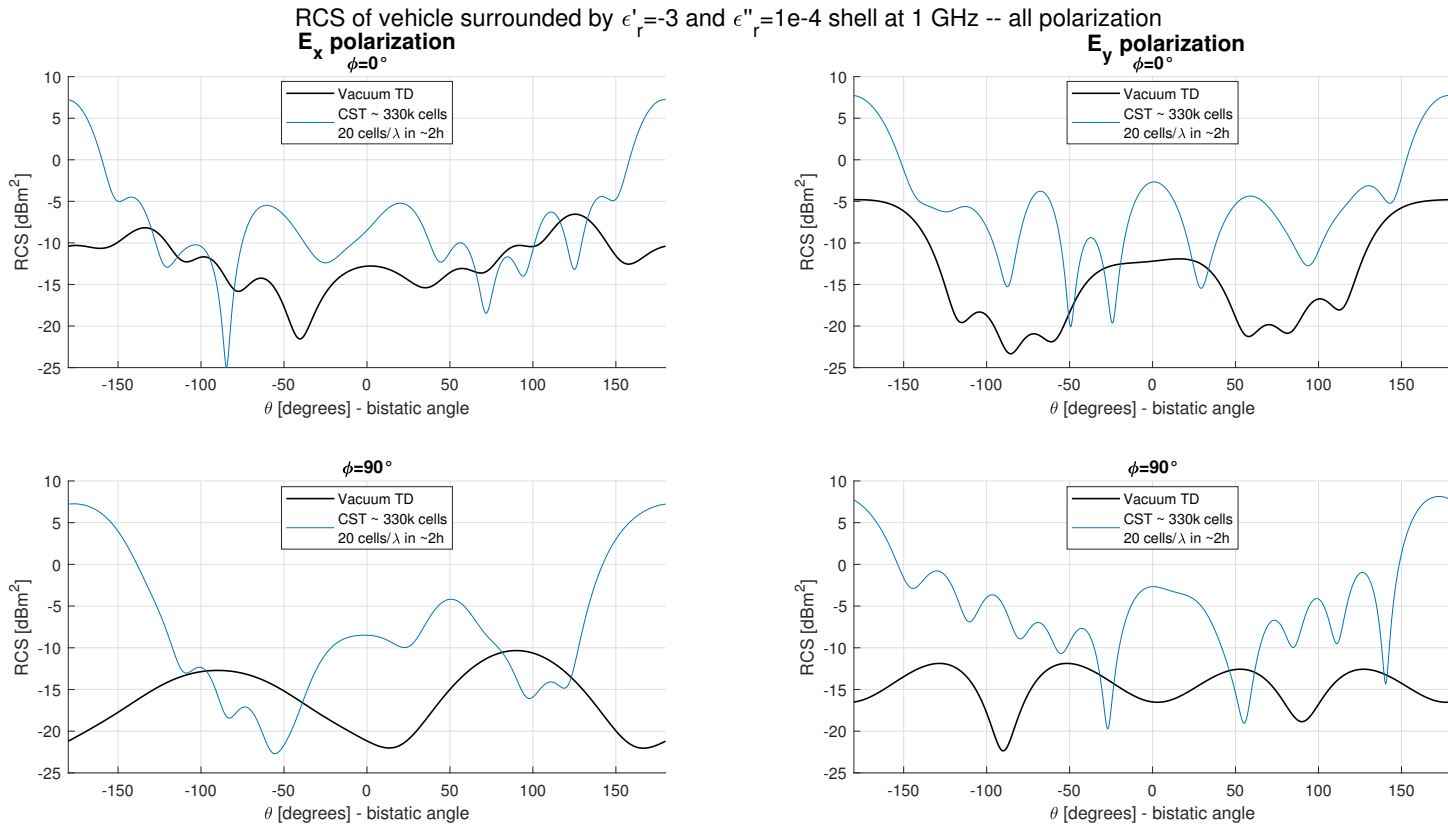


Fig. 5.13 RCS for model in figure 5.9a with negative shell with $\epsilon_r = -3 + j1 \cdot 10^{-4}$ around

Chapter 6

Summary and Conclusions

In this thesis the proposed analysis aims to assess the applicability of the CST Finite Difference Time Domain method to scattering problem with plasma-like dispersive media.

We exploited two way of model definition on CST: one was the solid-based definition, leading whenever occurred to concentric shells of defined dielectric, and the other was the space map material.

Space map material definition of CST is a powerful implementation for plasma dispersive material because the provided CFD by [1] have inhomogeneous distributions of physical quantities, such as dispersive parameters or equivalent permittivity. Moreover implemented parameters require complex values, because the imaginary component for dispersive material, with ν_c , or permittivity, with ϵ_r'' , leads to the stability of the simulations.

The modelling of inhomogeneous analytic plasmas was reported in Chapter 4 in two ways. The first one was with an hard discontinuity with the respect of background vacuum material, in this case unfortunately the RCS evaluated didn't seem to become accurate with the respect of mesh resolution on CST. The second one was with a continuous permittivity profile and in this case obtained results are considered accurate.

More realistic model of hypersonic plasmas were implemented in chapter 5, with analogous plasma distribution and in comparison with other studied models offered by literature, starting from the sphere proposed in [3] and then with a simple model

Summary and Conclusions

for a vehicle. The first plasma implementation was closer to realistic behaviour of hypersonic crafts, and it was extracted through CFD provided by [1]. The second implementation, inspired by [4], was a shell of uniform permittivity with strong cut-off condition.

Whenever a diffused and a relevant cut-off condition was met around the tested target, an RCS behaviour such a reflective layer was found thus increasing the back-scattering value. Moreover from provided CFD the cut-off condition is distributed principally on a limited region close to the front of the vehicle, while toward the rear this behaviour tends to disappear, therefore the evaluated RCS may have a lower back-scattering value due to altered scattering because the plasma shape may generate deflection and diffraction.

In conclusion obtained results are considered reliable and the cited literature reports similar cases that are comparable to our simulations. Proposed realistic models satisfies RCS behaviour in comparison with cited literature.

References

- [1] Salvatore Esposito. Radio communication and radar tracking of object in hypersonic suborbital flight. PhD thesis to be published. University of Politecnico di Torino.
- [2] Merrill I. Skolnik. *Introduction to Radar Systems*. McGraw-Hill Book Company, 2nd edition, 1981.
- [3] René Petervari, Alexander Nekris, and Tanja Bieker. Numerical Analysis of Radar-Plasma-Signatures of a Sphere in a Mach 10 Hypersonic Wind Tunnel Flow. In *2021 18th European Radar Conference (EuRAD)*, pages 86–89, 2022.
- [4] Abdulkadir C. Yucel, Luis J. Gomez, and Eric Michielssen. Internally Combined Volume-Surface Integral Equation for EM Analysis of Inhomogeneous Negative Permittivity Plasma Scatterers. *IEEE Transactions on Antennas and Propagation*, 66(4):1903–1913, 2018.
- [5] David M. Pozar. *Microwave Engineering*. John Wiley & Sons, Inc., 4th edition, 2012.
- [6] Fawwaz T. Ulaby, Umberto Ravaioli. *Fundamentals of Applied Electromagnetics*. Pearson, 7th edition, 2014.
- [7] George T. Ruck, Donald E. Barrick, William D. Stuart, Clarence K. Krichbaum. *Radar Cross Section Handbook*. Peninsula Publishing, 1970, reprint 2002.
- [8] Dassault Systèmes. CST Microwave Studio guide, 2019-2022.
- [9] Walton Gibson (2023). Scattered Field of a Conducting and Stratified Spheres (<https://www.mathworks.com/matlabcentral/fileexchange/20430-scattered-field-of-a-conducting-and-stratified-spheres>), MATLAB Central File Exchange. Retrieved April 3, 2023.
- [10] Jian-Ming Jin. *Theory and Computation of Electromagnetic Fields*. IEEE press - Wiley, 2nd edition, 2015.
- [11] Simon Ramo, John R. Whinnery, Theodore Van Duzer. *Fields and Waves in Communication Electronics*. John Wiley & Sons, 3rd edition, 1994.

References

- [12] Henry Giddens (2023). hgiddens/CST_App (https://github.com/hgiddens/CST_App), GitHub. Retrieved April 3, 2023.
- [13] Andrea Scarabosio, Javier Leonardo Araque Quijano, Jorge Tobon, Marco Righero, Giorgio Giordanengo, D. D'Ambrosio, L. Walpot, and Giuseppe Vecchi. Radiation and Scattering of EM Waves in Large Plasmas Around Objects in Hypersonic Flight. *IEEE Transactions on Antennas and Propagation*, 70(6):4738–4751, 2022.
- [14] Ji-Wei Qian, Hai-Li Zhang, Ming-Yao Xia, Modelling of Electromagnetic Scattering by a Hypersonic Cone-Like Body in Near Space, *International Journal of Antennas and Propagation*, vol. 2017, Article ID 3049532, 11 pages, 2017.

Appendix A

Homogeneous dielectric - spheres in vacuum - $k_0 \cdot a \approx 31.4$

In this appendix there are reported simulations on homogeneous dielectric spheres in vacuum background. Settings are the same as reported in subsection 3.2.4: source is a plane wave with electric field component along \hat{x} axis and propagating toward $-\hat{z}$ direction, while for equation (2.18) $k_0 \cdot a \approx 31.4$ as proposed in [13] section III.A: radius is $a = 2$ [m] and $f = 750$ [MHz]. Main solver adopted is Time Domain one, but Integral Equation Solver might be adopted as a reliable alternative. Following materials are implemented for spheres:

- PEC¹ sphere
- PTFE² sphere with $\epsilon_r = 2.1$ and two different geometries are considered:
 - filled material
 - hollowed with 5 mm thickness

Integral equation is a reliable solver and it makes a discretization on surface. This solver is implemented in this appendix as a more refined solution given by commercial software CST.

A recall on scattering definition is done from 3.2.4: *back-scattering* is the region for $\theta = 0$ [degrees] and *front-scattering* for $\theta = 180$ [degrees].

¹Perfect Electric Conducting

²Polytetrafluoroethylene

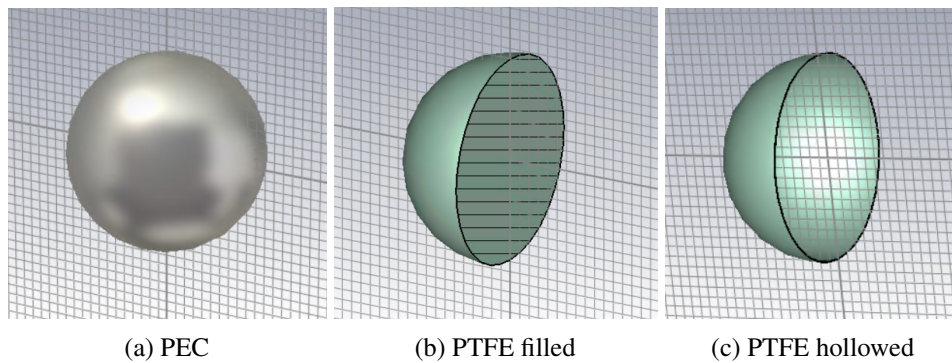


Fig. A.1 Sphere in vacuum CAD Models in CST

A.1 PEC sphere CAD model

First simulation is implemented on a PEC sphere in vacuum. In figure A.2 there are scattering solved in Time Domain and simulation have taken about 15 minutes, moreover the one more refined elapsed in 20 minutes. Mie Solution, the most reliable one, makes an evidence on back-scattering limitation on TDFD based solver, because in this simple case in vacuum background the differences from analytic solution have met yet.

CST allows Integral Equation Solver and scattering evaluation is reported in figure A.3: in this case the back-scattering is closer to Mie Solution.

A.2 PTFE sphere CAD model

Target material may be changed in a more realistic model: PTFE is a widely spread material in aerospace and may be implemented as target dielectric in atmospheric tracking analysis.

A.2.1 PTFE Filled sphere CAD model

Primarily PTFE sphere is filled and RCS evaluated with specified dielectric are reported in figure A.4 for Time Domain Solver and in figure A.5 for Integral Equation Solver: back-scattering in Mie Solution is lower than PEC sphere. On CST the RCS

is close to Mie Solution, but back-scattering is still not coincident with the respect of analytic solution provided through Mie Series.

A.2.2 PTFE Hollowed sphere CAD model

Targets does not have full filled dielectric and aerospace craft are detected by their sheath: a more rigorous model is a cavity inside PTFE sphere analysed in previous subsection. As shown in figure A.6 radar scattering decreases in a remarkably way, leading to an unideal detection.

Back-scattering evaluation through CST software is unideal, even for Integral Equation Solver as shown in figure A.6. Front-scattering track is lost as well in Time Domain Solver.

Comparison between CST Time Domain Solver and mie scattering of a PEC sphere with $ka=31.4377$
at frequency 750 MHz in ~15/20 minutes

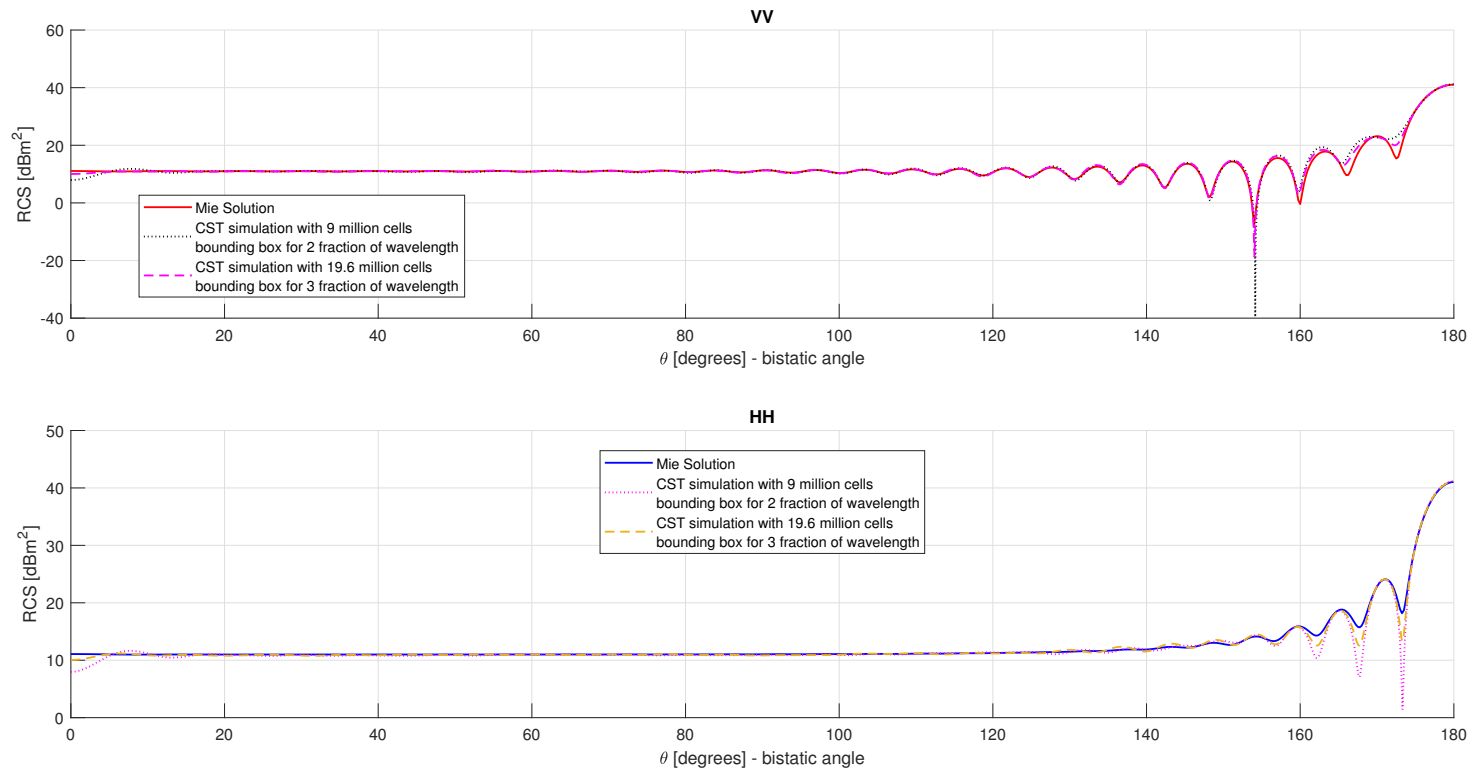


Fig. A.2 Time Domain Solver for PEC sphere with $k_0 \cdot a \approx 31.4$

Comparison between CST Integral Equation Solver and mie scattering of a PEC sphere with $ka=31.4377$ at frequency 750 MHz in ~5 minutes

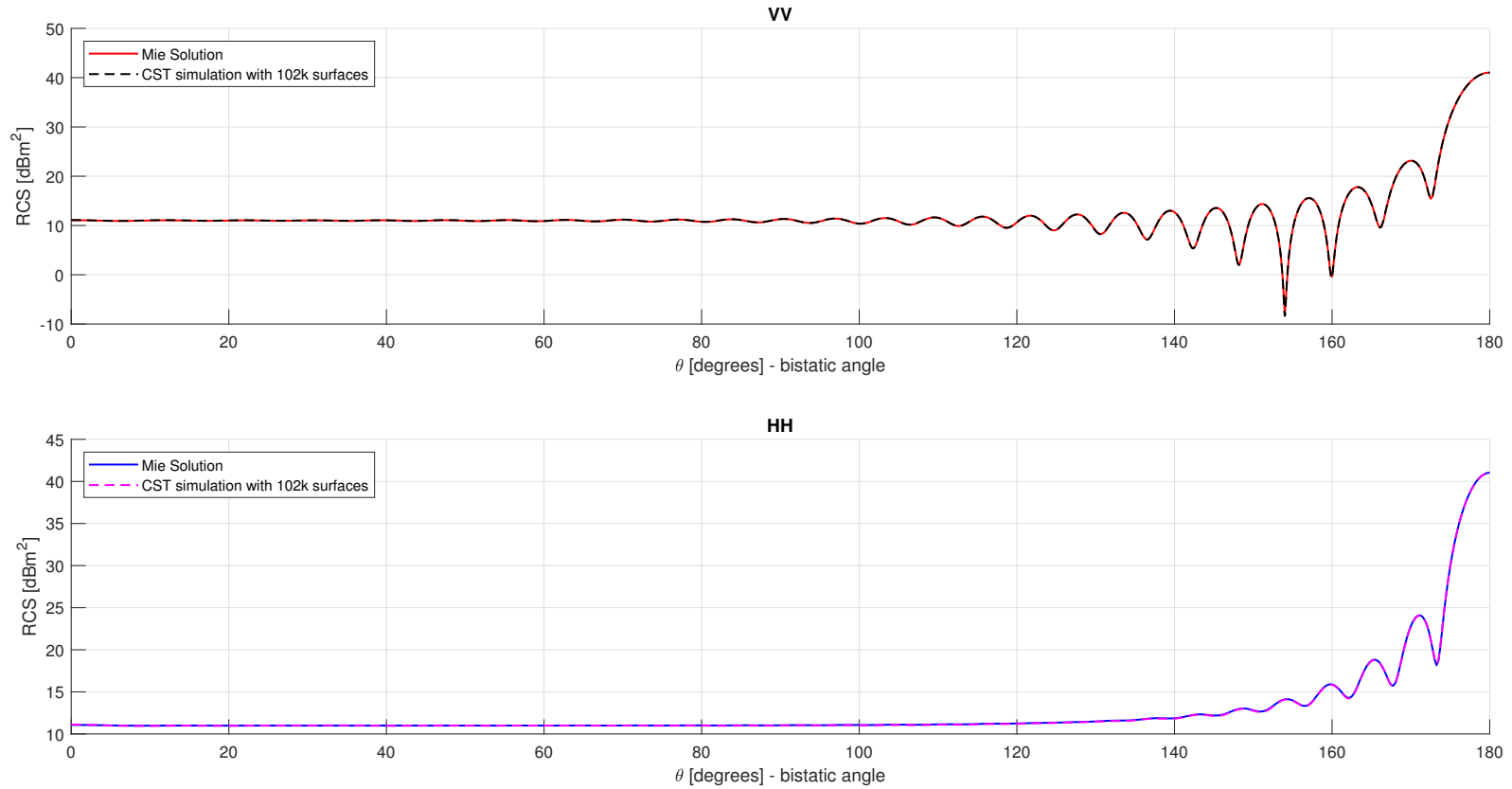


Fig. A.3 Integral Equation Solver for PEC sphere with $k_0 \cdot a \approx 31.4$

Comparison between CST Time Domain Solver and mie scattering of a filled PTFE sphere with $ka=31.4377$ at frequency 750 MHz

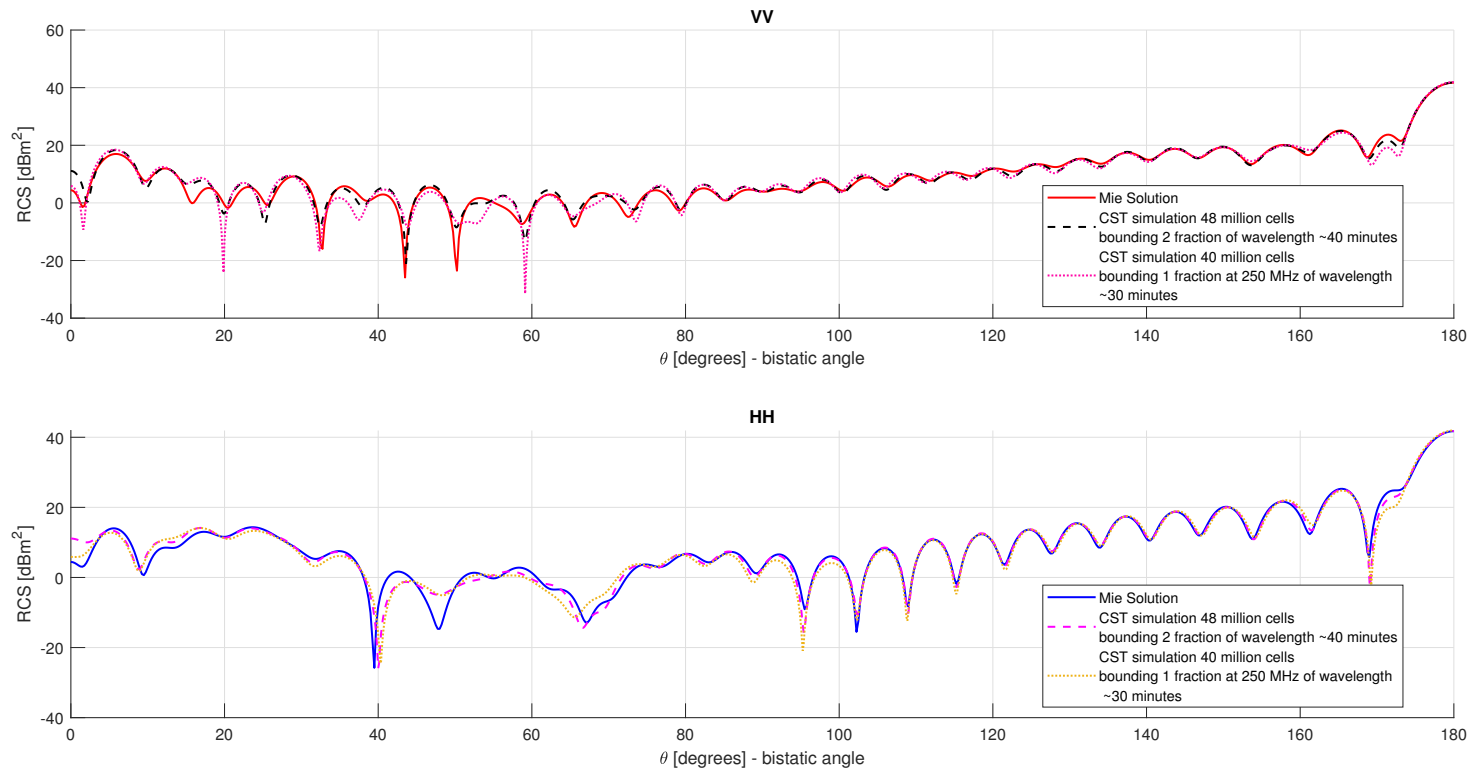


Fig. A.4 Time Domain Solver for PTFE filled sphere with $k_0 \cdot a \approx 31.4$

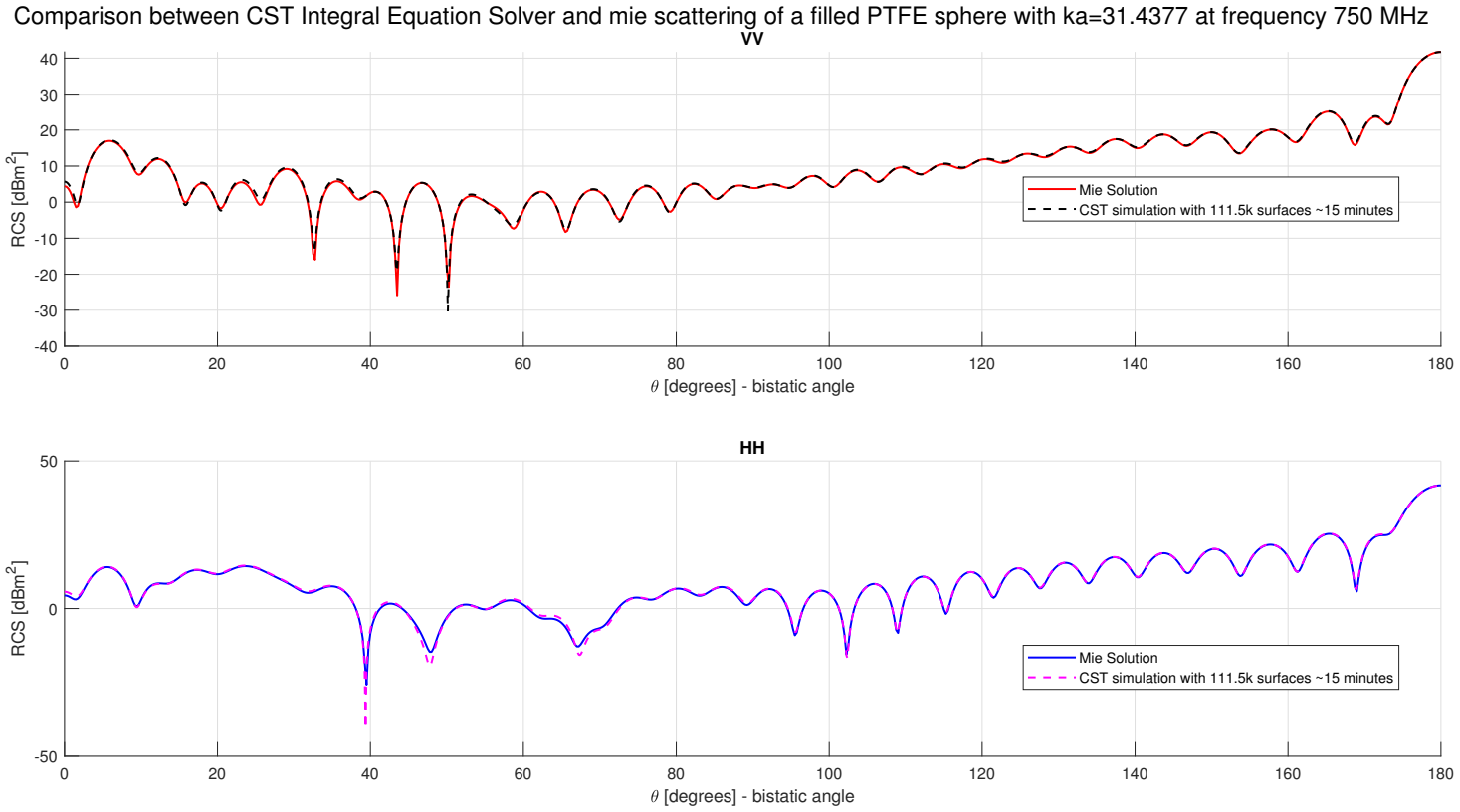


Fig. A.5 Integral Equation Solver for PTFE filled sphere with $k_0 \cdot a \approx 31.4$

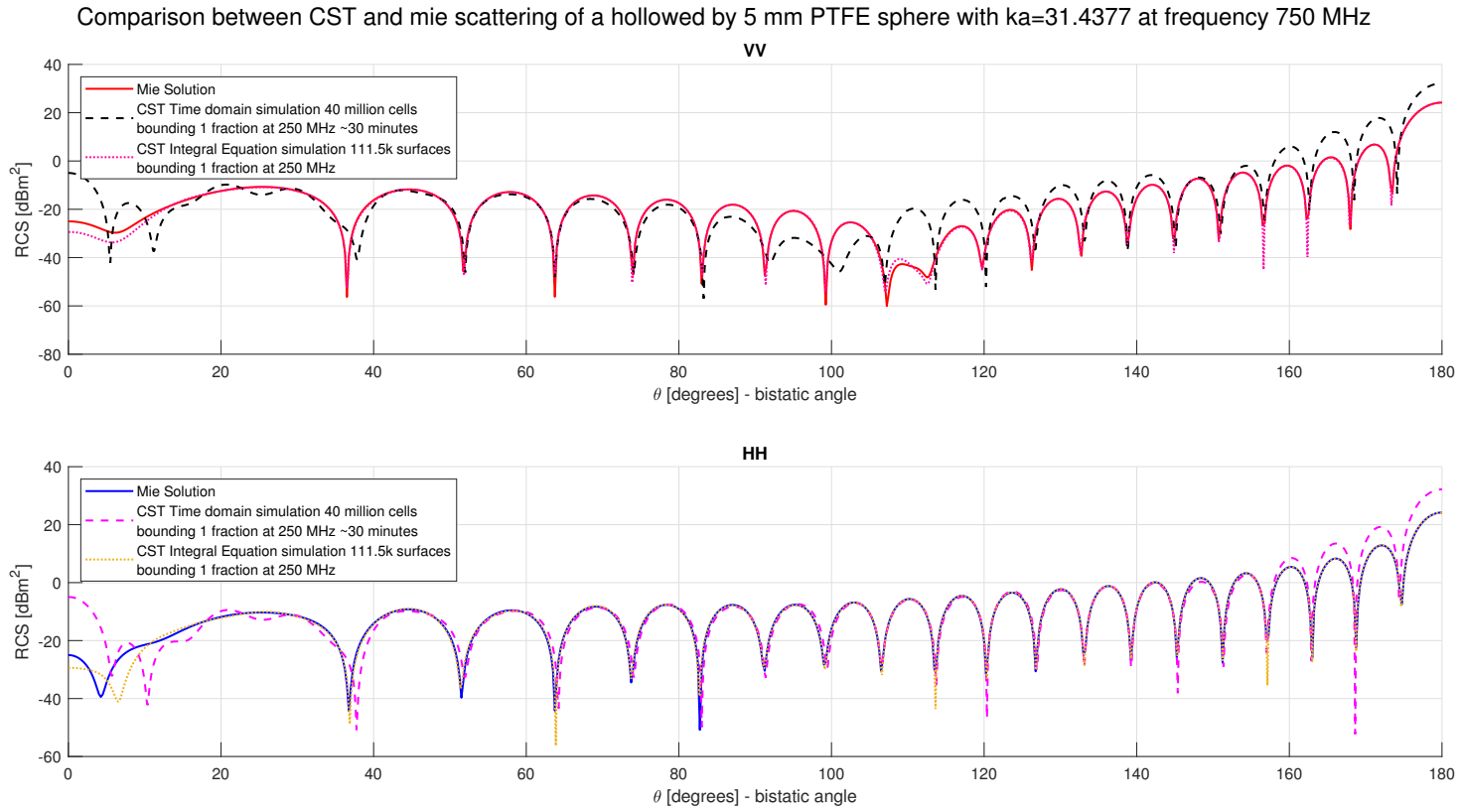


Fig. A.6 RCS of PTFE hollowed sphere in vacuum

A.3 PTFE filled sphere space map material

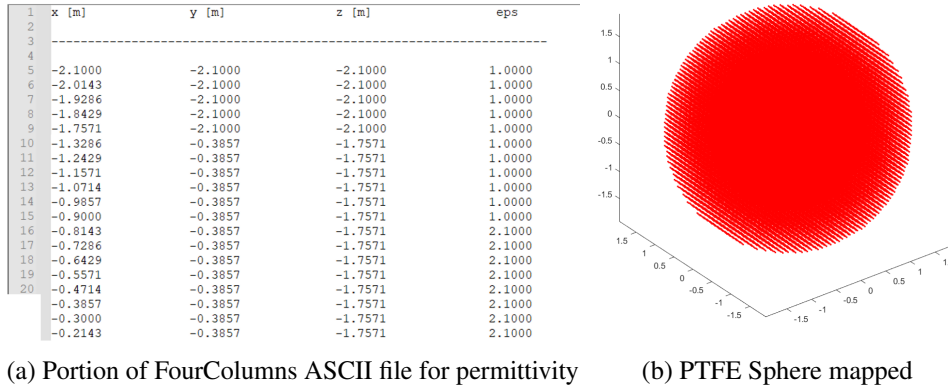


Fig. A.7 Instance of space map for a filled PTFE sphere by 2 meter radius

A.3 PTFE filled sphere space map material

Proposed geometry of PTFE filled sphere with 2 meter radius is implemented with space map material and in figure A.7 there is reported the behaviour of generated files for permittivities mapped in space, then in table A.1 there are reported widths and size of generated files in Byte.

Generated space map material has permittivity distribution of the spheres inside a box of vacuum permittivity, such giving continuity with background condition: this box is set by 10 cm thickness.

$f = 750 \text{ [MHz]} \Rightarrow \lambda_0 = c/f \approx 399.7 \text{ [mm]}$					
run order	1	2	3	4	5
Width [mm]	86	42	29.9	18	10
λ_0/width	≈ 4.65	≈ 9.52	≈ 13.4	≈ 22.2	≈ 40
Number of points	$125 \cdot 10^3$	$1.03 \cdot 10^6$	$2.6 \cdot 10^6$	$14.7 \cdot 10^6$	$74.6 \cdot 10^6$
File size	7.70 MB	64.3 MB	164 MB	918 MB	4.55 GB

Table A.1 Trends for different runs of space mapped permittivity for a PTFE filled sphere of 2 meter radius in width and ASCII generated file size

As shown in figure A.8 CAD model on CST is closer to Mie Solution than space map material. CST microwave studio software interpolates the imported space mapped material, thus leading to a less ideal model than CAD defined one. In figure A.9 there are reported space map models up to a width of 18 mm: bistatic angle has

Homogeneous dielectric - spheres in vacuum - fixed ka around 31.4

a defined trend with different behaviour from Mie Solution in few regions, but back-scattering becomes closer to analytic defined one with very low width. This may be a limit, because as seen in table A.1 extracted files for space map implementation may reach very high size.

A.4 Conclusions on homogeneous dielectric sphere EM evaluation in vacuum

These results reported in appendix are preliminary analyses for radar tracking: simulations explain main features and limits of TDFD software and CAD based EM simulators, such as back-scattering and front-scattering values and size of generated ASCII file.

Every model analysed in analytic solvers is an ideal model and whichever aircraft in atmosphere should remarkably change behaviour from PEC material analysis and from an only vacuum background condition.

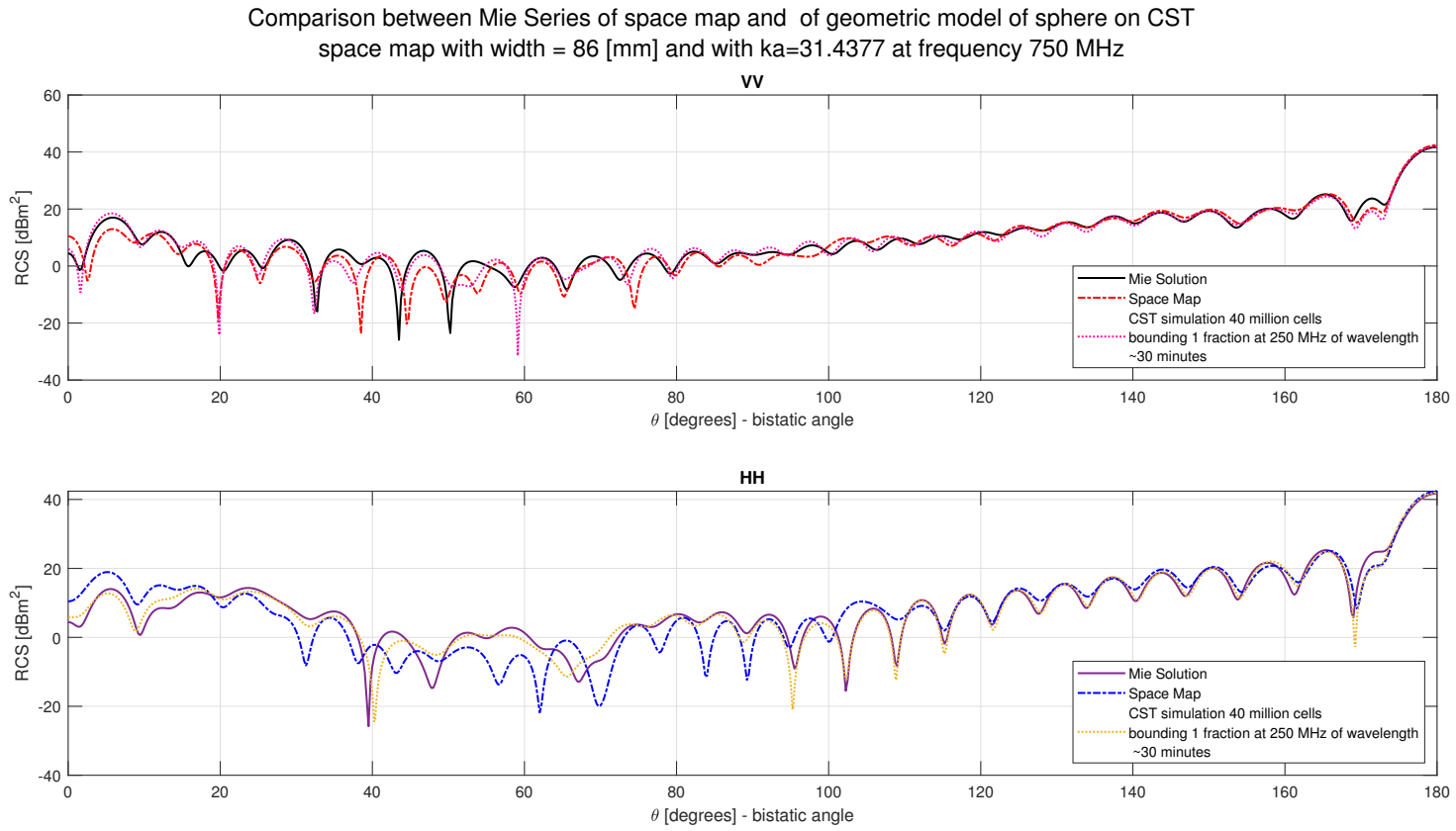


Fig. A.8 RCS of filled PTFE sphere space mapped with width on run1 in table A.1 and a CST simulation with CAD model

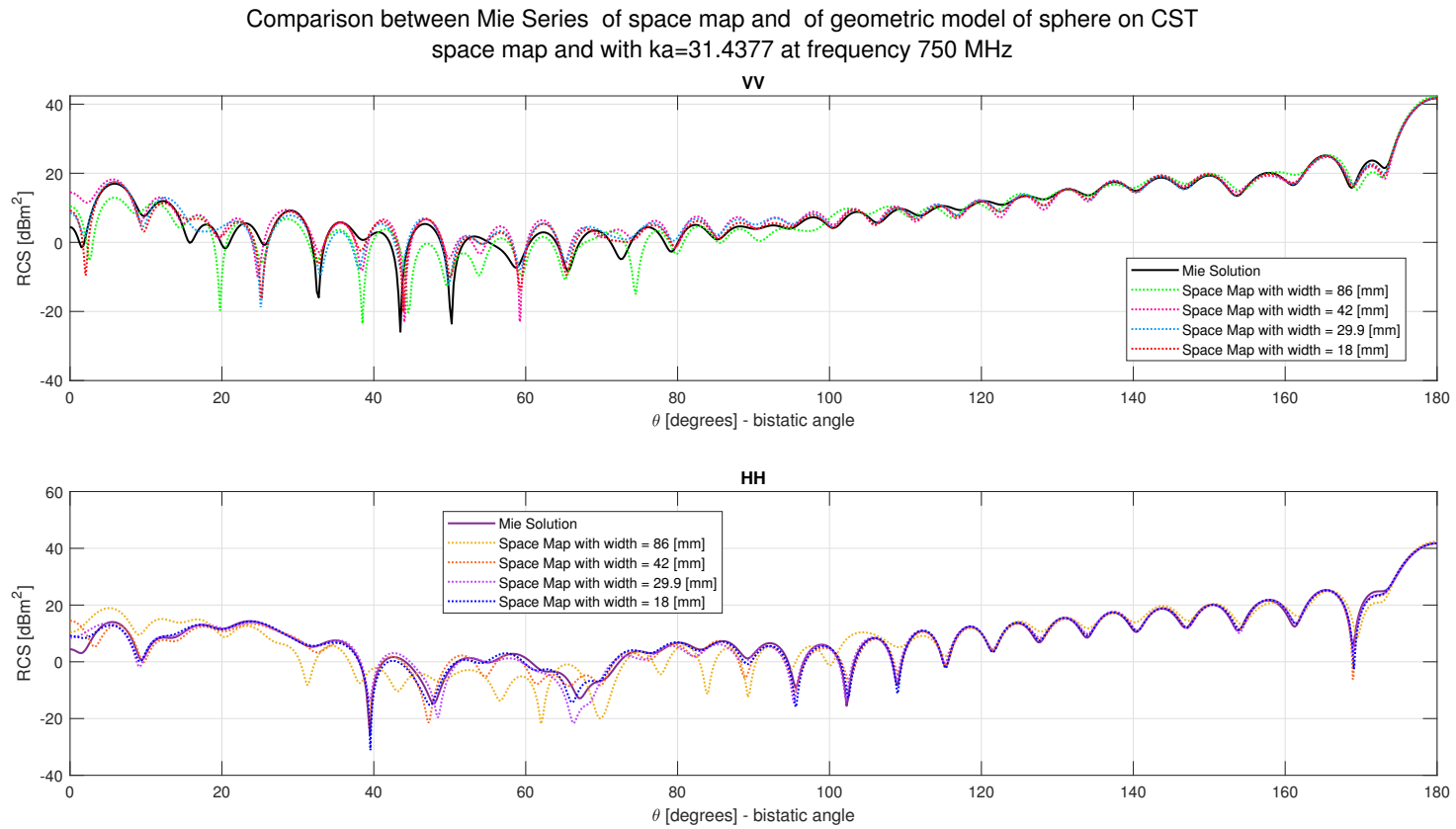


Fig. A.9 RCS of filled PTFE sphere space mapped with all widths reported in table A.1

Appendix B

Mie Solution for section 4.2 and imaginary component ϵ_r'' contribution

In this appendix the focus is on the analytic solution for proposed permittivity distribution related to equation 4.1 with ϵ_c variable implemented as in section 4.2:

- $\epsilon_c = 0.5$
- $\epsilon_c = 0.1$
- $\epsilon_c = -0.1$

B.1 Mie Solution evaluation

Relative permittivities toward PEC sphere surface are lower than $\epsilon_r = 1$ and they could be zero or negative values, therefore Mie Solution may oscillate: maximum number of harmonics should be as higher as possible and input permittivity distribution defined in equation (4.1) tends to be very tiny for accurate solution. In this subsection it is analysed the input dielectric required minimum step and imaginary component estimation for a correct Mie Solution: worst case is the one with highest $k_0 \cdot a$ parameter, belonging to highest working frequency, in this case set as $f = 250$ [MHz] with $k_0 \cdot a \approx 15.7$.

Mie Solution for continuous permittivity distribution and imaginary component of relative permittivity contribution

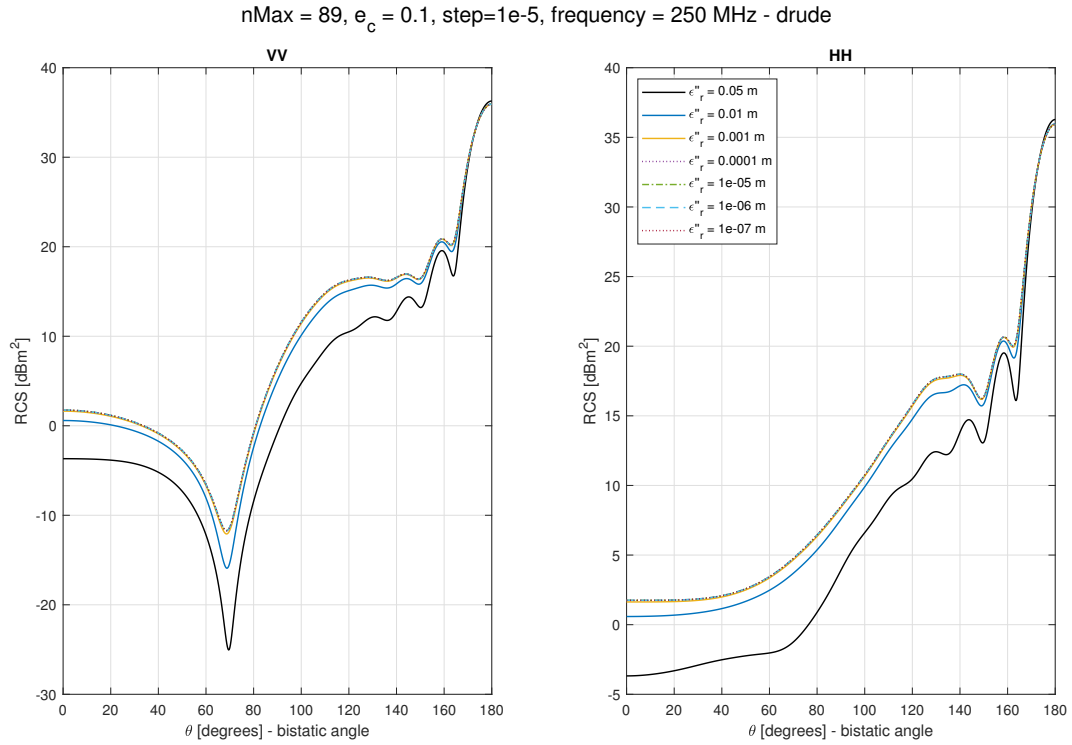


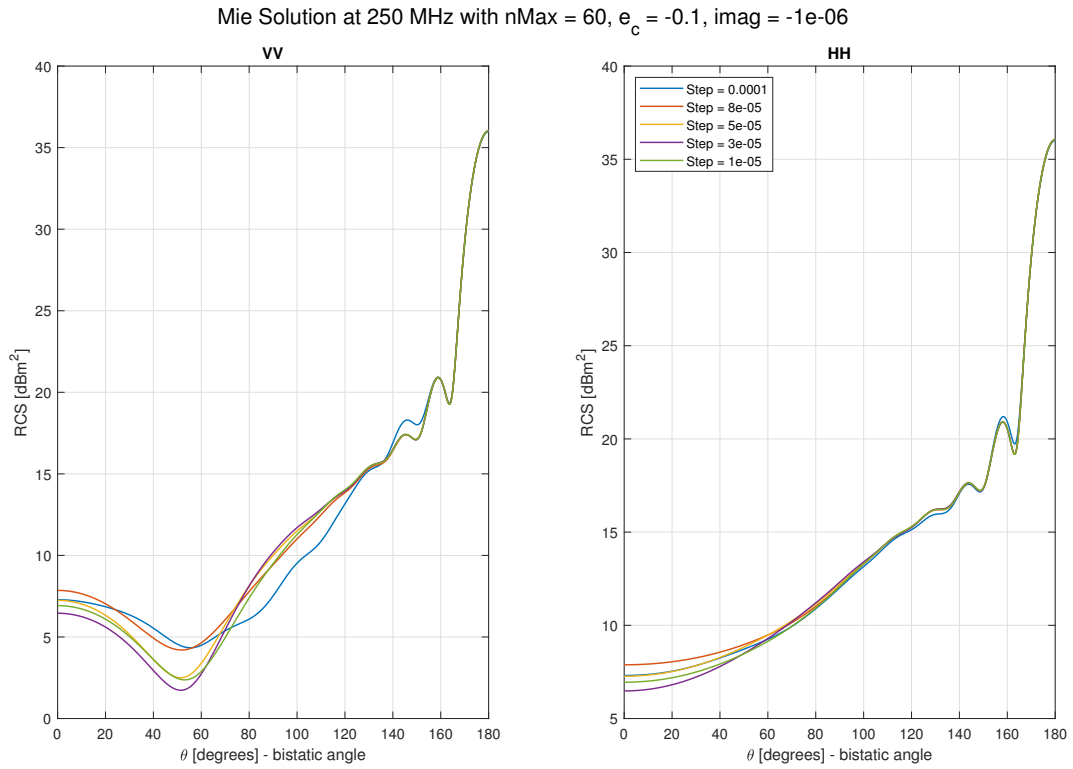
Fig. B.1 Convergence for imaginary part implementation for $\epsilon_c = 0.1$ in distribution equation (4.1)

B.1.1 Imaginary component contribution

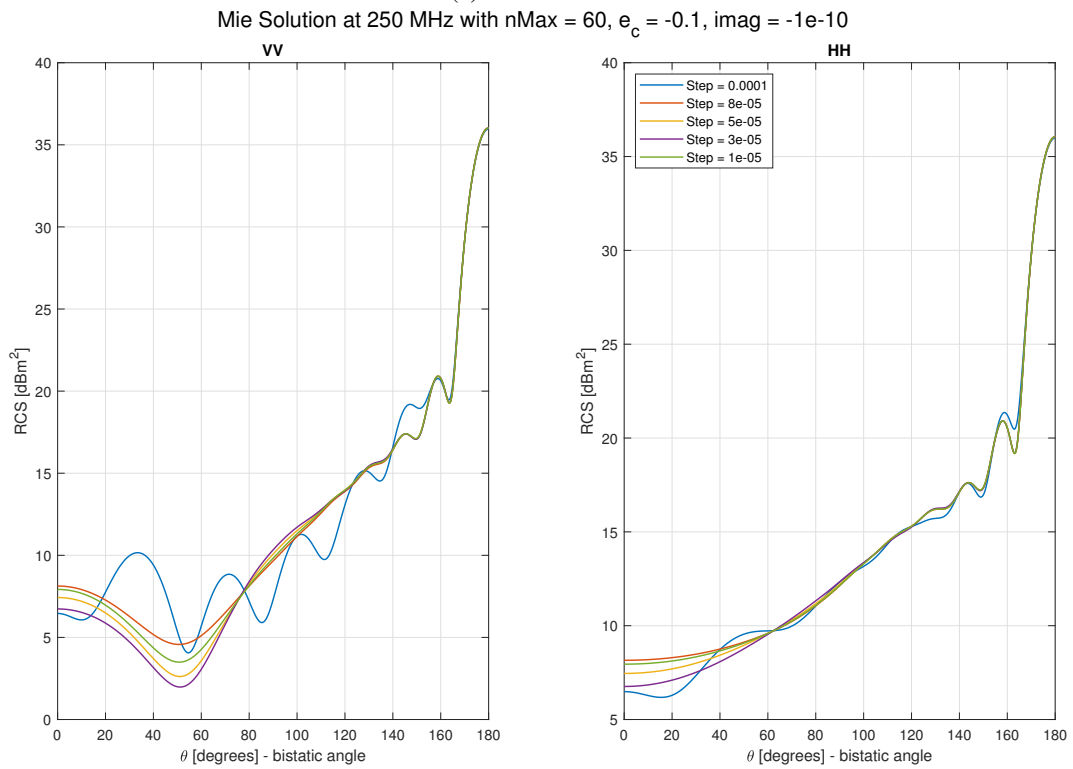
Permittivity is a complex quantity as mentioned in subsection 2.1.2: imaginary component may improve computation and should be implemented even for negligible ϵ_r'' . In figure B.1 there is shown how an imaginary component may change RCS behaviour from equation (4.1) with $\epsilon_c = 0.1$ for fixed step: higher imaginary components change behaviour of Mie Solution, while from $\epsilon_r'' = 1 \cdot 10^{-3}$ accuracy is reached.

In figure B.2 there are reported RCS for $\epsilon_c = -0.1$ and frequency $f = 250$ [MHz], worst case for implemented distribution in terms of oscillation due its negative permittivities towards target surface. A small imaginary quantity might be implemented in order to avoid RCS remodelling, so in figure B.2b proposed quantity is $\epsilon_r'' = 1 \cdot 10^{-10}$, but RCSs oscillate even for tiny steps, therefore an higher term is proposed such as $\epsilon_r'' = 1 \cdot 10^{-6}$ leading to lower oscillations but still not converging results. Finally the chosen imaginary component is $\epsilon_r'' = 1 \cdot 10^{-4}$.

B.1 Mie Solution evaluation



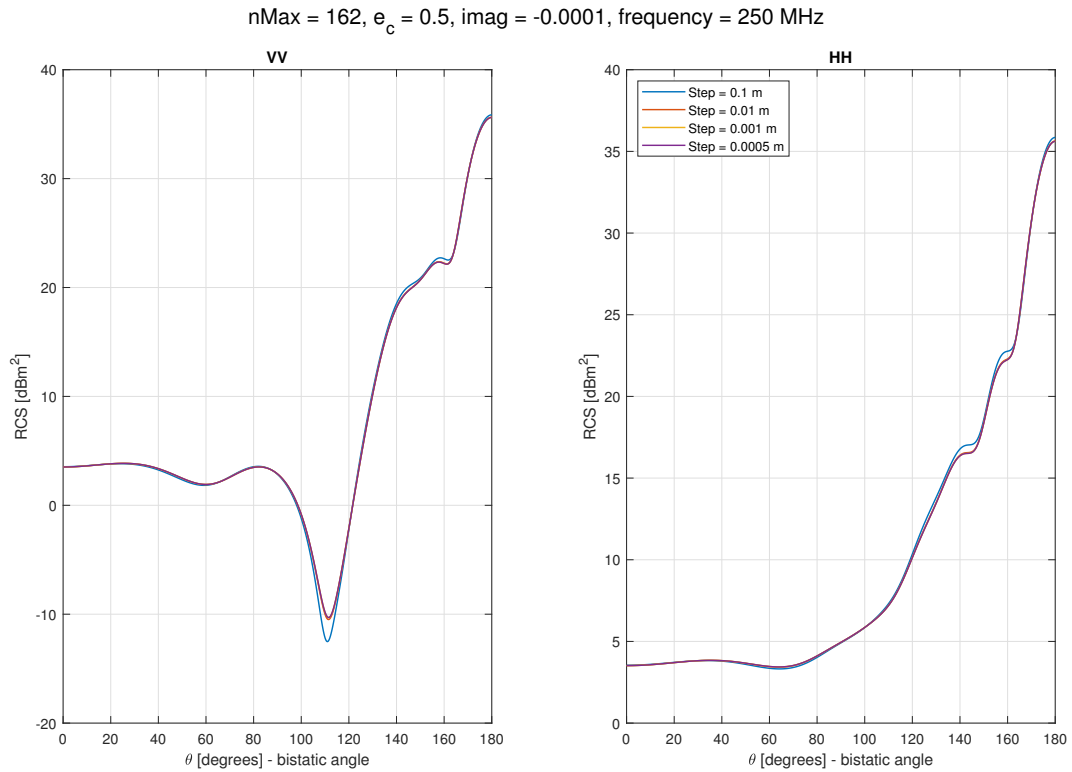
(a) $\epsilon'' = 1 \cdot 10^{-6}$



(b) $\epsilon'' = 1 \cdot 10^{-10}$

Fig. B.2 RCS of ϵ_r from equation (4.1) Mie Solution with $\epsilon_c = -0.1$ and additive imaginary component

Mie Solution for continuous permittivity distribution and imaginary component of relative permittivity contribution



B.1.1.1 Step for input dielectric

Estimation of correct Mie Solution has to be done with a very refined input step thus giving accuracy in results.

$$\epsilon_c = 0.5$$

Simplest case is for positive and large permittivities, and as shown in figure B.3 accuracy occurs from a $step = 10$ [cm] with 162 maximum number of harmonics.

$$\epsilon_c = 0.1$$

In this case permittivities are still positive, but towards a value very close to zero. In figure B.4 accuracy is similar to previous case: $step = 10$ [cm] with 162 number of maximum harmonics.

$$\epsilon_c = -0.1$$

B.1 Mie Solution evaluation

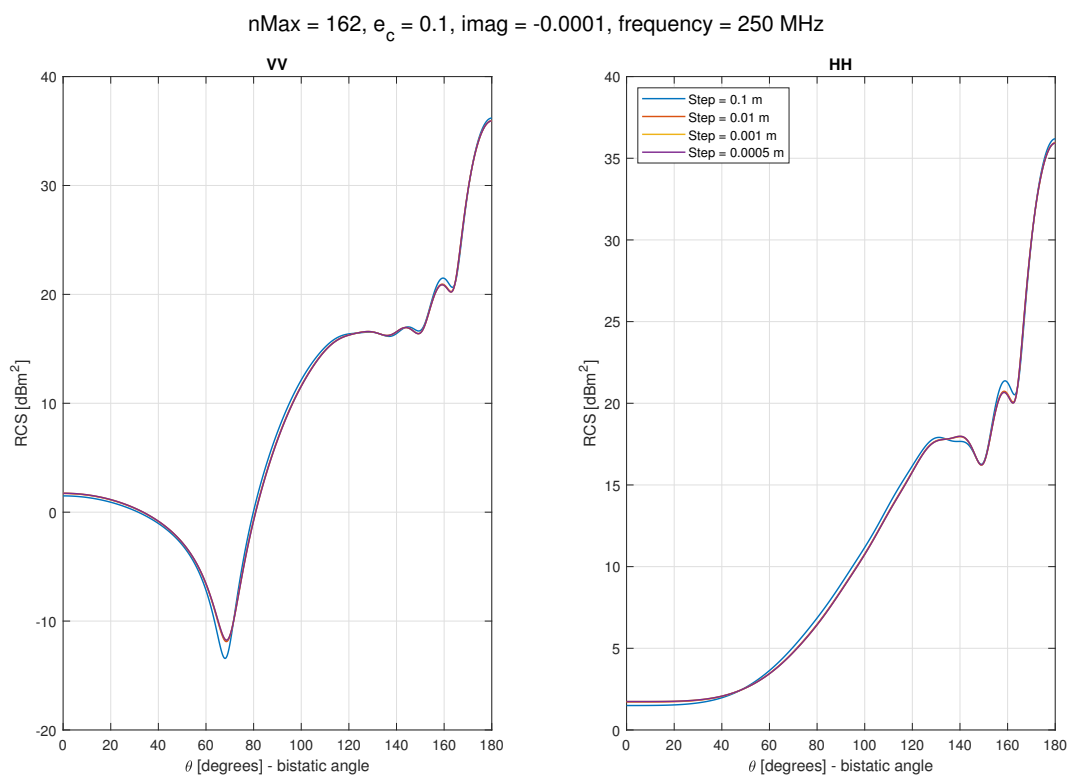


Fig. B.4 RCS convergence for ϵ_r by equation (4.1) with $\epsilon_c = 0.1$

Mie Solution for continuous permittivity distribution and imaginary component of relative permittivity contribution

This last parameter is the worst case and leads to hard oscillations as shown in figure B.5a: in this case there is no accuracy for some steps as previously seen with higher ϵ_c values. In figure B.5b accuracy is reached from a $step = 100$ [μm], much lower than previous cases.

B.2 Implementation of a relevant imaginary component

In this subsection a relevant imaginary component is chosen with $\epsilon_c = -0.1$ for distribution relation in (4.1). Analysis are done on permittivities, therefore being ϵ_c negative substitutions for zero and negative permittivities with $\epsilon_r' = 1 \cdot 10^{-3}$ occur as shown in figure B.6. Chosen imaginary component is $\epsilon_r'' = 0.05$: RCSs may have different back-scattering, in this case around $1 dBm^2$ of difference as shown in figure B.7

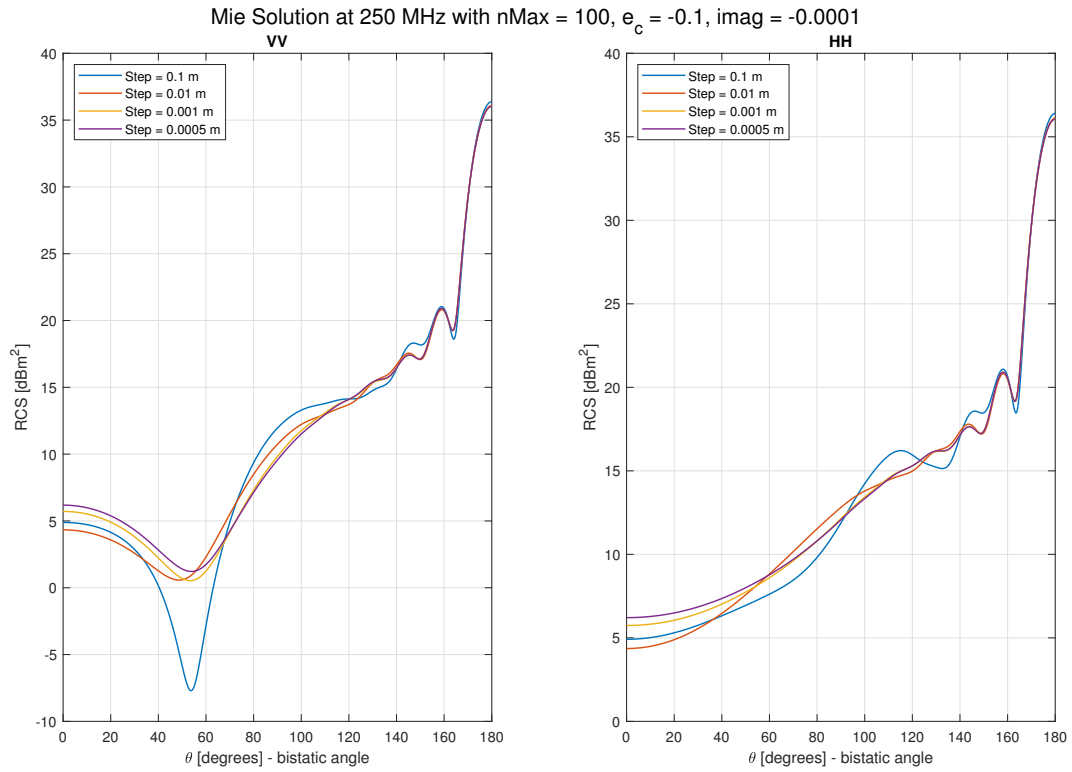
B.2.1 Permittivity distribution with negative and zero values substituted with very tiny positive values

In figure B.8 it is shown the accuracy for proposed continuous inhomogeneous plasma, reached from $step = 1$ [cm]: RCSs are lower for most the bistatic angle with the respect of previous case with $\epsilon_r'' = 1 \cdot 10^{-4}$ as shown in figure B.5b and accuracy is more relaxed then previous $step = 100$ [μm].

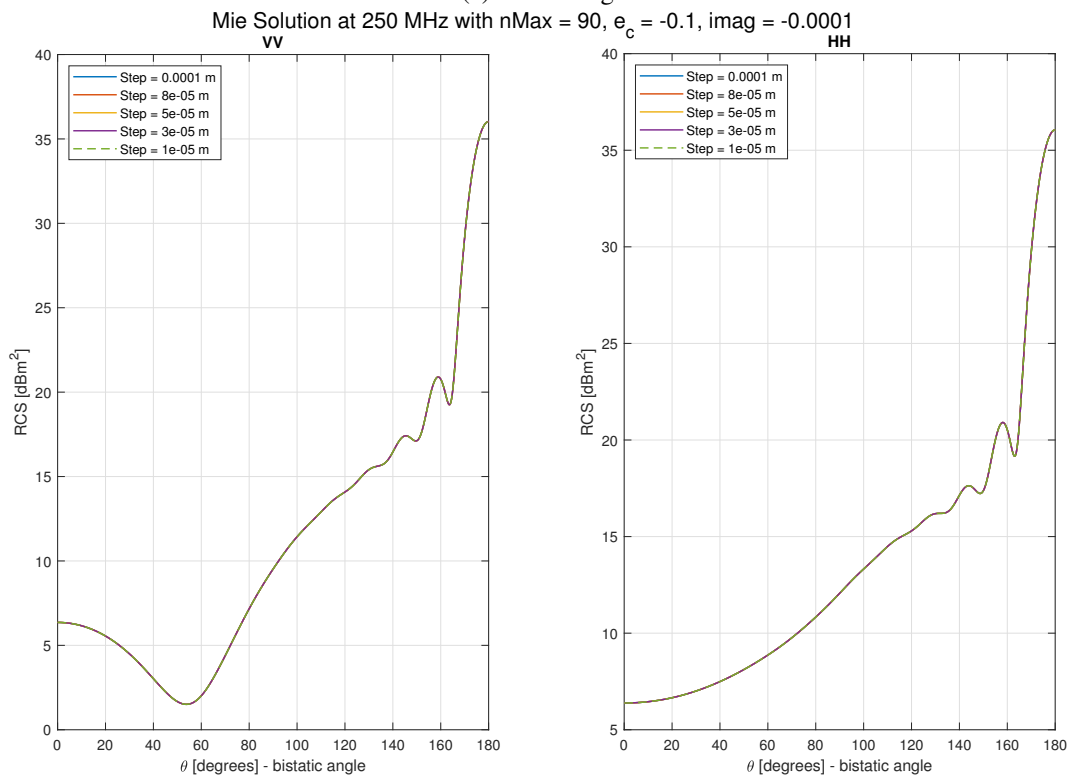
In analytic solution there is a decrease for required minimum resolution due to imaginary component increasing, moreover on CST there is analysed the trend for RCS with mesh increasing. For positive permittivity material, three meshes are proposed: **2 million cells** as lowest resolution; **5 million cells** as intermediate resolution and **10 million cells** as highest resolution.

In figure B.9 there are proposed simulations with an imaginary component.

B.2 Implementation of a relevant imaginary component



(a) Oscillating



(b) Convergent

Fig. B.5 RCS of ϵ_r from equation (4.1) Mie Solution for $\epsilon_c = -0.1$

Mie Solution for continuous permittivity distribution and imaginary component of relative permittivity contribution

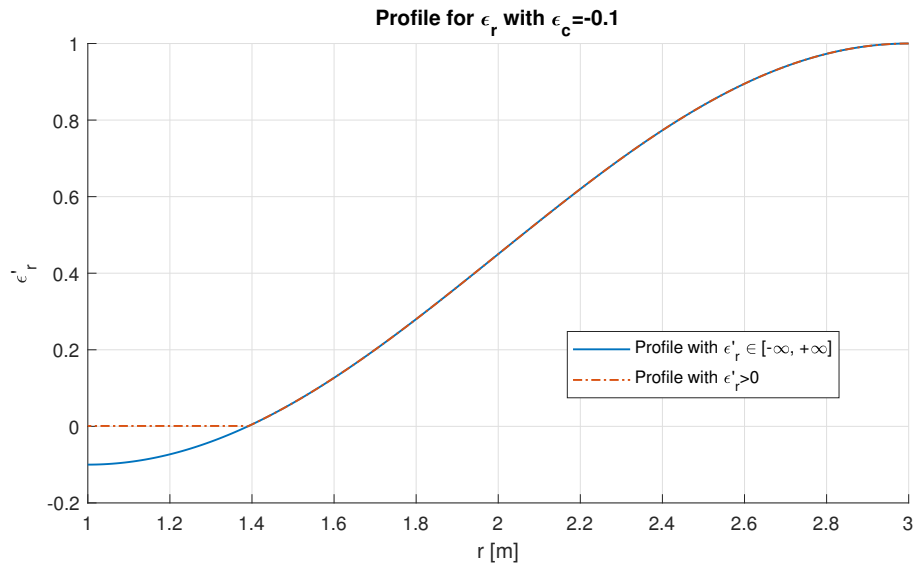


Fig. B.6 Profile of permittivity distribution

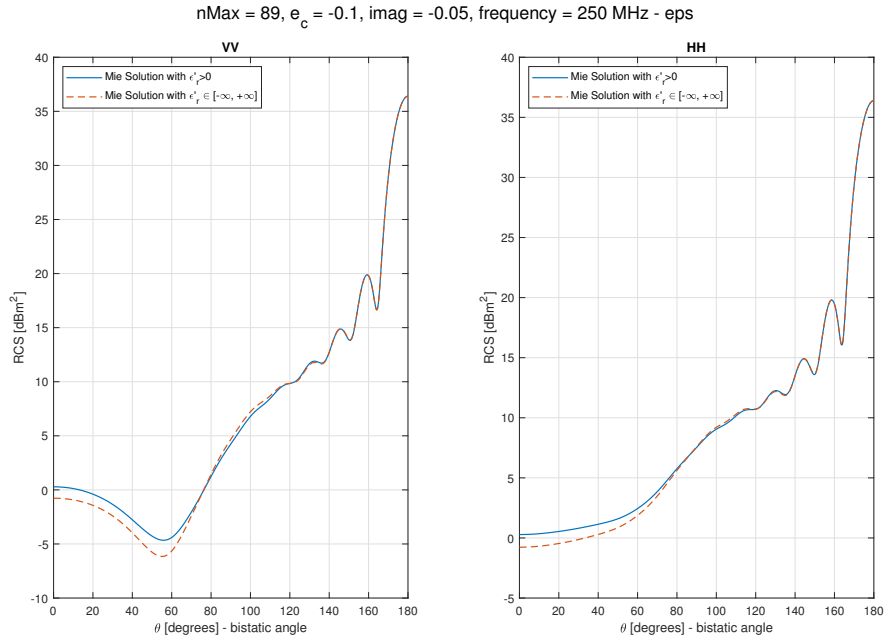


Fig. B.7 RCS for permittivity distribution in equation (4.1) with $\epsilon_c = -0.1$ and $\epsilon_r'' = 0.05$ with and without substitution $\forall \epsilon_r' < 0 \Rightarrow \epsilon_r' = 1 \cdot 10^{-3}$

B.2 Implementation of a relevant imaginary component

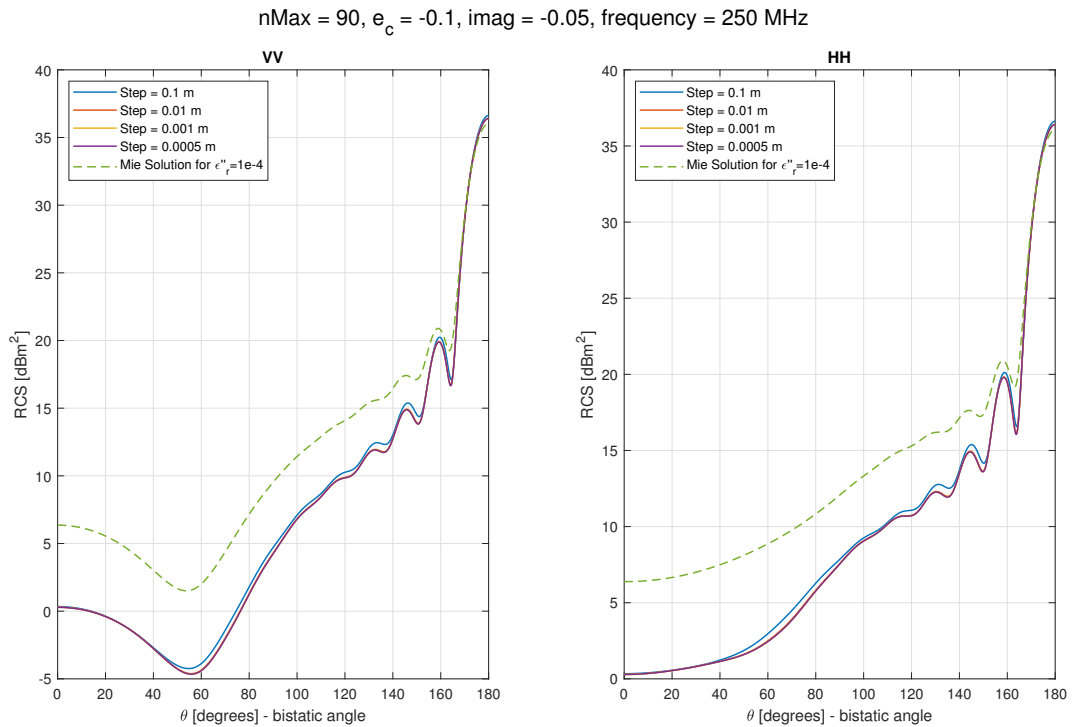


Fig. B.8 Accuracy for Mie Solution of ϵ_r from equation (4.1) with $\epsilon_c = -0.1$ and $\epsilon_r'' = 0.05$

B.2.2 Conclusions

For both implementations as mesh increases RCS generated by CST simulations reach a closer accuracy with the respect of corresponding Mie Solution, thus leading to a required increase of CST mesh as well previously done with Mie Solution resolution. This may be a bottleneck, because as mesh increases, time computation and required resources in memory become larger as well.

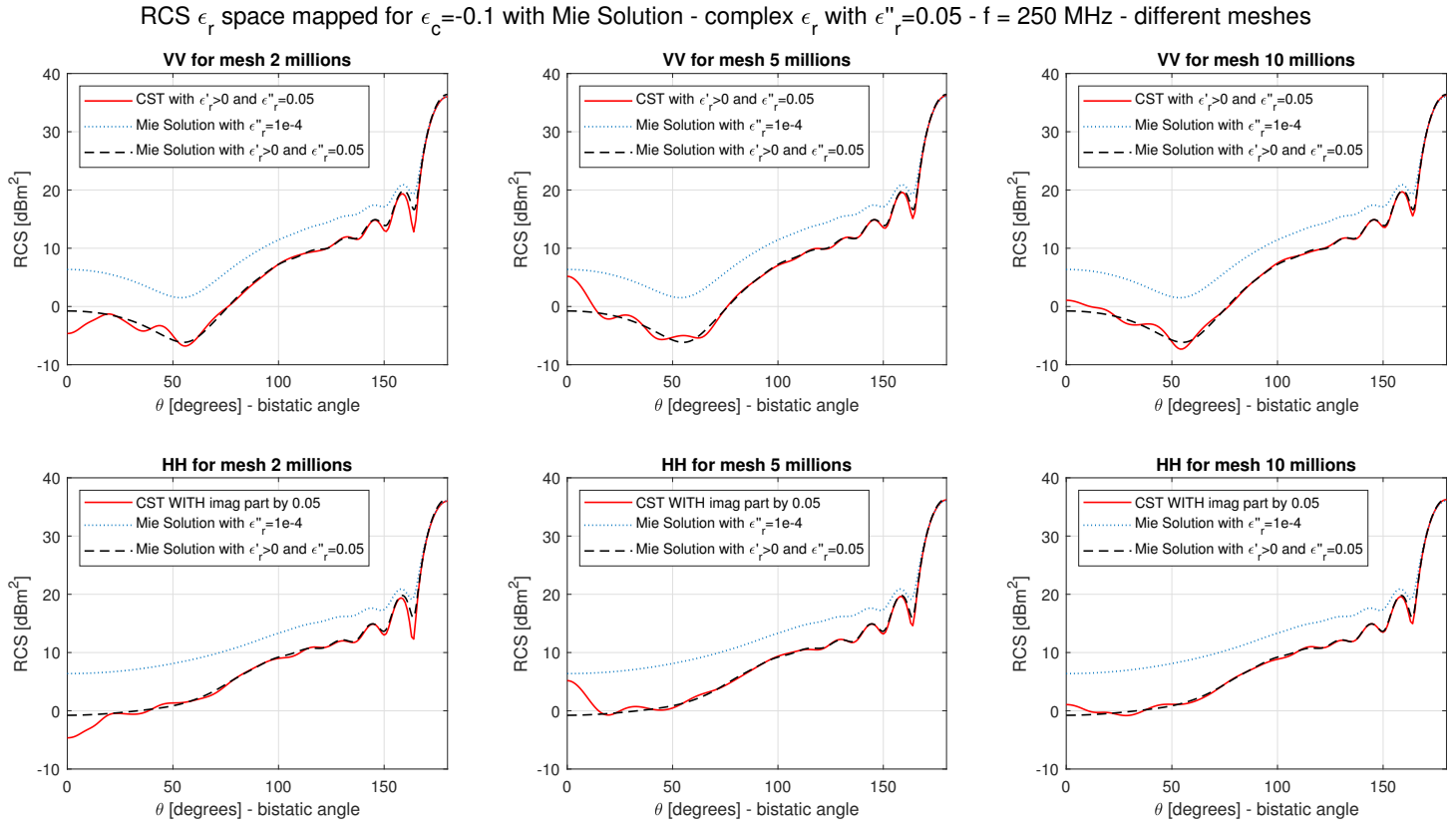


Fig. B.9 RCS with $\epsilon_c = -0.1$ from profile defined in (4.1) - $\epsilon_r \in \mathbb{C}$

Appendix C

MATLAB code for shells with permittivity profile and CST geometry implementation

In this Appendix there is reported the MATLAB code for the generation of the geometry of concentric shells in 4.2.1.1 and shown in figure 4.9.

For the implementation of Mie Series Solution implemented functions are from [9], while the implementation of the functions for CST interaction is from [12].

The cosine profile in lines 41 and 92 is the one in equation (4.1). From line 203 the script creates CST project. From line 375 there is a function inspired by an internal method from [12] for material generation, in this case for dispersive Drude Model material implementation.

```
1  %%%%%%%%%%%%%%%%%%%%%%%%%%%%%%%%%%%%%%%%%%%%%%%%%%%%%%%%%%%%%%%%%%%%%%%%% cosine plasma distribution implementation in CST
2  %%%%%%%%%%%%%%%%%%%%%%%%%%%%%%%%%%%%%%%%%%%%%%%%%%%%%%%%%%%%%%%%%%%%%%%%% not as Space MAP but as geometric concentric shells
3  clear all
4  close all
5  clc
6
7  % in this path there are the functions for Mie Solution provided by Walton
8  % Gibson's script
9  addpath('..\functions')
10
11 % this command is to choose if geometry is based on Drude material , with false
    value ,
12 % or permittivity , with true value that removes negative permittivities and
13 % substitutes them with a fixed low value
14 remove_negative_eps = false; % Drude dispersion model is implemented
```

MATLAB code for shells with permittivity profile and CST geometry implementation

```

15
16 % physical parameter
17 frequency = 100e6; % working frequency in Hz
18 step = 0.037; % step of shells implemented, in m
19
20 %%%%%%%%%%%%%%%%%%%%%%%%%%%%%%%%%%%%%%%%%%%%%%%%%%%%%%%%%%%%%%%%%%%%%%%%% From examples.m file provided by Walton Gibson's script
21 nTheta = 721;
22 theta = linspace(0, pi, nTheta); % bistatic scattering angles
23
24 % This may change
25 nMax = 80; % maximum mode number for Mie Solution
26 %%%%%%%%%%%%%%%%%%%%%%%%%%%%%%%%%%%%%%%%%%%%%%%%%%%%%%%%%%%%%%%%%%%%%%%%%
27
28 %%%%%%%%%%%%%%%%%%%%%%%%%%%%%%%%%%%%%%%%%%%%%%%%%%%%%%%%%%%%%%%%%%%%%%%%% Geometry dimensions
29 Rin = 1; % PEC core sphere radius
30 Rout = 3; % plasma radius outer shell
31 %e_r at sphere core surface
32 e_c = 0.1; % key parameter for sinusoidal distribution
33 imag_part = 1e-4; % imaginary relative permittivity
34
35 %%%%%%%%%%%%%%%%%%%%%%%%%%%%%%%%%%%%%%%%%%%%%%%%%%%%%%%%%%%%%%%%%%%%%%%%% Mie Solution for cosine distribution %%%%%%%%%%%%%%%%%%%%%%%%%%%%%%%%%%%%%%%%%%%%%%%%%%%%%%%%%%%%%%%%%%%%%%%%%
36 r = [Rout:-0.0001:Rin]; % r variable discretized for convergent result
37
38 e_ext = 1; %e_r at outer shell
39
40 % Cosine profile
41 e_r = ((e_c+e_ext)/2)*(1 + ((e_c-e_ext)/(e_c+e_ext))*cos(pi*(r-Rin)/(Rout-Rin)) );
42
43 %%%%%%%%%%%%%%%%%%%%%%%%%%%%%%%%%%%%%%%%%%%%%%%%%%%%%%%%%%%%%%%%%%%%%%%%% for permittivity distribution on CST substituted negative
44 %%%%%%%%%%%%%%%%%%%%%%%%%%%%%%%%%%%%%%%%%%%%%%%%%%%%%%%%%%%%%%%%%%%%%%%%% permittivities whenever a permittivity material has to be defined
45 e_r_replaced = e_r;
46 e_r_replaced( e_r_replaced <= 0 ) = 1e-3; % substituted with a low value
47 % for Mie Solution
48 if remove_negative_eps
49     e_r_imag = [e_r_replaced 1.0]-1i*imag_part; % implement substitutions
50 else
51     e_r_imag = [e_r 1.0]-1i*imag_part; % implement original permittivities
52 end
53
54 %%%%%%%%%%%%%%%%%%%%%%%%%%%%%%%%%%%%%%%%%%%%%%%%%%%%%%%%%%%%%%%%%%%%%%%%% from examples.m file from Walton Gibson's script %%%%%%%%%%%%%%%%%%%%%%%%%%%%%%%%%%%%%%%%%%%%%%%%%%%%%%%%%%%%%%%%%%%%%%%%%
55 mu = ones(size(e_r_imag)); % same sizes and all ones for unmagnetized plasma
56 isPEC = 1; % innermost region is conducting
57
58 % Mie Solution for corresponding permittivity profile
59 [An, Bn] = mieLayeredTerms(mu, e_r_imag, r, isPEC, frequency, nMax);
60
61 for k = 1:nTheta
62     [eTheta_imag_mie(k,:), a] = mieScatteredField(An, Bn, theta(k), 0, frequency);
63     [a, ePhi_imag_mie(k,:)] = mieScatteredField(An, Bn, theta(k), pi/2,
64         frequency);
65 end
66 %%%%%%%%%%%%%%%%%%%%%%%%%%%%%%%%%%%%%%%%%%%%%%%%%%%%%%%%%%%%%%%%%%%%%%%%%
67 % plot Mie Solution with accurate results

```

```

68 fig_RCS = figure ;
69 subplot(1, 2, 1)
70 plot( theta*180/pi, 20*log10(eTheta_imag_mie), 'r', 'linewidth', 1 )
71 subplot(1, 2, 2)
72 plot( theta*180/pi, 20*log10(ePhi_imag_mie), 'r', 'linewidth', 1 )
73
74 disp(['Number of spheres: ', num2str(floor((Rout-Rin)/step)+1)])
75
76 % linear discretized shells with defined step
77 r_linear = [Rout:-step:Rin];
78
79 %%% to remove coincidence with inner core sphere radius of innermost shell
80 if r_linear(end) == Rin
81     warning('Removed last point on discretized radius')
82     r_linear = r_linear(1:end-1);
83 end
84
85 %%%%%%%%%%%%%%%%%%%%%%%%%%%%%%%%%%%%%%%%%%%%%%%%%%%%%%%%%%%%%%%%%%%%%%%%%%%
86 w = 2*pi*frequency;
87 epsilon0 = 8.8541878128e-12; % vacuum permittivity
88 % sigma value for CST permittivity imaginary component in S/m
89 sigma = imag_part * w * epsilon0
90
91 % new cosine profile for given step
92 e_r = ((e_c+e_ext)/2)*(1 + ((e_c-e_ext)/(e_c+e_ext))*cos(pi*(r_linear-Rin)/(Rout-
    Rin)) );
93
94 %%%%%%%%%%%%%%%%%%%%%%%%%%%%%%%%%%%%%%%%%%%%%%%%%%%%%%%%%%%%%%%%%%%%%%%%%%% MIE Solution with provided step %%%%%%%%%%%%%%%%%%%%%%%%%%%%%%%%%%%%%%%%%%%%%%%%%%%%%%%%%%%%%%%%%%%%%%%%%%%
95 if remove_negative_eps % if chosen material is non-dispersive
96     % removal of negative values and implementation
97     %of imaginary component
98     e_r(e_r<=0) = 1e-3;
99     e_r = e_r-j*imag_part;
100 else % if chosen material is dispersive
101     % if Drude is required let's evaluate collision frequency to have same
102     % imag part
103     eps_inf = 1; % background material of Drude model
104     w = 2*pi*frequency; % angular working frequency
105
106     % plasma frequency in rad/s
107     w_pe_2 = w^2 * ( eps_inf - e_r );
108     w_pe = sqrt( w_pe_2 );
109
110     % nu_c is low and may be extracted through approximation
111     nu_c = ( w_pe.^2 - sqrt( w_pe.^4 - 4 * w^4 * imag_part^2 ) ) ./ ( 2*w*
        imag_part);
112
113     % manual adjustment for outer shell that is e_r=1
114     w_pe(1) = 15e5; % much lower than expected
115     nu_c(1) = nu_c(2)+5e5;
116     nu_c = real(nu_c); % only real values required
117
118     % re-evaluation of permittivity with obtained Drude coefficients
119     epsilon_drude = eps_inf - ( w_pe.^2 ) ./ ( w^2 - 1i*w*nu_c );

```

MATLAB code for shells with permittivity profile and CST geometry implementation

```

120
121     % error evaluated from the original one, but RCS are close to the ideal
122     % one
123     error_Drude = abs( epsilon_drude - e_r );
124     figure
125     plot( error_Drude )
126     set(gca, 'Yscale', 'log')
127     xlabel('Original \epsilon_r profile')
128     ylabel('Absolute values of error with Drude coefficients')
129     title('error with new generated permittivity from Drude Coefficients')
130
131     % new permittivity is defined through Drude coefficients
132     e_r = epsilon_drude;
133 end
134
135 % core as PEC for simplicity
136 isPEC = 1; % if sphere core is conductive
137
138 e_r(end+1) = 1.0-j*imag_part; % last entry required for Mie Solution
139 e_r(1) = 1 +j*0; % removed imaginary component for outer shell
140 mu = ones(size(e_r)); % mu as 1 for all
141
142 %%% from examples.m file from Walton Gibson's script %%%
143 %%% Mie Solution for new discretization
144 [An, Bn] = mieLayeredTerms(mu, e_r, r_linear, isPEC, frequency, nMax);
145
146 for k = 1:nTheta
147     [eTheta(k,:), a] = mieScatteredField(An, Bn, theta(k), 0.0, frequency);
148     [a, ePhi(k,:)] = mieScatteredField(An, Bn, theta(k), 0.5*pi, frequency);
149 end
150 %%%
151
152 % plot RCS of Mie Solution with accurate and discretized result
153 % for CST implementation
154 figure( fig_RCS )
155 subplot(1, 2, 1)
156 hold on
157 plot(theta*180/pi, 20.0*log10(abs(eTheta)), '--b', 'linewidth', 1);
158 xlabel('\theta [degrees] - bistatic angle')
159 ylabel('RCS [dBm^2]')
160 grid on
161 legend('Mie Solution with step=1e-4', ['Mie Solution with step=', num2str(step)], 'location', 'North')
162 title('VV')
163 xlim([0 180])
164
165 subplot(1, 2, 2)
166 hold on
167 plot(theta*180/pi, 20.0*log10(abs(ePhi)), '--b', 'linewidth', 1);
168 xlabel('\theta [degrees] - bistatic angle')
169 ylabel('RCS [dBm^2]')
170 grid on
171 legend('Mie Solution with step=1e-4', ['Mie Solution with step=', num2str(step)], 'location', 'North')

```

```

172 title('HH')
173 xlim([0 180])
174
175 sgtitle(['nMax = ', num2str(nMax), ', imag part = ', ...
176         num2str( imag_part ), ', sigma = ', num2str(sigma) ,...
177         ' [S/m], remove neg eps = ', char(string(remove_negative_eps)) ,...
178         '\epsilon_c=', num2str(e_c), ', frequency = ', ...
179         num2str(frequency/1e6), ' MHz' ])
180
181 % verify if data
182 if isnan(eTheta(1)) || isnan(ePhi(1))
183     error(['NaN for Mie Solution'])
184 end
185
186 if ~remove_negative_eps % is false then Drude Model has to be implemented
187     plasma_freq_linear = w_pe;
188 end
189 epsilon_linear = e_r;
190 epsilon_linear(end) = []; % without Mie Solution last element has to be removed
191 clear w_pe e_r % changed names of variables
192
193 figure
194 subplot(2,1,1)
195 plot( r_linear, real(epsilon_linear), 'r', 'linewidth', 1 );
196 title('Real \epsilon')
197 subplot(2,1,2)
198 plot( r_linear, imag(epsilon_linear), 'r', 'linewidth', 1 );
199 title('Imag \epsilon')
200 sgtitle('Profile of generated permittivity')
201
202
203 %% CREATE CST PROJECT RELATED TO RESULTS OBTAINED ABOVE
204 disp(['Will be generated ', num2str(length(r_linear)), ' circles'])
205
206 %%% For file naming
207 if remove_negative_eps
208     Drude_or_eps = 'eps';
209 else
210     Drude_or_eps = 'Drude';
211 end
212
213 % path for CST script of Henry Giddens
214 addpath('C:\Users\Mascarino\Documents\MATLAB\github_repo\CST_App')
215
216 folder = 'E:\users\Mascarino\CST_simulations';
217 filename = ['PLASMA_PEC_sinusoidal_Plasma_', Drude_or_eps ,...
218            '_with_e_c_', num2str(length(r_linear)), '_spheres_with_epsilon_c_', ...
219            replace(num2str(e_c), '.', '_'), '_and_frequency_', ...
220            num2str(frequency/1e6), '_MHz.cst'];
221
222 % create object to communicate with CST from Henry Giddens' script
223 CST = CST_MicrowaveStudio(folder, filename);
224
225 % project settings, required when created the file

```

MATLAB code for shells with permittivity profile and CST geometry implementation

```
226 frequency_range = [frequency/1e6-0.1*(frequency/1e6) ,...
227     frequency/1e6+0.1*(frequency/1e6)]; % MHz
228 monitor_freq = frequency/1e6; %MHz
229 frequency_unit = 'MHz';
230 meter_unit = 'm';
231 if meter_unit == "m"
232     scale_factor = 1;
233 elseif meter_unit == "mm"
234     scale_factor = 1e3;
235 else
236     error('Undefined scale factor for corresponding meter unit')
237 end
238
239 %%% project general settings - required only when created the file
240 if exist( [folder, '\', filename], 'file' ) ~= 2
241     CST.defineUnits('Geometry', meter_unit, 'Frequency', frequency_unit)
242     CST.setSolver('time')
243     CST.setFreq( min(frequency_range), max(frequency_range))
244 else % condition satisfied when file already exists
245     warning('File already exist')
246 end
247
248 %%% CREATE COLORMAP
249 % starting from the colormap used in Matlab is possible to interpolate it
250 % and create corresponding colours in CST. Is a visible effect
251 % useful during geometry creation
252
253 % from https://stackoverflow.com/questions/33110109/interpolating-a-matlab-
254     colormap
255 colormap = jet;
256 hsv=rgb2hsv( colormap );
257 cm_data=interp1( linspace(0,1,size( colormap ,1)),hsv, linspace(0, 1, length(r_linear
258     )));
259 cm_data=hsv2rgb( cm_data );
260 %%% Material Creation
261 for index = 1:length( r_linear )
262     % there is a difference between Drude model in addDrudeMaterial,
263     % where negative epsilons occur, and NormalMaterial method
264     % from Giddens' script in which negative epsilons are removed.
265     % This belongs to all previous elaborations done above in the code
266     if remove_negative_eps
267         if index == 1 % outer shell does not have imaginary component
268             CST.addNormalMaterial(['material', num2str(index)], real(epsilon_linear
269                 (index)), 1, cm_data(index,:))
270         else
271             CST.addNormalMaterial(['material', num2str(index)], real(epsilon_linear
272                 (index)), 1, cm_data(index,:), 'sigma', sigma)
273         end
274     else
275         % function reported below, extracted and inspired by Giddens'
276         % method for dispersive material definition
```

```

275         addDrudeMaterial(CST, ['material', num2str(index)], plasma_freq_linear(
                index), nu_c(index), cm_data(index,:))
276     end
277
278 end
279 CST.save % save CST project
280 %%%%%%%%%%%%%%%%%%%%%%%%%%%%%%%%%%%%%%%%%%%%%%%%%%%%%%%%%%%%%%%%%%%%%%%%%
281
282 %%%%%%%%%%%%%%%%%%%%%%%%%%%%%%%%%%%%%%%%%%%%%%%%%%%%%%%%%%%%%%%%%%%%%%%%% Geometry Creation
283 % as previously done for material, even the geometry has to be defined
284 % through a cycle for
285
286 % in the cycle there are generated hollowed spheres related to r_linear
287 % dimensions, so the "last" hollowed circle for geometry will be done
288 % separately, related to the radius of the core sphere
289
290     tic()
291     for index = 1:length( r_linear )-1
292         % a sphere is created through Giddens' script method
293         CST.addSphere(0,0,0, r_linear(index)*scale_factor, 0, 0,...
294             ['Sphere', num2str(index)], 'Spheres', ...
295             ['material', num2str(index)])
296
297         % corresponding thickness of the sphere is related to next sphere
298         thickness = (r_linear(index)-r_linear(index+1))*scale_factor;
299         if thickness <= 0, error(['Wrong thickness for index ', ...
300             num2str(index)], end
301
302         % Sphere becomes hollowed by corresponding thickness
303         VBA = ['Solid.ShellAdvanced "', 'Spheres:Sphere', num2str(index), ...
304             '", "Inside", "', num2str(thickness),"', "true"'];
305         CST.addToHistory(['Create hollowed sphere: ', num2str(index)], VBA);
306     end
307
308     % last sphere has to be created outside for cycle
309     index = index + 1; % increase index as last sphere,
310     % that should correspond to r_linear size
311
312     % let's verify all previsions are respected
313     if length( r_linear ) ~= index, ...
314         error('error: last sphere index doesn't correspond!'), end
315
316     % add last sphere of r_linear through Giddens' script method
317     CST.addSphere(0,0,0, r_linear(index)*scale_factor, 0, 0,...
318         ['Sphere', num2str(index)], 'Spheres', ['material', num2str(index)])
319
320     % thickness belongs to core radius
321     thickness = (r_linear(index)-Rin)*scale_factor;
322     if thickness <= 0, error(['Wrong thickness for last index']), end
323
324     % shelling the last sphere
325     VBA = ['Solid.ShellAdvanced "', 'Spheres:Sphere', num2str(index), ...
326         '", "Inside", "', num2str(thickness),"', "true"'];
327     CST.addToHistory(['Create hollowed sphere: ', num2str(index)], VBA);

```

MATLAB code for shells with permittivity profile and CST geometry implementation

```
328
329     CST.save % save file
330
331 disp('Geometry done')
332 disp(['Elapsed time in minutes ', num2str(toc()/60)])
333
334 %%%%%%%%%%%%%%%%%%%%%%%%%%%%%%%%%%%%%%%%%%%%%%%%%%%%%%%%%%%%%%%%%%%%%%%%%%% CORE sphere
335 % Creating core sphere in PEC
336 CST.addSphere(0,0,0, Rin*scale_factor, 0, 0, 'Core', 'Inner', 'PEC')
337 VBA = ['StoreParameter "', 'core_done', '", "', num2str(1), '"'];
338 CST.addToHistory('Core Done', VBA)
339
340 %%%%%%%%%%%%%%%%%%%%%%%%%%%%%%%%%%%%%%%%%%%%%%%%%%%%%%%%%%%%%%%%%%%%%%%%%%% CREATE PLANEWAVE
341 %%% creation of a plane wave with E along x
342     Normal = [0, 0, -1]; % normal direction in x y z coordinates
343     EVector = [1, 0, 0]; % E field direction in x y z coordinates
344     Polarization = 'Linear';
345     Phase_difference = -90.0;
346 %%% VBA definition inspired by method inside CST repository of Henry
347 %%% Giddens
348     VBA = sprintf(['With PlaneWave\n'...
349                 '\t.Reset\n'...
350                 '\t.Normal (%d, %d, %d)\n'...
351                 '\t.EVector (%d, %d, %d)\n'...
352                 '\t.Polarization ("%s")\n'...
353                 '\t.PhaseDifference (%d)\n'...
354                 '\t.Store\n'...
355                 'End With' ],...
356                 Normal(1), Normal(2), Normal(3), EVector(1), ...
357                 EVector(2), EVector(3), Polarization, Phase_difference);
358     CST.addToHistory('Create PlaneWave', VBA)
359 %%%%%%%%%%%%%%%%%%%%%%%%%%%%%%%%%%%%%%%%%%%%%%%%%%%%%%%%%%%%%%%%%%%%%%%%%%%
360
361 %%%%%%%%%%%%%%%%%%%%%%%%%%%%%%%%%%%%%%%%%%%%%%%%%%%%%%%%%%%%%%%%%%%%%%%%%%% Monitor freq
362 %%% create the monitor for working frequency through Giddens' script method
363 CST.addFieldMonitor('Farfield', monitor_freq)
364
365 CST.save
366
367 disp('Project modeling finished')
368
369 %%%%%%%%%%%%%%%%%%%%%%%%%%%%%%%%%%%%%%%%%%%%%%%%%%%%%%%%%%%%%%%%%%%%%%%%%%% function extracted from CST_MicrowaveStudio script
370 %%%%%%%%%%%%%%%%%%%%%%%%%%%%%%%%%%%%%%%%%%%%%%%%%%%%%%%%%%%%%%%%%%%%%%%%%%% by Henry Giddens and
371 %%%%%%%%%%%%%%%%%%%%%%%%%%%%%%%%%%%%%%%%%%%%%%%%%%%%%%%%%%%%%%%%%%%%%%%%%%% rewritten to create Drude Material for concentric spheres
372
373 %%%%%%%%%%%%%%%%%%%%%%%%%%%%%%%%%%%%%%%%%%%%%%%%%%%%%%%%%%%%%%%%%%%%%%%%%%% there is no an existing method for specific material
374 function addDrudeMaterial(obj,name,plasma_freq,collision_freq,C,varargin)
375
376     p = inputParser;
377     p.addParameter('transparency', 0);
378     p.parse(varargin{:});
379
380     transparency = p.Results.transparency;
381
```

```
382     VBA = sprintf(['With Material\n' ,...
383         '. Reset\n' ,...
384         '. Name "%s"\n' ,...
385         '. DispModelEps "Drude"\n' ,...
386         '. DispModelMu "None"\n' ,...
387         '. EpsInfinity 1\n' ,...
388         '. DispCoeff1Eps "%e"\n' ,...
389         '. DispCoeff2Eps "%e"\n' ,...
390         '. Transparency %d\n' ,...
391         '. Colour "%f" , "%f" , "%f"\n' ,...
392         '. Create\n' ,...
393         'End With' ] ,...
394         name , plasma_freq , collision_freq ,...
395         transparency , C(1) , C(2) , C(3));
396
397     obj.addToHistory(['define Drude material: ' , name] , VBA);
398 end
```